Management of stem rot of peanut using optical sensors, machine learning, and fungicides

Xing Wei

Dissertation submitted to the faculty of the Virginia Polytechnic Institute and State University in partial fulfillment of the requirements for the degree of

Doctor of Philosophy
In
Plant Pathology, Physiology and Weed Science

Hillary L. Mehl
Song Li
David B. Langston Jr.
Maria Balota
Wade E. Thomason
David S. McCall

April 30, 2021
Blacksburg, VA

Keywords: soilborne plant diseases, plant disease detection, *Arachis hypogaea*, *Sclerotium rolfsii*, *Athelia rolfsii*, sensors, spectral reflectance, thermal imaging, hyperspectral band selection

Management of stem rot of peanut using optical sensors, machine learning, and fungicides

Xing Wei

ABSTRACT

Stem rot of peanut (*Arachis hypogaea* L.), caused by a soilborne fungus *Athelia rolfsii* (Curzi) C. C. Tu & Kimbr. (anamorph: *Sclerotium rolfsii* Sacc.), is one of the most important diseases in peanut production worldwide. Though new varieties with increased partial resistance to this disease have been developed, there is still a need to utilize fungicides for disease control during the growing season. Fungicides with activity against *A. rolfsii* are available, and several new products have been recently registered for control of stem rot in peanut. However, fungicides are most effective when applied before or during the early stages of infection. Current scouting methods can detect disease once signs or symptoms are present, but to optimize the timing of fungicide applications and protect crop yield, a method for early detection of soilborne diseases is needed. Previous studies have utilized optical sensors combined with machine learning analysis for the early detection of plant diseases, but these studies mainly focused on foliar diseases. Few studies have applied these technologies for the early detection of soilborne diseases in field crops, including peanut. Thus, the overall goal of this research was to integrate sensor technologies, modern data analytic tools, and properties of standard and newly registered fungicides to develop improved management strategies for stem rot control in peanuts. The specific objectives of this work were to 1) characterize the spectral and thermal responses of peanut to infection with *A. rolfsii* under controlled conditions, 2) identify optimal wavelengths to detect stem rot of peanut using hyperspectral sensor and machine learning, and 3) evaluate the standard and newly registered peanut fungicides with different modes

of action for stem rot control in peanuts using a laboratory bioassay. For Objective 1, spectral reflectance and leaf temperature of peanut plants were measured by spectral and thermal sensors in controlled greenhouse experiments. Differences in sensor-based responses between *A. rolfsii*-infected and non-infected plants were detected 0 to 1 day after observation of foliar disease symptoms. In addition, spectral responses of peanut to the infection of *A. rolfsii* were more pronounced and consistent than thermal changes as the disease progressed. Objective 2 aimed to identify specific signatures of stem rot from reflectance data collected in Objective 1 utilizing a machine learning approach. Wavelengths around 505, 690, and 884 nm were repeatedly selected by different methods. The top 10 wavelengths identified by the recursive feature selection methods performed as well as all bands for the classification of healthy peanut plants and plants at different stages of disease development. Whereas the first two objectives focused on disease detection, Objective 3 focused on disease control and compared the properties of different fungicides that are labeled for stem rot control in peanut using a laboratory bioassay of detached peanut tissues. All of the foliar-applied fungicides evaluated provided inhibition of *A. rolfsii* for up to two weeks on plant tissues that received a direct application. Succinate dehydrogenase inhibitors provided less basipetal protection of stem tissues than quinone outside inhibitor or demethylation inhibitor fungicides. Overall, results of this research provide a foundation for developing sensor/drone-based methods that use disease-specific spectral indices for scouting in the field and for making fungicide application recommendations to manage stem rot of peanut and other soilborne diseases.

Management of stem rot of peanut using optical sensors, machine learning, and fungicides

Xing Wei

GENERAL AUDIENCE ABSTRACT

Plant diseases are a major constraint to crop production worldwide. Developing effective and economical management strategies for these diseases, including selection of proper fungicide chemistries and making timely fungicide application, is dependent on the ability to accurately detect and diagnose their signs and/or symptoms prior to widespread development in a crop. Optical sensors combined with machine learning analysis are promising tools for automated crop disease detection, but research is still needed to optimize and validate methods for the detection of specific plant diseases. The overarching goal of this research was to use the peanut-stem rot plant disease system to identify and evaluate sensor-based technologies and different fungicide chemistries that can be utilized for the management of soilborne plant diseases. The specific objectives of this work were to 1) characterize the temporal progress of spectral and thermal responses of peanut to infection and colonization with *Athelia rolfsii*, the causal agent of peanut stem rot 2) identify optimal wavelengths to detect stem rot of peanut using hyperspectral sensor and machine learning, and 3) evaluate standard and newly registered peanut fungicides with different modes of action for stem rot control in peanuts using a laboratory bioassay. Results of this work demonstrate that spectral reflectance measurements are able to distinguish between diseased and healthy plants more consistently than thermal measurements. Several wavelengths were identified using machine learning approaches that can accurately differentiate between peanut plants with symptoms of stem rot and non-symptomatic plants. In addition, a new method was developed to select the top-ranked,

non-redundant wavelengths with a custom distance. These selected wavelengths performed better than using all wavelengths, providing a basis for designing low-cost optical filters to specifically detect this disease. In the laboratory bioassay evaluation of fungicides, all of the foliar-applied fungicides provided inhibition of *A. rolfsii* for up to two weeks on leaf tissues that received a direct application. Percent inhibition of *A. rolfsii* decreased over time, and the activity of all fungicides decreased at a similar rate. Overall, the findings of this research provide a foundation for developing sensor-based methods for disease scouting and making fungicide application recommendations to manage stem rot of peanut and other soilborne diseases.

DEDICATION

This dissertation is dedicated to my eldest brother, Wei, who introduced me to the marvelous world of agricultural research and inspired me to pursue my dreams of studying abroad; and to my beloved wife, Marian, and adorable daughter, Jasmine, for their endless love, care, and encouragement.

ACKNOWLEDGEMENTS

With a grateful heart, I would like to thank the people who trusted in me and made it possible to approach the finish line of my Ph.D. I am fortunate to have the opportunity to work with three co-advisors. First, my sincere appreciation to Dr. Hillary L. Mehl, who encouraged me to explore my full potential, provide countless suggestions in professional development including conducting experiments, sharing my research in regional and national scientific meetings, and writing. I thank Dr. David B. Langston Jr. for taking me into this program and sharing his expertise in plant pathology and fungicides. I thank Dr. Song Li for sharing his expertise in data science and training me in machine learning and programming. I want to thank my committee members, Dr. Maria Balota, Dr. Wade E. Thomason, and Dr. David S. McCall, for sharing instruments, providing ideas in experiment design, and helpful insights in data collection and analysis.

I appreciate my fellow lab mates in Mehl and Langston Lab for their excellent technical support in field and greenhouse experiments. I enjoyed working with you all: Linda Byrd-Masters, Steve Byrum, Ed Hobbs, Saleh Ahmed, Christian Aguilar, Bhupendra Acharya, Tian Zhou, Joseph Opoku, Navjot Kaur, Curtis Guilford, Loni Askew, Zoe Dunlow, Fitz Cherry, Robert Wilson, Amy Taylor, Marian Luis, and Jon Stein. I thank the Li Lab members, including Qi Song, Haidong Yan, Jiyong Lee, Marcela Aguilera, Kshitiz Dhakar, Hazem Sharaf, and Xuemei Zhang, for their help in machine learning analysis and programming. I also thank other colleagues at TAREC and SPES who helped with my academic program and made this journey memorable.

Last but not least, I would like to thank every member of my wonderful family, including my parents Zhixuan and Yulan, my parents-in-law Ben and Janet, my brothers and sisters-in-law including Wei, Zhen, Dong, Yi, Suhui, and Fei, and my wife Marian and daughter Jasmine, for their continuous love, encouragement, and support.

TABLE OF CONTENTS

LIST OF TABLES

CHAPTER 1: Literature review

CHAPTER 2: Spectral and thermal responses of peanut to infection and colonization with *Athelia rolfsii*

CHAPTER 3: Identifying optimal wavelengths to detect peanut infection with *Athelia rolfsii* using hyperspectral sensor and machine learning

CHAPTER 4: Detection of soilborne disease utilizing sensor technologies: Lessons learned from studies on stem rot of peanut

CHAPTER 5: Comparison of standard and newly registered peanut fungicides with different modes of action through bioassay of detached plant tissues with *Athelia rolfsii*

LIST OF FIGURES

CHAPTER 2: Spectral and thermal responses of peanut to infection and colonization with *Athelia rolfsii*

CHAPTER 3: Identifying optimal wavelengths to detect peanut infection with *Athelia rolfsii* using hyperspectral sensor and machine learning

CHAPTER 1: Literature Review

Peanut production in the United States

Peanut (*Arachis hypogaea* L.) is cultivated in tropical and subtropical areas worldwide, mainly for its seeds which contain high-quality protein and oil content (Stalker 1997; Venkatachalam and Sathe 2006). Peanut seeds contain protein (20 to 30%), edible oil (40 to 56%), carbohydrate (10 to 20%), and many other beneficial minerals such as calcium, iron, magnesium, phosphorus, potassium, zinc, sodium, copper, and selenium (Dean et al. 2009; Davis et al. 2016; Ayoola et al. 2012). The United States (3.23 million metric tons) is the fourth largest peanut producer following China (17.09 million), India (6.65 million), and Nigeria (4.25 million) in 2017/18 (USDA-FAS 2019). The area planted in peanuts in the U.S. was 576,879 hectares in 2018 (USDA-NASS 2019). Most peanuts in the U.S. are grown in three regions: Southeastern U.S. (Georgia, Alabama, and Florida), Southwestern U.S. (Texas, Oklahoma, and New Mexico), and Eastern U.S. (or Atlantic region) (North Carolina, South Carolina, and Virginia) (NPB 2019).

Several pests and diseases affect peanut production in the U.S. The most economically important diseases of peanut include foliar diseases, such as early and late leaf spot (causal organisms: *Cercospora arachidicola* and *Phaeoisariopsis personata*), tomato spotted wilt (causal organism: *Tomato spotted wilt virus*), and soilborne fungal diseases including stem rot (SSR) (causal organism: *Athelia rolfsii*), Sclerotinia blight (causal organism: *Sclerotinia minor*), and Cylindrocladium black rot (causal organism: *Cylindrocladium parasiticum*). Estimated economic losses caused by reduced yields and costs of management practices to control diseases were near $140 million in 2008 Georgia peanut production (Kemerait 2012). In this study, we will focus on investigating SSR, one of the soilborne diseases of peanut.

Economic importance of stem rot of peanut

As one of the most economically important diseases of peanut, SSR can be found in all major peanut-growing areas in the world. Yield loss caused by SSR is typically less than 25% but can be up to 80% (Backman and Brenneman 1997). Stem rot is more severe in the southeastern U.S. than other peanut production regions, where annual yield losses caused by SSR average from 7 to 10% (Backman and Brenneman 1997). In recent years, this disease became more prevalent in the Virginia-Carolina region due to warm climate trends that favored disease spread.

Causal organism and disease cycle of stem rot

Stem rot is caused by the soilborne fungal pathogen, *Athelia rolfsii* (Curzi) C.C. Tu & Kimbr., well-recognized by its anamorph synonym *Sclerotium rolfsii* Sacc. This fungus has a wide host range of 500 plant species across 100 plant families, including field, vegetable, and ornamental crops (Aycock 1966; Mullen 2001; Ridge and Shew 2014; Xie et al. 2014). In the tropics and subtropics such as the southeastern U.S., the widespread occurrence of diseases caused by *A. rolfsii* is favored by sufficiently high temperatures that favor the survival and growth of this pathogen (Punja 1985). Stem rot usually occurs during the mid to late growing season when the plant canopy covers the soil between rows and produces a warm and humid environment conducive to pathogen growth (Aycock 1966; Shokes et al., 1996). During the infection process, *A. rolfsii* will first destroy host epidermal cells before hyphal penetration. Afterward, the mycelium spreads through both intercellular and intracellular movement (Higgins 1927). The death of host cells is due to the production of large amounts of oxalic acid and cell wall degrading enzymes such as polygalacturonase and cellulase during pathogenesis (Husain 1958; Bateman and Beer 1965; Bateman 1969, 1972; Punja et al. 1985).

Athelia rolfsii is characterized by its white fluffy mycelium and brown round sclerotia, which are usually found at or near the soil line around the affected plant parts. The pathogen can colonize either living plant tissues or plant debris. The primary and secondary inoculums of *A. rolfsii* are hypha that developed from infected plant debris and germinating sclerotia in the soil, and hypha from infected plant tissues during the growing season, respectively. The development and spread of *A. rolfsii* are favored by warm to hot temperatures (27 to 30ºC) and humid conditions (Backman and Brenneman 1997; Mullen 2001). The initial symptoms of peanut plants infected with *A. rolfsii* are water-soaked necrotic lesions on stems, roots, pegs or pods, while the foliar symptoms include wilting of a single lateral branch, the main stem, or the entire plant (Backman and Brenneman 1997; Punja et al. 1985).

Management practices of stem rot

Several disease control strategies have been developed to control SSR. Only a few peanut varieties show partial resistance to this disease (Brenneman et al. 1990; Gorbet et al. 2004). In general, peanut varieties with erect growth habits are less susceptible to the disease than those with spreading growth habits (Backman and Brenneman 1997). Biological control agents such as *Trichoderma* spp. were reported to be effective in suppressing SSR severity (Backman and Brenneman 1997). Nevertheless, there are no commercialized biocontrol products available to the market because no durable formulation can be applied in the field (Backman and Brenneman 1997). Cultural practices, including deep plowing to bury crop debris, crop rotations with grass crops such as corn, sorghum or pasture grasses, and weed control, can be used to reduce overwintering of *A. rolfsii* inoculum in the soil (Backman and Brenneman 1997). However, during

the growing season, multiple applications of fungicides are typically needed to provide adequate management of this disease.

It is difficult for foliar-sprayed fungicides to penetrate into lower stems inside plant canopy and roots, pegs and pods underground because of the density of plant leaves, but it is in these plant tissues in the lower canopy that infection of soilborne pathogens initially occurs. To facilitate the penetration of fungicides into lower plant canopies, growers are recommended to apply fungicides at night when the peanut leaves are folded (Augusto et al., 2010a, 2010b), or apply irrigation shortly after fungicide spray to wash the fungicide residues on the foliage into the inner and lower plant tissues (Woodward 2006) or into soils and uptake by plant root systems.

Peanut fungicide chemistries for stem rot control

The peanut fungicides labeled for SSR control are mainly from three chemical groups: demethylation inhibitors (DMI) (e.g., tebuconazole, prothioconazole, metconazole), quinone outside inhibitors (QoI) (e.g., azoxystrobin, fluoxastrobin, pyraclostrobin), and succinate dehydrogenase inhibitors (SDHI) (e.g., penthiopyrad, benzovindiflupyr, flutolanil) (Anco 2017; Mehl 2019). DMI fungicides interfere with one specific enzyme, C14-demethylase, which is involved in sterol biosynthesis in cell membranes of fungi (FRAC 2019). Therefore, DMI fungicides can cause abnormal growth and death of the fungus (Mueller et al. 2013). Both QoI and SDHI fungicides inhibit fungal respiration, but they have different target sites on the respiratory system of fungi. QoI fungicides target the cytochrome bc1 (ubiquinol oxidase) at quinone outer binding site (complex III), while SDHI fungicides act at the succinate-dehydrogenase in the complex II of the fungal respiratory system (FRAC 2019).

Based on their mobility in a plant, fungicides can be categorized into two groups, contacts or systemics. Contact fungicides cannot penetrate plant tissues, while systemic fungicides can be absorbed and translocated inside plants. Systemic fungicides can be further divided into three categories based on the distances of these fungicides mobile from the site of application: local systemics or translaminar (very short distance such as across a leaf from upper surface to lower surface), xylem-mobile systemics (extensively upward through the plant), and phloem-mobile systemics (bi-directional mobility) (McGrath 2004). Most DMI fungicides, including prothioconazole, are xylem-mobile systemics. Most QoI fungicides are local systemics, while some including azoxystrobin are xylem-mobile systemics (McGrath 2004). Most SDHI fungicides, including the new fungicide benzovindiflupyr, are local systemics (McGrath 2004; Rambach et al. 2015). In peanut, a previous study showed that prothioconazole + tebuconazole, azoxystrobin, and flutolanil provided acropetal protection in peanut shoots (indicating xylem systemicity), and prothioconazole + tebuconazole also had basipetal protection (suggesting one or both fungicides possibly have some phloem mobility) (Augusto and Brenneman 2012). However, it is not precisely known how mobile these different fungicides are in peanut plants.

Also, there are no current reports on the residual activity of these different fungicides in peanut, which can be influenced by the application rate, method, and systemicity of the fungicide product, the targeted disease and the level of disease pressure, and environmental factors such as rain and sun-exposure (Augusto et al. 2010a; Miorini et al. 2017).

Timing of fungicide application

Peanut fungicides labeled for SSR control can be applied on a calendar schedule or following the onset of disease symptoms. However, calendar-based sprays are often confounded

by year-to-year differences in host and environmental factors, and applications of fungicides after disease onset can result in poor fungicide performance (Hagan et al. 2007; Rideout et al. 2008). Even when calendar-based sprays are used, growers always face the question of when an SSR fungicide versus leaf spot only fungicide should be applied. Scouting is essential for selecting proper fungicide chemistries and making timely applications, but the erratic distribution of SSR in the field (Aycock 1966) makes scouting for the disease time and labor-intensive. More efficient disease detection methods for SSR have the potential to improve the timing of fungicide applications, disease control, and thus peanut crop yields.

Applications of remote sensing in plant disease detection

Previous studies have demonstrated the potential applications of remote sensing technologies for the detection and quantification of plant physiological changes due to abiotic and biotic stresses including plant diseases (Nilsson 1991, 1995; Chaerle and Straeten 2000; Bauriegel et al. 2011; Mahlein 2016). Various types of optical sensors have been used for plant disease detection, including RGB-imaging, multi- and hyperspectral reflectance sensors, thermal sensors, fluorescence imaging, and light detection and ranging (LiDAR) sensors (Mahlein 2016). Among these sensors, spectral reflectance sensors and infrared thermography (IRT) are of particular interest in plant disease detection and plant phenotyping (Chaerle and Van Der Straeten 2000; Mahlein 2016; Perez-Bueno et al. 2019). The technical innovation and improvement of spectral and thermal sensors make them suitable for mounting on unmanned aerial vehicles (UAVs) for large-scale mobile mapping applications (SphereOptics 2017). Advantages of using remote sensing to assess plant disease include non-destructive sampling, objective measurements compared to visual disease assessment, and the potential to conduct automatic disease assessment

for large-scale field applications (Nilsson 1995; Mahlein 2016). On the other hand, the lack of an efficient method to analyze the great amount of complex data collected limits the use of remote sensing to assess plant diseases (Moran et al. 1997; Mahlein 2016). Machine learning algorithms are a very promising approach to analyze these sophisticated and large amounts of sensor data more efficiently (Singh et al. 2016).

Applications of machine learning in plant disease detection

Machine learning (ML) refers to the scientific study of computerized algorithms and statistical models that computer systems can use to perform specific tasks without being explicitly programmed (Samuel 1959; Mitchell 1997). Along with sensor technologies, ML approaches have been increasingly applied in precision crop management such as yield prediction and detection of abiotic and biotic stresses including insects, diseases, and weeds (Liakos et al. 2018). Machine learning algorithms are capable of generalizing trends or patterns from large amounts of data efficiently (Singh et al. 2016), which is essential for applying crop management practices based on sensor technologies such as fungicide applications in a timely manner.

Various ML algorithms such as support vector machine (SVM), *k* nearest neighbors (KNN), random forests (RF), and partial least square regression (PLSR) have been applied for the detection and classification of different plant disease systems (Table 1). For example, Rumpf et al. (2010) developed a procedure using SVM and hyperspectral reflectance for the early detection and differentiation of three foliar diseases on sugar beet. The classification accuracy of healthy and diseased sugar beet leaves was between 65% and 90% depending on the type and stage of disease using SVM (Rumpf et al. 2010). In another study, Heim et al. (2018) trained an RF classifier based on hyperspectral reflectance data of fungicide treated and untreated lemon myrtle leaves and

achieved an overall accuracy of 78% for the detection of myrtle rust (*Austropuccinia psidii*) on lemon myrtle trees. One last example, Gold et al. (2019) employed both partial least square-discrimination analysis (PLS-DA) and RF to examine the spectral responses of four potato cultivars to inoculation with *Phytophthora infestans* and attained an overall accuracy of ~ 70% in discrimination between *P. infestans*-inoculated and non-inoculated potato leaves.

Applications of spectral sensors in plant disease detection

Spectral reflectance sensors can be used to measure light-reflected directly from leaf surfaces or internal leaf structures, and the amount of light reflected from leaves is dependent on multiple biophysical and biochemical interactions (Mahlein 2016). Leaf reflectance in the visible (400 to 700 nm), near-infrared (700 to 1,100 nm) and short-wave infrared (1,100 to 2,500 nm) range is related to leaf pigment content, leaf structure, and the composition of leaf chemicals and water content, respectively (Carter and Knapp 2001; Jacquemound and Ustin 2001; Mahlein 2016). Infection and colonization of plants by pathogens can cause changes in reflectance due to deteriorations in leaf structure and chemical composition inside leaf tissues during pathogenesis, followed by chlorotic and necrotic leaf tissues or the formation of fungal structures on plant leaves (Mahlein 2016). Mahlein et al. (2010, 2013) utilized a non-imaging hyperspectral spectroradiometer to detect and differentiate three leaf diseases (Cercospora leaf spot, sugar beet rust, and powdery mildew) in sugar beet plants through the examination of spectral signatures of healthy and diseased sugar beet leaves. The authors also developed specific spectral disease indices for each disease (Mahlein et al. 2013).

A reduction of information-rich hyperspectral data to the most significant wavelengths associated with the plant disease under investigation is needed for the efficient use of spectral

reflectance measurements for disease detection (Stafford 2000; Mahlein et al. 2013). Spectral vegetation indices (SVIs) can then be developed based on these selected specific wavelengths and used to detect biochemical or physiological changes in plants. Previous studies have shown that SVIs could also be possibly used to detect plant diseases (Thenkabail et al. 2000; Ashourloo et al. 2014). However, common SVIs cannot be used for the identification or quantitative assessment of a specific disease so far because these indices lack disease specificity (Mahlein et al. 2013). In order to utilize spectral sensors for disease detection, it is necessary to identify the most critical wavelengths at which light reflectance indirectly correlates with plant responses to specific pathogen infection. Spectral vegetation or disease indices developed based on a few specific wavelengths are commonly used to simplify the analysis of complex spectral data. Several spectral wavelengths and indices have been identified for specific crop-disease systems (Table 2).

Applications of thermography in plant disease detection

The infrared thermography (IRT) of measured objects can be acquired with thermographic cameras by detecting the emitted infrared radiation from the objects in the range of 8 to 14 μm (Chaerle and Straeten 2000). IRT has been employed to visualize surface temperature changes of leaves, plants, or canopies due to abiotic and biotic stresses (Table 3). The leaf temperature is closely related to plant transpiration (Jones 1999; Jones et al. 2002) which can be affected by a variety of plant pathogens in different ways (Oerke et al. 2006; Mahlein 2016). Infection and colonization of leaves by foliar pathogens such as leaf spot or rusts can cause localized changes in plant transpiration rate, while systemic infections (e.g. *Fusarium* spp.) or diseases caused by pathogens that infect root systems (e.g. *Rhizoctonia solani*) often impact the transpiration rate and water flow of the whole plant or plant tissues (Mahlein 2016). Chaerle et al. (2004) also

demonstrated the potential of pre-symptomatic detection of plant infection utilizing IRT when investigating tobacco mosaic virus with thermal imaging. Moreover, Wang et al. (2012) detected *Fusarium* wilt of cucumber and found certain internal metabolic processes related to water status by employing IRT to monitor changes in leaf temperatures in a greenhouse study.

Rationale and objectives

Though research efforts using spectral reflectance measurements and thermal imaging for plant disease detection are increasing, most previous studies have focused on detection of foliar diseases of various crops and trees (Baranowski et al., 2015; Gold et al., 2019; Heim et al., 2018; Mahlein et al., 2010; Patrick et al., 2017; Xavier et al., 2019). Only a few studies have reported the utilization of these technologies on soilborne disease detection (Hillnhütter et al. 2011; Wang et al. 2012; Perez-Bueno et al. 2019). This is due in part to the fact that foliar diseases are easier to detect with optical sensors while soilborne diseases are concealed beneath the plant canopy or soil surface. In addition, it is difficult to identify specific foliar signatures of diseases that affect stems or roots because other factors including both abiotic and biotic stresses may produce similar responses in the plant.

To our current knowledge, there is no report of using sensor-based methods for the detection of stem rot caused by *A. rolfsii* in peanut. Therefore, the ultimate goal of this study is to provide growers or crop consultants a new sensor-based scouting method/tool that can be used to determine when and where fungicide applications are needed. The specific objectives of this research were to, 1) characterize the spectral and thermal responses of peanut to infection with *A. rolfsii* under controlled conditions, 2) identify optimal wavelengths to detect stem rot of peanut using hyperspectral sensor and machine learning, and 3) evaluate the standard and newly registered

peanut fungicides with different modes of action for stem rot control in peanuts using a laboratory bioassay.

Literature Cited

Anco, D. 2017. Peanut Disease Management. In 2017 South Carolina Pest Management Handbook. Clemson Cooperative Extension. *APT-17.* Page 190 – 201. Available at, https://dc.statelibrary.sc.gov/bitstream/handle/10827/24248/CU_ES_PMH_SC_Pest_Management_Handbook_2017.pdf?sequence=1&isAllowed=y. Accessed on December 31, 2019.

Ashourloo, D., Aghighi, H., Matkan, A. A., Mobasheri, M. R., and Rad, A. M. 2016. An investigation into machine learning regression techniques for the leaf rust disease detection using hyperspectral measurement. *IEEE Journal of Selected Topics in Applied Earth Observations and Remote Sensing*, *9*(9), 4344-4351.

Ashourloo, D., Mobasheri, M. and Huete, A. 2014. Evaluating the effect of different wheat rust disease symptoms on vegetation indices using hyperspectral measurements. *Remote Sensing*, *6*(6), 5107-5123.

Augusto, J. and Brenneman, T. B. 2012. Assessing systemicity of peanut fungicides through bioassay of plant tissues with *Sclerotium rolfsii*. *Plant disease*, *96*(3), 330-337.

Augusto, J., Brenneman, T. B., Culbreath, A. K. and Sumner, P. 2010a. Night spraying peanut fungicides I. Extended fungicide residual and integrated disease management. *Plant disease*, *94*(6), 676-682.

Augusto, J., Brenneman, T. B., Culbreath, A. K. and Sumner, P. 2010b. Night spraying peanut fungicides II. Application timings and spray deposition in the lower canopy. *Plant disease*, *94*(6), 683-689.

Aycock, R. 1966. Stem rot and other diseases caused by *Sclerotium rolfsii*. *N. C. Agric. Exp. Stn. Tech. Bull*. 174.

Ayoola, P. B., Adeyeye, A., and Onawumi, O. O. 2012. Chemical evaluation of food value of groundnut (*Arachi hypogaea*) seeds. *American Journal of Food and Nutrition*, *2*(3), 55–57.

Backman, P.A., and T.B. Brenneman. 1997. Stem rot, pp. 36-37. In Compendium of Peanut Diseases, 2nd ed. N.Kokalis-Burelle, D.M. Porter, R Hodrfguez-Kabana, D.H. Smith and P. Subrahmanyam eds. American Phytopathological Society Press, St. Paul, MN.

Baranowski, P., Jedryczka, M., Mazurek, W., Babula-Skowronska, D., Siedliska, A., and Kaczmarek, J. 2015. Hyperspectral and thermal imaging of oilseed rape (*Brassica napus*) response to fungal species of the genus *Alternaria*. *PloS one*, *10*(3), e0122913.

Bateman, D. F. 1969. Some characteristics of the cellulase system produced by *Sclerotium rolfsii* Sacc. *Phytopathology*, *59*(1), 37-42.

Bateman, D. F. 1972. The polygalacturonase complex produced by *Sclerotium rolfsii*. *Physiological Plant Pathology*, *2*(2), 175-184.

Bateman, D. F., and Beer, S. V. 1965. Simultaneous production and synergistic action of oxalic acid and polygalacturonase during pathogenesis by *Sclerotium rolfsii*. *Phytopathology*, *55*(11), 204-11.

Bauriegel, E., Giebel, A., Geyer, M., Schmidt, U., Herppich, W.B., 2011. Early detection of Fusarium infection in wheat using hyper-spectral imaging. *Computers and Electronics in Agriculture* 75, 304-312.

Brenneman, T. B., Branch, W. D., and Csinos, A. S. 1990. Partial resistance of Southern Runner, *Arachis hypogaea*, to stem rot caused by *Sclerotium rolfsii*. *Peanut Science*, *17*(2), 65-67.

Calderón, R., Navas-Cortés, J., and Zarco-Tejada, P. 2015. Early detection and quantification of Verticillium wilt in olive using hyperspectral and thermal imagery over large areas. *Remote Sensing*, *7*(5), 5584-5610.

Calderón, R., Navas-Cortés, J.A., Lucena, C., Zarco-Tejada, P.J., 2013. High-resolution airborne hyperspectral and thermal imagery for early detection of Verticillium wilt of olive using fluorescence, temperature and narrow-band spectral indices. *Remote Sensing of Environment 139*, 231-245.

Carter, G. A. and Knapp, A. K. 2001. Leaf optical properties in higher plants: linking spectral characteristics to stress and chlorophyll concentration. *American journal of botany*, *88*(4), 677-684.

Chaerle, L. and Van Der Straeten, D., 2000. Imaging techniques and the early detection of plant stress. *Trends in Plant Science 5*, 495-501.

Chaerle, L., Caeneghem, W.V., Messens, E., Lambers, H., Van Montagu, M., Van Der Straeten, D., 1999. Presymptomatic visualization of plant–virus interactions by thermography. *Nature Biotechnology 17*, 813-816.

Chaerle, L., Hagenbeek, D., De Bruyne, E., Valcke, R., Van Der Straeten, D., 2004. Thermal and chlorophyll-fluorescence imaging distinguish plant-pathogen interactions at an early stage. *Plant and Cell Physiology 45*, 887-896.

Charness, G., Gneezy, U., and Kuhn, M. A. 2012. Experimental methods: Between-subject and within-subject design. *Journal of Economic Behavior & Organization*, *81*(1), 1-8.

Davis, J.P., K.M. Price, L.L. Dean, D.S. Sweigart, J.M. Cottonaro, and T.H. Sanders., 2016. Peanut Oil Stability and Physical Properties Across a Range of Industrially Relevant Oleic Acid/Linoleic Acid Ratios. *Peanut Science*: *43*(1), 1-11.

Dean, L. L., Hendrix, K. W., Holbrook, C. C., and Sanders, T. H. 2009. Content of some nutrients in the core of the core of the peanut germplasm collection. *Peanut Science*, *36*(2), 104-120.

Fungicide Resistance Action Committee (FRAC). 2019. FRAC Code List© 2019. Available at, https://www.frac.info/docs/default-source/publications/frac-code-list/frac-code-list-2019.pdf?sfvrsn=98ff4b9a_2. Accessed on December 31, 2019.

Gold, K.M., Townsend, P.A., Herrmann, I., Gevens, A.J., 2019. Investigating potato late blight physiological differences across potato cultivars with spectroscopy and machine learning. *Plant Science*, 110316.

Gorbet, D. W., Kucharek, T. A., Shokes, F. M., and Brenneman, T. B. 2004. Field evaluations of peanut germplasm for resistance to stem rot caused by *Sclerotium rolfsii. Peanut Science*, *31*(2), 91-95.

Hagan, A. K., Bowen, K. L., Campbell, H. L. and Wells, L. 2007. Calendar-based and AU-Pnuts advisory programs with pyraclostrobin and chlorothalonil for the control of early leaf spot and stem rot on peanut. *Peanut science*, *34*(2), 114-121.

Heim, R. H. J., Wright, I. J., Chang, H. C., Carnegie, A. J., Pegg, G. S., Lancaster, E. K., Falster, D.S., and Oldeland, J. 2018. Detecting myrtle rust (*Austropuccinia psidii*) on lemon myrtle trees using spectral signatures and machine learning. *Plant pathology*, *67*, 1114-1121.

Heim, R., Wright, I., Allen, A., Geedicke, I., Oldeland, J., 2019. Developing a spectral disease index for myrtle rust (*Austropuccinia psidii*). *Plant Pathology, 68,* 738-745.

Higgins, B. B. 1927. Physiology and parasitism of *Sclerotium rolfsii* Sacc. *Phytopathology*, *17*, 417-448.

Hillnhütter, C., Mahlein, A. K., Sikora, R. A., and Oerke, E. C. 2011. Remote sensing to detect plant stress induced by *Heterodera schachtii* and *Rhizoctonia solani* in sugar beet fields. *Field Crops Research*, *122*(1), 70-77.

Husain, A. 1958. Production of cellulolytic enzymes by *Sclerotium rolfsii*. *Phytopathology*, *48*(6), 338-340.

Jacquemoud, S. and Ustin, S. L. 2001. Leaf optical properties: A state of the art. Pages 223-332. In: *Proceedings of the 8th International Symposium of Physical Measurements & Signatures in Remote Sensing*., 8-12 January 2001, CNES, Aussois, France.

Jones, H. G., Stoll, M., Santos, T., Sousa, C. D., Chaves, M. M., and Grant, O. M. 2002. Use of infrared thermography for monitoring stomatal closure in the field: application to grapevine. *Journal of Experimental Botany*, *53*(378), 2249-2260.

Jones, H.G., 1999. Use of thermography for quantitative studies of spatial and temporal variation of stomatal conductance over leaf surfaces. *Plant, Cell & Environment 22,* 1043-1055.

Kemerait, Jr., R.C. 2012. Peanut. In 2008 Geogia Plant Disease Loss Estimates Compiled by D.B. Langston, Jr. The Univerisity of Geogina Cooperative Extension, College of Agricltual and Environmental Sciences and College of Family and Consumer Sciences. *Ap-102-1*. 8p.

Liakos, K. G., Busato, P., Moshou, D., Pearson, S., and Bochtis, D. 2018. Machine learning in agriculture: A review. *Sensors*, *18*(8), 2674.

Mahlein, A. K., Steiner, U., Dehne, H. W., and Oerke, E. C. .2010. Spectral signatures of sugar beet leaves for the detection and differentiation of diseases. *Precision Agriculture*, *11*(4), 413-431.

Mahlein, A.-K., 2016. Plant Disease Detection by Imaging Sensors – Parallels and Specific Demands for Precision Agriculture and Plant Phenotyping. *Plant Disease 100*, 241-251.

Mahlein, A.K., Rumpf, T., Welke, P., Dehne, H.W., Plümer, L., Steiner, U., Oerke, E.C., 2013. Development of spectral indices for detecting and identifying plant diseases. *Remote Sensing of Environment 128*, 21-30.

McGrath, M.T. 2004. What are Fungicides. *The Plant Health Instructor*. DOI: 10.1094/PHI-I-2004-0825-01. Updated 2016.

Mehl, H. L. 2019. Peanut Diseases. In 2019 Virginia Peanut Production Guide. Viginia Cooperative Extension. SPES-67NP. Page 91 -104. Available at, https://www.sites.ext.vt.edu/newsletter-archive/peanut-production/2019. Accessed on December 31, 2019.

Miorini, T. J., Raetano, C. G., and Everhart, S. E. 2017. Control of white mold of dry bean and residual activity of fungicides applied by chemigation. *Crop protection*, *94*, 192-202.

Mitchell, T. 1997. Machine Learning. New York: McGraw Hill. ISBN 0-07-042807-7. OCLC 36417892.

Moran, M. S., Inoue, Y., and Barnes, E. M. 1997. Opportunities and limitations for image-based remote sensing in precision crop management. *Remote sensing of Environment*, *61*(3), 319-346.

Mueller, D. S., Wise, K. A., Dufault, N. S., Bradley, C. A., and Chilvers, M. A.,eds. 2013. Fungicides for Field Crops. American Phytopathological Society,St. Paul, MN.

Mullen, J. 2001. Southern blight, Southern stem blight, White mold. *The Plant Health Instructor*. DOI: 10.1094/PHI-I-2001-0104-01. *Updated 2006.*

National Peanut Board (NPB). 2019. Peanut country, U.S.A. Avaiable at, https://www.nationalpeanutboard.org/peanut-info/peanut-country-usa.htm. Accessed on December 15, 2019.

Nilsson, H., 1995. Remote Sensing and Image Analysis in Plant Pathology. *Annual Review of Phytopathology 33*, 489-528.

Nilsson, H.E., 1991. Hand-held radiometry and IR-thermography of plant diseases in field plot experiments. *International Journal of Remote Sensing 12*, 545-557.

Oerke, E. C., Steiner, U., Dehne, H. W., and Lindenthal, M. 2006. Thermal imaging of cucumber leaves affected by downy mildew and environmental conditions. *Journal of experimental botany*, *57*(9), 2121-2132.

Omran, E.-S.E., 2017. Early sensing of peanut leaf spot using spectroscopy and thermal imaging. *Archives of Agronomy and Soil Science* 63, 883-896.

Patrick, A., Pelham, S., Culbreath, A., Holbrook, C. C., De Godoy, I. J., and Li, C. 2017. High throughput phenotyping of tomato spot wilt disease in peanuts using unmanned aerial systems and multispectral imaging. *IEEE Instrumentation & Measurement Magazine*, *20*(3), 4-12.

Pérez-Bueno, M. L., Pineda, M., Vida, C., Fernández-Ortuño, D., Torés, J. A., de Vicente, A.,Cazorla, F.M., and Barón, M. 2019. Detection of White Root Rot in Avocado Trees by Remote Sensing. *Plant disease*, PDIS-10.

Pinter, P.J., Stanghellini, M.E., Reginato, R.J., Idso, S.B., Jenkins, A.D., Jackson, R.D., 1979. Remote Detection of Biological Stresses in Plants with Infrared Thermometry. *Science 205*, 585-587.

Punja, Z. K., Huang, J. S., and Jenkins, S. F. 1985. Relationship of mycelial growth and production of oxalic acid and cell wall degrading enzymes to virulence in *Sclerotium rolfsii*. *Canadian Journal of plant pathology*, *7*(2), 109-117.

Punja, Z.K., 1985. The Biology, Ecology, and Control of *Sclerotium Rolfsii*. *Annual Review of Phytopathology* 23, 97-127.

Rambach, O., Bartlett, D., Bieri, S., Haas, H. U., Scalliet, G., Stalker, A. and Dale, S. 2015. Benzovindiflupyr, a new SDHI fungicide to control foliar diseases. In *11e Conférence Internationale sur les Maladies des Plantes, Tours, France, 7 au 9 décembre 2015* (pp. 473-482). Association Française de Protection des Plantes (AFPP).

Rideout, S.L., Brenneman, T.B., Culbreath, A.K., Langston, D.B., 2008. Evaluation of Weather-Based Spray Advisories for Improved Control of Peanut Stem Rot. *Plant Disease 92*, 392-400.

Ridge, G. and Shew. B. 2014. *Sclerotium rolfsii* (Southern blight of vegetables and melons). Available online at, https://wiki.bugwood.org/Sclerotium_rolfsii_(Southern_blight_of_vegetables_and_melons). Accessed on December 6, 2019.

Rumpf, T., Mahlein, A. K., Steiner, U., Oerke, E. C., Dehne, H. W., and Plümer, L. 2010. Early detection and classification of plant diseases with support vector machines based on hyperspectral reflectance. *Computers and electronics in agriculture*, *74*(1), 91-99.

Samuel, A. L. 1959. Some studies in machine learning using the game of checkers, *IBM Journal of Research and Development*, **3**(3), 210–229.

Sankaran, S., Mishra, A., Maja, J. M., and Ehsani, R. 2011. Visible-near infrared spectroscopy for detection of Huanglongbing in citrus orchards. *Computers and electronics in agriculture*, *77*(2), 127-134.

Sawe, B.E. 2017. Top Peanut (Groundnut) Producing Countries. Available at, https://www.worldatlas.com/articles/top-peanut-groundnut-producing-countries.html. Accessed on March 6, 2018.

Shokes, F.M., Różalski, K., Gorbet, D.W., Brenneman, T.B., Berger, D.A., 1996. Techniques for Inoculation of Peanut with *Sclerotium rolfsii* in the Greenhouse and Field. *Peanut Scien*ce 23:124-128.

Singh, A., Ganapathysubramanian, B., Singh, A. K., and Sarkar, S. 2016. Machine learning for high-throughput stress phenotyping in plants. *Trends in plant science*, *21*(2), 110-124.

SphereOptics. 2017. Remote Sensing & Proximal Sensing. Avaiable at, https://sphereoptics.de/en/application/remote-sensing-proximal-sensing/. Accessed on December 15, 2019.

Stalker, H.T., 1997. Peanut (*Arachis hypogaea* L.). *Field Crops Research* 53, 205-217.

Thenkabail, P. S., Smith, R. B. and De Pauw, E. 2000. Hyperspectral vegetation indices and their relationships with agricultural crop characteristics. *Remote sensing of Environment*, *71*(2), 158-182.

United States Department of Agriculture (USDA) – Foreign Agricultural Service. 2019. World Agricultural Production. Page 26. Available at,

https://apps.fas.usda.gov/psdonline/circulars/production.pdf. Accessed on December 15, 2019.

United States Department of Agriculture, National Agricultural Statistics Service (USDA-NASS). 2019. Acreage. ISSN: 1949-1522. The NASS, Agricultural Statistics Board, USDA, Washington DC. 16p.

Venkatachalam, M., Sathe, S.K., 2006. Chemical Composition of Selected Edible Nut Seeds. *Journal of Agricultural and Food Chemistry 54*, 4705-4714.

Wang, M., Ling, N., Dong, X., Zhu, Y., Shen, Q., Guo, S., 2012. Thermographic visualization of leaf response in cucumber plants infected with the soil-borne pathogen *Fusarium oxysporum* f. sp. *cucumerinum*. *Plant Physiology and Biochemistry 61*, 153-161.

Woodward, J. E. 2006. Optimizing efficacy and economic benefits of fungicides for peanut disease control via pre-plant analysis of disease risk and irrigation timing. Ph.D. dissertation, University of Georgia, Athens.

Xavier, T. W., Souto, R. N., Statella, T., Galbieri, R., Santos, E. S., S Suli, G., and Zeilhofer, P. 2019. Identification of Ramularia Leaf Blight Cotton Disease Infection Levels by Multispectral, Multiscale UAV Imagery. *Drones*, *3*(2), 33.

Xie, C., Huang, C. H., and Vallad, G. E. 2014. Mycelial compatibility and pathogenic diversity among *Sclerotium rolfsii* isolates in the southern United States. *Plant disease*, *98*(12), 1685-1694.

Table 1. Examples of machine learning (ML) algorithms in plant disease detection and classification

Disease	**Crop**	**ML Algorithms***	**Sensor**	**Reference**
Cercospora leaf spot Sugar beet rust Powdery mildew	Sugar beet	SVM, RELIEF	Non-imaging spectroradiometer	Rumpf et al. 2010, Mahlein et al. 2013
Beet cyst nematode and Rhizoctonia root and crown rot	Sugar beet	SAM	Hyperspectral images	Hillnhutter et al. 2011
Fusarium head blight	Wheat	SAM	Hyperspectral images	Bauriegel et al. 2011
Huanglongbing	Citrus	KNN, QDA, LDA, SIMCA	Non-imaging spectroradiometer	Sankaran et al. 2011
Verticillium wilt	Olive	LDA, SVM	Hyperspectral and thermal images	Calderon et al. 2015
Leaf rust	Wheat	PLSR, SVR, GPR	Non-imaging spectroradiometer	Ashourloo et al. 2016
Myrtle rust	Lemon myrtle	RF	Non-imaging spectroradiometer	Heim et al. 2019
Late blight	Potato	RF, PLS-DA	Non-imaging spectroradiometer	Gold et al. 2019

*Abbreviations: SVM, support vector machine; SAM, spectral angle mapper; KNN, *k*-nearest neighbor; QDA, quadratic discriminant analysis; LDA, linear discriminant analysis; SIMCA, soft independent modeling of classification analogies; PLSR, partial least square regression; SVR, support vector regression; GPR, Gaussian process regression; RF, random forests; PLS-DA, partial least square discrimination analysis.

Table 2. Overview of disease-related spectral indices in previous studies

Disease	**Crop**	**Index***	**Equation**	**Reference**
Myrtle rust	Lemon myrtle	LMMR	$\left(\frac{R545}{R555}\right)^{\frac{5}{3}} * \frac{R1050}{R2195}$	Heim et al. 2019
Cercospora leaf spot	Sugar beet	CLSI	$\frac{R698 - R570}{R698 + R570} - R734$	Mahlein et al. 2013
Sugar beet rust	Sugar beet	SBRI	$\frac{R570 - R513}{R570 + R513} + \frac{1}{2} * R734$	Mahlein et al. 2013
Powdery mildew	Sugar beet	PMI	$\frac{R520 - R584}{R520 + R584} + R724$	Mahlein et al. 2013
Early leaf spot	Peanut	ELSI	$b1 * \frac{R600}{R437} - b2$, where b1 and b2 are the regression coefficient	Omran 2017
Late leaf spot	Peanut	LLSI	$b1 * \frac{R701}{R569} - b2$, where b1 and b2 are the regression coefficient	Omran 2017
Tomato spot wilt	Peanut	NDRE	$\frac{R717 - R840}{R717 + R840}$	Patrick et al. 2017
Fusarium head blight	Wheat	HBI	665-675 nm and 550-560 nm	Bauriegel et al. 2011

*Abbreviations: LMMR, lemon myrtle-myrtle rust index; CLSI, *Cercospora* leaf spot index; SBRI, sugar beet rust index; PMI, powdery mildew index; ELSI, early leaf spot index; LLSI, late leaf spot index; NDRE, normalized difference red-edge; HBI, head blight index.

Table 3. Overview of plant disease effects on leaf or canopy temperature by infrared thermography (IRT) in previous studies

Disease (pathogen)	**Crop**	**Scale (leaf, plant, or canopy)**	**Response***	**Reference**
Pythium root rot (*Pythium aphanidermatum*)	Sugar beet	Leaf (field study)	3℃ to 5℃ (+)	Pinter et al. 1979
Cotton root rot (*Phymatotrichum omnivorum*)	Cotton	Leaf (field study)	3℃ to 5℃ (+)	Pinter et al. 1979
White root rot (*Rosellinia necatrix*)	Avocado	Canopy	(Tc – Ta)** (+)	Perez-Bueno et al. 2019
Tobacco mosaic (Tobacco mosaic virus)	Tobacco	Leaf (plant-pathogen interaction)	0.3℃ to 0.4℃ (+)	Chaerle et al. 1999
Early and late leaf spot (*Cercospora arachidicola* and *Cercosporidium personatum*)	Peanut	Leaf and plant (field study)	Pre-symptomatic:1.3℃ (-) Diseased: 2.2℃ (+)	Omran 2017
Verticillium wilt (*Verticillium dahliae* Kleb)	Olive	Tree-crown level	(Tc – Ta) (+)	Calderon et al. 2013
Fusarium wilt *(Fusarium oxysporum* f. sp. *cucumerinum*)	Cucumber	Leaf (greenhouse study)	Light (+) Dark (-)	Wang et al. 2012

Note: * '+' = an increase in temperature, '-' = a decrease in temperature; **Tc = canopy temperature, Ta = air temperature.

CHAPTER 2: Spectral and thermal responses of peanut to infection and colonization with *Athelia rolfsii*

Xing Wei,[1,2] David B. Langston, Jr.,[1,2] and Hillary L. Mehl[1,2,3]

[1]Tidewater Agricultural Research and Extension Center, Virginia Tech, Suffolk, VA 23437, U.S.A.; [2]School of Plant and Environmental Sciences, Virginia Tech, Blacksburg, VA 24061, U.S.A.; [3]Current address: United States Department of Agriculture, Agricultural Research Service, Arid-Land Agricultural Research Center, Tucson, AZ 85701, U.S.A.

Author Contributions: Conceptualization, X.W., D.B.L., and H.L.M; methodology, X.W., D.B.L. and H.L.M.; formal analysis, X.W.; investigation, X.W.; resources, D.B.L., and H.L.M.; writing—original draft preparation, X.W.; writing—review and editing, X.W., D.B.L., and H.L.M.; supervision, D.B.L. and H.L.M.; funding acquisition, D.B.L. and H.L.M. All authors have reviewed the manuscript prior to publication.

Note: The first look version of this manuscript was published by the journal PhytoFrontiers™ on 22 Feb 2021.

Citation: Wei, X., Langston Jr., D. B., and Mehl, H. L. 2021. Spectral and thermal responses of peanut to the infection and colonization with *Athelia rolfsii*. PhytoFrontiers. doi: https://doi.org/10.1094/PHYTOFR-07-20-0008-R

Keywords: Southern stem rot, *Sclerotium rolfsii*, *Arachis hypogaea*, soilborne disease detection, spectral reflectance, thermal imaging

Funding: This work was funded by the Virginia Peanut Board and Virginia Agricultural Council.

Abstract

Soilborne fungal diseases, including southern stem rot (SSR, causal *agent Athelia rolfsii*), are major constraints to peanut production worldwide. Scouting for disease via visual observation is time and labor-intensive, but sensor technologies are a promising tool for plant disease detection. Prior research has focused on foliar diseases, and few studies have applied sensor-based tools for early detection of soilborne diseases. This study characterized the temporal progress of spectral and thermal responses of peanut plants during infection and colonization with *A. rolfsii* under controlled environment. In greenhouse experiments, *A. rolfsii*-inoculated and mock-inoculated lateral stems of peanut were inspected daily for symptoms, and leaf spectral reflectance and temperature were measured using a handheld spectrometer and thermal camera, respectively. Following onset of visual disease symptoms, leaflets on inoculated stems had greater spectral reflectance in the visible region compared to those on mock-inoculated stems. Leaflets on the inoculated stems also had greater normalized leaf temperatures as compared to leaflets on mock-inoculated stems. Overall, results indicate that signatures of disease development can be detected during peanut infection and colonization with *A. rolfsii* using spectral reflectance and thermal imaging technologies, and spectral signatures of disease are more consistent and specific compared to thermal ones. Though only one peanut variety, one pathogen isolate, and one single measurement were assessed per evaluation date, temporal progress of spectral and thermal

responses on a daily basis characterized in this study can be used to develop sensor-based methods to detect southern stem rot and other soilborne diseases ultimately in the field.

Introduction

Athelia rolfsii (Curzi) C.C. Tu & Kimbr., well-recognized by its anamorph synonym *Sclerotium rolfsii* Sacc., is an economically important soilborne fungal pathogen that can cause disease on more than 500 plant species, including field, vegetable, and ornamental crops (Aycock 1966; Mullen 2001). The disease caused by *A. rolfsii* on peanut (*Arachis hypogaea* L.) is known as southern stem rot (SSR). SSR has long been one of the most important diseases of cultivated peanut worldwide. In the southeastern U.S., peanut yield loss due to SSR is typically less than 25%, but can be up to 80% when weather conditions are favorable for disease development, which include hot temperatures (~30 °C) and relative humidity > 90% (Backman and Brenneman 1997; Punja 1985). Peanut infection with *A. rolfsii* usually occurs during the mid to late growing season when the plant canopy covers the soil between rows and produces a warm, humid environment conducive to pathogen infection and growth (Aycock 1966; Shokes et al. 1996).

Despite considerable research efforts to develop management strategies for SSR of peanut, control of this disease remains a challenge. Only a few peanut cultivars show partial resistance to SSR (Brenneman et al. 1990; Gorbet et al. 2004). Deep tillage and crop rotation can both reduce losses to SSR, but often multiple applications of fungicides during the growing season are needed to provide adequate control (Backman and Brenneman 1997; Hagan et al. 2004; Rideout et al. 2008). Many fungicides are labeled for SSR control in peanut including demethylation inhibitors (DMI) (e.g., tebuconazole, prothioconazole, metconazole), quinone outside inhibitors (QoI) (e.g., azoxystrobin, fluoxastrobin, pyraclostrobin), and succinate dehydrogenase inhibitors (SDHI) (e.g.,

penthiopyrad, benzovindiflupyr, flutolanil). These fungicides can be applied on a calendar schedule or once disease symptoms and signs are observed. However, calendar-based sprays are often confounded by year-to-year differences in host and environmental factors that impact disease onset, and fungicides are most effective when applied prior to crop infection with a fungal pathogen. Even when calendar-based sprays are used, growers always face a question of when to apply an SSR fungicide versus a leaf spot only fungicide. Scouting can be implemented to select proper fungicide chemistries (based on which diseases are present) and to make timely fungicide applications. However, the erratic distribution of SSR in the field make it labor- and time-intensive for crop scouts to detect the disease in large commercial fields. A more effective and precise disease detection method for SSR is needed to select proper disease management strategies and improve fungicide efficacy through better application timing. Such a method will increase the probability of successful, cost-effective disease management that will protect peanut crop yields and maximize grower profits.

Previous studies have demonstrated potential applications of remote sensing technologies for the detection of plant physiological changes due to abiotic and biotic stresses, including plant diseases (Bauriegel et al. 2011; Chaerle and Straeten 2000; Mahlein 2016; Mahlein et al. 2018; Moran et al. 1997; Nilsson 1991, 1995). Among various types of sensors used in remote sensing, spectral reflectance sensors and infrared thermography (IRT) are most frequently used to detect plant pathogens and plant diseases (Chaerle et al. 1999; Gold et al. 2019; Heim et al. 2018; Mahlein et al. 2010, 2013; Wang et al. 2012). Spectral reflectance sensors can be used to measure light reflected directly from leaf surfaces or internal leaf structures. The amount of light reflected from leaves is mainly affected by leaf pigment content in the visible region (400 to 700 nm), cell structure in the near-infrared region (700 to 1,100 nm), and leaf biochemical and water content in

the shortwave infrared region (1,100 to 2,500 nm) (Carter and Knapp 2001; Jacquemoud and Ustin 2001; Mahlein 2016). Thus, the changes in reflectance caused by plant pathogens can be characterized by deteriorations in leaf pigment content, cell structure, and leaf biochemical and water content during plant disease development (Mahlein 2016).

The IRT of measured objects can be acquired with thermographic cameras by detecting the emitted infrared radiation from the objects in the range of 8 to 14 μm (Chaerle and Straeten 2000). IRT can be used to visualize surface temperature differences of leaves, plants, or canopies, which are correlated with, in part, changes in transpiration due to plant pathogen infection (Jones 1999; Jones et al. 2002; Mahlein 2016; Oerke et al. 2006). Colonization and infection of foliar pathogens can cause localized changes in plant transpiration rates, while plant pathogens primarily impacting stems and roots often have an effect on the transpiration rate and water flow of whole plants or plant tissues (Mahlein 2016).

Though increasing research efforts are made in using spectral reflectance measurements and thermal imaging for plant disease detection, most previous studies have focused on detection of foliar plant diseases of various crops and trees (Baranowski et al. 2015; Heim et al. 2018; Mahlein et al. 2010; Patrick et al. 2017; Xavier et al. 2019). Only a few reported the utilization of these technologies for early detection of soilborne diseases (Hillnhütter et al. 2011; Pérez-Bueno et al. 2019; Raza et al. 2020; Wang et al. 2012). Foliar diseases can be readily detected with the naked eye or with optical sensors since they directly alter above-ground plant parts as lesions develop on leaves. However, it is difficult to identify specific foliar signatures of diseases that occur on stems or roots because a variety of other abiotic and biotic stresses may cause general changes in the optical or thermal properties of above-ground plant parts.

To our knowledge, there are no previous reports of using sensor-based methods for the detection of SSR symptoms in peanut. Therefore, the present study was designed to characterize the temporal progress of spectral and thermal responses of peanut plants during infection and colonization with *A. rolfsii*. We hypothesized that 1) peanut plants colonized by *A. rolfsii* will have different leaf spectral reflectance and leaf temperature as compared to disease-free plants, and 2) spectral reflectance and leaf temperature of *A. rolfsii*-infected plants will change over time as disease progresses.

Materials and Methods

Greenhouse studies. Four independent experiments were conducted in a greenhouse at the Virginia Tech Tidewater Agricultural Research and Extension Center (AREC) in Suffolk, VA. In each experiment, three seeds of peanut cultivar 'Sullivan' treated with *Rhizobium leguminosarum* biovar *phaseoli* (N-DURE™, INTX Microbials, LLC, Kentland, IN) were planted in a plastic pot (26.4 cm in diameter by 22.5 cm in height) (Model: 1200 Series, Greenhouse Megastore) containing a 3:1 mixture of pasteurized field soil and potting mix. Three to four weeks after planting, one vigorous plant per pot was selected for further experiments, while the two extra plants were uprooted. Imidacloprid (Admire Pro, Bayer Crop Science, Research Triangle Park, NC) was applied preventatively for thrips control at the peanut seedling stage. The temperature inside the greenhouse was set at 24.4 ℃ (day) and 21.1 ℃ (night) using a greenhouse controller (Model: GHK12X2, BARTLETT Instrument company, Fort Madison, IA). Drip irrigation was applied daily 3-minutes per day using a 12 station Sterling Controller (Sterling-12, Superior Control Inc., Torrance, CA).

The experimental unit was one lateral stem of a peanut plant. The experiment was arranged in a completely randomized design with two treatments (lateral stem mock-inoculated and inoculated with *A. rolfsii* as described below) and six replicates per treatment. After inoculation, plants were evaluated daily for 14 to 16 days. The experiment was repeated four times with peanut planting dates of 19 October and 21 December in 2018, and 8 January and 22 February in 2019.

Pathogen and inoculation. An isolate of *A. rolfsii* collected from a peanut field at the Tidewater AREC research farm in 2017 was used in the current study. The inoculation method was adapted from a clothespin technique described by Shokes et al. (1996). To prepare inoculum, clothespins were boiled in distilled water for 30 minutes twice (water was changed in-between times) to remove tannins then placed in 500-ml flasks filled with 100-ml full-strength potato dextrose broth (PDB) (Becton, Dickinson and Company, Sparks, MD) and autoclaved for 20 minutes. After cooling, PDB was removed from the flasks and clothespins were either kept as they were for mock-inoculation treatment, or inoculated with a 3-day old actively growing culture of *A. rolfsii* on potato dextrose agar (~ 20 of 5-mm diameter agar pieces per flask) (Becton, Dickinson and Company, Sparks, MD). Then, the clothespins were incubated at room temperature (21.1 to 23.3 ℃) until clothespins were colonized with mycelium of *A. rolfsii* (approximately 5 days after inoculation). To inoculate plants, clothespins colonized with *A. rolfsii* were clamped on lateral stems of peanut plants. Non-colonized clothespins were clamped on mock-inoculated control stems. In the first experiment, one lateral stem of each individual plant was either inoculated or mock-inoculated, whereas in the three remaining experiments, treatments were applied to two symmetrical lateral stems of the same plant.

Inoculation treatments were made approximately 70 days after planting, and plants were placed inside a moisture chamber to facilitate pathogen infection and disease development. A

moisture chamber was setup by covering a bench with a clear polyethylene film inside the greenhouse. Two cool mist humidifiers (Model: Vicks® 1.2-gal, Kaz USA, Inc., Marlborough, MA) were placed inside the moisture chamber with maximum setting to provide ≥ 90% relative humidity. Two WatchDog sensors (Model: 1,000 series, Spectrum Technologies, Inc., Aurora, IL) were mounted in the greenhouse with one inside and one outside the moisture chamber to record the temperature and relative humidity every 15 minutes.

Disease assessment. Starting at 2 days after inoculation (DAI), plants were inspected daily for visual disease symptoms and sensor responses. For daily measurement, plants were moved out of the moisture chamber in the morning (~ 10 AM) and placed on another bench inside the greenhouse to allow the foliage to air-dry. Plants were moved back into the moisture chamber after all the measurements were completed. With the exception of when daily measurements were taken, plants were incubated inside the moisture chamber for the entire duration of the experiment (14 to 16 days) for the first three experiments. For the fourth experiment, plants were moved permanently outside the moisture chamber 7 DAI because plants were undergoing heat stress due to the high temperature inside the moisture chamber (Fig. S1).

Disease severity was evaluated using a scale adapted from Shokes et al. (1996) where 1 = healthy; 2 = necrotic lesions on the inoculated lateral stem but no foliar symptoms; 3 = necrotic lesions plus 25 to 50% of leaves symptomatic (wilting, leaf curling and discoloration); 4 = necrotic lesions plus >50% of leaves symptomatic (wilting, leaf curling and discoloration); and 5 = necrotic lesions plus withering of all the leaves and stem. Disease progress for each experiment was plotted by averaging disease ratings on each evaluation date (6 replicates per treatment per experiment).

Spectral reflectance measurement. The second youngest mature leaf on each lateral stem was labeled with a twist tie prior to inoculation. Spectral reflectance (200 nm to 1,100 nm with an

optical resolution of ~ 0.4 nm) of the same designated leaflet on the labeled leaf was collected daily (once per day) in the afternoon using a handheld spectrometer system. The handheld spectrometer system included a Jaz spectrometer (Model: JAZ-COMBO, Ocean Optics, Dunedin, FL) and an attached SpectroClip probe (Model: SpectroClip-R, Ocean Optics, Dunedin, FL) that had an active illuminated area with a 5 mm diameter. The spectrometer was set to 'Boxcar Width' of 5 (the number of adjacent pixels to be averaged together), and 'Scans to Average' of 10 (the number of discrete spectra to be summed together) to reduce machinery noises in data collected. A Pulsed Xenon light source (spectral range of 190 to 1,100 nm) embedded in the spectrometer was used during the measurement. The WS-1 diffuse reflectance standard from Ocean Optics was used as a white reference. The reflectivity of WS-1 was >98% from 250 to 1,500 nm.

The spectral reflectance curves of each leaflets on each evaluation date were plotted and inspected visually for abnormal spectra removal. A spectral index for southern stem rot of peanut (SSRI) was calculated with the reflectance at 550 nm and 790 nm, using the equation $SSRI = \frac{(R790-R550)}{(R790+R550)}$. Reflectance at 550 nm was selected because the greatest visual differences between spectra of *A. rolfsii*-infected and non-infected peanut plants were observed at this wavelength (Fig. S2). Reflectance at 790 nm was selected for the normalization of the index to 0 to 1 scale. The equation of SSRI was adapted from the normalized difference vegetation index (NDVI), where NDVI $= \frac{(ir-red)}{(ir+red)}$, ir radiance (750 – 800 nm) and red radiance (630 – 690 nm) (Rouse et al. 1974).

Thermal imaging system. Digital and thermal images of each plant were taken daily (once per day) in the afternoons immediately prior to spectral reflectance measurements with a FLIR T420 camera (FLIR Systems, Wilsonville, OR). The FLIR camera used in this study had one thermal lens and one built-in digital lens. The thermal lens had a spectral range of 7.5 to 13.0 µm, a field of view of 25° x 19°, and a focal plane array (FPA) uncooled microbolometer in a format

of 320 x 240 pixels. The built-in digital lens had a field of view of 53° x 41°. The FLIR camera was mounted about 130 cm above the plant (~ 183 cm above the ground) with conduit clamps onto the ceiling structures of the greenhouse. Plants were placed on a wood board covered with a white needled cotton batting (The Warm Company, Lynnwood, WA) to provide a uniform thermal background. The soil surface inside each pot was also covered with the cotton batting prior to image acquisition.

The thermal images of each lateral stem and whole plant were first inspected visually. Mean normalized leaf temperature was calculated by subtracting air temperature [Ta] from leaf temperature [Tc]. Leaf temperature for each plant was calculated by averaging temperatures from three regions of interest (ROI) on each thermal image. The ROIs were selected from three different leaflets on the upper to the middle of treated lateral stems (approximately 2^{nd} to 5^{th} youngest mature leaves) using a polygon selection tool in FLIR ResearchIR Max4 software (FLIR Systems, Wilsonville, OR). Each ROI contained 3x3 pixels.

Data analysis. Six replications per treatment per experiment across 14 to 16 evaluation dates, including a total of 656 spectrum files and 522 thermal images, were used in the final analysis. The repeated measures on SSRI and normalized leaf temperature (Tc – Ta) over time were analyzed by invoking the REPEATED statement in the MIXED procedure (PROC MIXED) in SAS (version 9.4; SAS Institute, Inc., Cary, NC). Inoculation treatment (between-subject factor), days after inoculation (DAI; within-subject factor), and treatment × DAI interaction were included in the MODEL statement as fixed effects. Five common covariance structures, including compound symmetry (CS), Huynh-Feldt (HF), Unstructured (UN), Autoregressive (AR(1)), and Toeplitz (TOEP) were tested during the selection of covariance structure for mixed model analysis (Wolfinger 1993; Wolfinger and Chang 1995). The Huynh-Feldt (HF) and Unstructured (UN)

were not fitted for the model. The rest of three structures had close Akaike Information Criterion (AIC), AIC Corrected (AICC), and Bayesian Information Criterion (BIC) values. The Autoregressive (AR(1)) structure was selected because it takes into account that two measurements close to each other are more correlated and measurements that are farther apart are less correlated (Kincaid 2005), which applied to this study. The REPEATED statement incorporated DAI as a REPEATED effect, each treated stem for the SUBJECT option, and AR(1) for the TYPE option. If there was a significant inoculation treatment by DAI interaction effect, the treatment effect was then assessed on each day of evaluation in each experiment using LSMEANS statement in the MIXED procedure. Means between treatments on each evaluation date were separated using a t-test at α level of 0.05. Relationships between disease severity, SSRI, normalized leaf temperature (Tc – Ta), and ambient environmental conditions during sensor measurements were evaluated using the CORR procedure (PROC CORR) in SAS 9.4.

Results

Disease symptoms and progress. Necrotic lesions were observed on the *A. rolfsii*-inoculated lateral stems of peanut plants 3 to 5 DAI (Fig. 1A). The first foliar symptom observed was drooping of top terminal leaves (Fig. 1B). However, these foliar symptoms were reversible, and wilting was observed mostly during the afternoon on each day of measurement. As the disease progressed over time, wilting symptoms became irreversible and more severe, including leaf curling, prevalent veins, and leaf discoloration (Fig. 1C). All leaflets on the stems inoculated with *A. rolfsii* became withered 12 to 16 DAI (Fig. 1D).

After the onset of foliar symptoms, disease developed rapidly until the *A. rolfsii*-inoculated stems withered (Fig. 2). Wilting symptoms were observed on some of the control plants in the

third and fourth experiment due to either heat or drought stress. However, these symptoms disappeared after either relocating plants outside the moisture chamber in the greenhouse or watering (data not shown). The disease progressed more rapidly in the fourth experiment that was conducted in May than in the three experiments conducted during the winter and early spring. This coincided with higher temperatures inside the moisture chamber the first week after inoculation of the fourth experiment (Fig. S1). The irreversible foliar wilting symptoms on the *A. rolfsii*-inoculated stems were observed (mean disease severity of scale 3 and above) beginning on 12, 9, 12, and 6 DAI in the first, second, third, and fourth experiment, respectively (Fig. 2). Because of the differences in disease development among the four greenhouse experiments, sensor measurements were analyzed and reported separately for each experiment.

Spectral reflectance. In each of the four experiments, the mean percent spectral reflectance curves of leaflets on *A. rolfsii*-inoculated and mock-inoculated stems were similar prior to the observation of irreversible foliar wilting symptoms. Following onset of wilting symptoms, leaflets on the *A. rolfsii*-inoculated stems had greater percent spectral reflectance than leaflets on the mock-inoculated stems in the visible (VIS) region (Fig. S2). Reflectance data in the near-infrared (NIR) region were more variable and noisy as compared to data in the VIS region. The greatest difference in percent reflectance between *A. rolfsii*-inoculated and mock-inoculated stems was observed at 550 nm (Fig. S2).

In all four experiments, southern stem rot spectral index (SSRI) varied by days after inoculation (DAI) ($P<0.0001$), and there was a significant inoculation treatment by DAI interaction ($P<0.0001$). Therefore, the inoculated treatment effect was assessed on each day of evaluation in each experiment. The *A. rolfsii*-inoculated and mock-inoculated peanut stems had similar SSRI values until 12, 10, 13, and 7 DAI for the first, second, third, and fourth experiment,

respectively. Afterwards, SSRI for the *A. rolfsii*-inoculated treatments began to decrease (Fig. 2). The decrease in SSRI values of *A. rolfsii*-inoculated stems resulted from the increase in the reflectance of infected stems at 550 nm as wilting symptoms became more severe. The differences in SSRI values between *A. rolfsii*-inoculated and mock-inoculated peanut stems were detected 0 to 1 days after the irreversible foliar wilting symptoms were observed (mean disease severity of scale 3 and above).

There was a significant negative correlation between southern stem rot spectral index (SSRI) values and disease severity ratings in all four experiments (P<0.001, Table S1). The only environmental parameter measured that was correlated with SSRI was air temperature; there was a weak but negative correlation between SSRI and greenhouse air temperature in three of the four experiments (Table S2).

Thermal imaging. Initially, leaf temperatures were similar between *A. rolfsii*-inoculated and mock-inoculated lateral stems, indicated by similar false blue colors (cool temperature) in the thermal images. Starting at 7 to 10 DAI, all leaflets on *A. rolfsii*-inoculated stems had greater temperatures compared to leaflets on mock-inoculated stems indicated by false orange color in thermal images (Fig. 3). These differences via visual inspection of thermal images were found starting when reversible drooping symptoms of the terminal leaves on the *A. rolfsii*-inoculated stems were first observed (data not shown).

Normalized leaf temperature varied by days after inoculation (DAI) in all four experiments (P<0.0001), but impacts of inoculation treatment on leaf temperature were inconsistent (Fig. 4). In the first through third experiment, mean leaf temperature was less than the air temperature, but inoculated lateral stems were 0.4 to 1.6°C warmer than mock-inoculated ones (P<0.05) (Fig. 5). In addition, the second and third experiment had a significant inoculation treatment by DAI

interaction (P<0.001). In the second experiment, leaflets on the *A. rolfsii*-inoculated stems had consistently greater mean normalized temperatures than leaflets on mock-inoculated stems by 0.7 to 4.0℃ starting at 9 DAI (Fig. 4B). In the third experiment, leaflets on the *A. rolfsii*-inoculated stems had greater mean normalized temperatures than leaflets on mock-inoculated stems by 0.3 to 2.3℃ as early as 12 DAI (Fig. 4C). Differences in normalized leaf temperatures between *A. rolfsii*-inoculated and mock-inoculated stems were first detected 9 and 12 DAI, the same day that the irreversible foliar wilting symptoms were observed in experiments two and three respectively (Fig. 4).

In two of the four experiments, there was a weak but significant positive correlation between disease severity and normalized leaf temperature (P<0.05, Table S1) indicating that as disease severity increased, there was a greater difference between air and leaf temperatures (i.e. leaf temperature increased). Normalized leaf temperature had a weak negative correlation with air temperature and solar radiation respectively, and a positive relationship with relative humidity in the greenhouse (Table S3). As air temperature and solar radiation increased, there was a smaller difference between air and leaf temperatures. Conversely, as relative humidity increased, there was a greater difference between air and leaf temperatures.

Discussion

The current study quantified the temporal changes in peanut leaf spectral reflectance and temperature during early stages of infection and colonization by *A. rolfsii* under controlled conditions. Differences in spectral reflectance and leaf temperature between *A. rolfsii*-infected and non-infected peanut plants were detected 0 to 1 day after establishment of foliar disease symptoms (> 25% of the leaves on the *A. rolfsii*-inoculated stem showing wilting symptoms that were non-

reversible). Spectral responses of peanut to the infection of *A. rolfsii* were more pronounced and consistent than thermal changes as disease progressed. Our work demonstrates the potential of using spectral reflectance and thermal imaging technologies to detect soilborne diseases like southern stem rot of peanut. In addition, the spectral and thermal signatures found in this study can be ultimately used to develop a new sensor-based, nondestructive scouting tool of plant diseases caused by *A. rolfsii* in peanut and other crops such as potato and tomato in the field.

Our study demonstrated that the index developed based on spectral reflectance provided consistent differentiation between *A. rolfsii*-infected from non-infected peanut lateral stems. The spectral disease index was developed using reflectance of one wavelength each in the VIS and NIR regions. In response to infection with *A. rolfsii*, peanut plants had a noticeable increase of spectral reflectance in the VIS region, and a less obvious increase of reflectance in the NIR region. Reflectance in the VIS region is related to leaf pigments of the plants and often corresponds to a reduction in chlorophyll activity (Carter and Knapp 2001). This is consistent with other studies focused on the detection of foliar diseases, which often cause chlorotic and necrotic lesions or formation of fungal structures on plant leaves (Heim et al. 2018; Mahlein et al. 2010, 2013). In contrast, changes in reflectance in the NIR region often correspond to alteration of cell structure of leaves (Mahlein 2016). Whereas foliar pathogens can directly alter leaf cell structures, peanut infection with *A. rolfsii* occurs on the root or stem tissues and may not have an immediate impact on leaf cell structures. This may explain, in part, why peanut infected with *A. rolfsii* had a less obvious increase of reflectance in NIR region as compared to non-infected plants. The spectral disease index was developed based on visual assessment of spectral reflectance curves of peanut leaves on healthy and diseased lateral stems in this study. It may be possible to develop more precise indices for early plant disease detection using machine learning algorithms such as support

vector machine (SVM), *k* nearest neighbors (KNN), and random forests (Heim et al. 2019b; Mahlein et al. 2013; Rumpf et al. 2010). In addition, further work is needed to determine the extent to which indices can distinguish between a specific disease (i.e. SSR), other diseases, and abiotic stress including physical injury to plants. If SSR-specific indices can be developed, it may eventually be possible to mount a multispectral camera on unmanned aerial vehicles (UAV) and identify SSR hotspots remotely as an alternative method for scouting large-scale commercial fields.

In this study, leaflets on *A. rolfsii*-infected peanut stems generally had greater leaf temperatures than leaflets on non-infected stems. Since leaf temperature is negatively correlated with transpiration (Pallas et al. 1967), the wilting response to infection with *A. rolfsii* infection presumably reduced the transpiration of leaves compared to those on non-infected peanut plants. However, the variable environmental factors inside the greenhouse likely influenced the thermal responses of peanut plants to the infection of *A. rolfsii,* and this may have contributed to differences between *A. rolfsii*-infected and non-infected plants being less pronounced than they would be under strictly controlled conditions. Thus, results of the current study indicate that it will be difficult to utilize thermal sensors to characterize temporal progress of SSR in the field since both biotic and abiotic stresses contribute to thermal responses. However, if thermal sensors are combined with other sensors or diagnostic tools (Oerke 2019), they may have improved disease detection accuracy and efficiency. In addition, thermal images taken at different times a day might still be useful to detect groups of plants undergoing temperature stress, which could indicate potential SSR hotspots in the field.

Though results of the current study provide a basis for detecting southern stem rot of peanut using sensors, it had several limitations. Only one peanut variety, one pathogen isolate, and one

biotic stress were evaluated to determine whether spectral and thermal sensor could be utilized for early detection of a soilborne plant disease that affects roots or stems like southern stem rot of peanut. Future research should evaluate the effects of host cultivar, different pathogen genotypes, and different abiotic and biotic stresses in order to develop robust sensor-based methods for early plant disease detection (Gold et al. 2019, 2020a, 2020b). Even though responses of peanut to the infection of *A. rolfsii* were evaluated on a daily basis for 14 to 16 days, there was only a single measurement of spectral reflectance and thermal imaging per experimental unit on each evaluation date. Diurnal patterns of spectral reflectance had been reported previously in other crops such as wheat and corn (Pinter et al. 1983; Ranson et al. 1985). Thus, spectral and thermal responses of peanut to the infection of *A. rolfsii* may also vary at different times of day, and additional studies are needed to determine the optimal time of day to detect southern stem rot of peanut with spectral and thermal sensors under field conditions.

Integrated pest management (IPM) is a critical practice to achieve sustainable crop production, and disease detection and identification is an important component of IPM. Disease management is most effective when practices are applied prior to onset of disease or in early disease establishment (pre-symptomatic and early symptomatic) (Agrios 2009; Gold et al. 2020a; Zarco-Tejada et al. 2018). In the current study, sensors did not distinguish infected peanut from non-infected plants prior to the appearance of visual foliar disease symptoms. However, sensors may still be a useful tool for IPM since preventative management practices can be applied to non-diseased plants occurring in the same field as diseased plants to prevent further yield losses. The patchy distribution and low mobility of soilborne pathogens make sensor-based detection methods suitable for site-specific management (Hillnhütter et al. 2010; Oerke et al. 2014), which can reduce chemical use and their negative impacts on the environment and risk of inducing fungicide

resistance due to chemical overuse (Heim et al. 2019a; Mahlein et al. 2018). In addition, records of sensor-based detection methods in one planting season can be applicable for future crops in following seasons (Hillnhütter et al. 2010). Regardless, this study serves as a proof-of-concept for utilizing sensor-based technologies for early detection of soilborne diseases in peanut and provides a foundation for incorporating new technologies into precision scouting and application of inputs.

Acknowledgments

We thank Drs. Maria Balota, David McCall, and Wade Thomason for their suggestions on the data collection and analysis. We thank Dr. Song Li for reviewing the manuscript before submission. We thank Linda Byrd-Masters, Robert Wilson, Amy Taylor, Jon Stein, and Daniel Espinosa for excellent technical assistance. We thank the reviewers and editor for their constructive suggestions to improve this manuscript. Mention of trade names or commercial products in this article is solely for the purpose of providing specific information and does not imply recommendation or endorsement by Virginia Tech or the U.S. Department of Agriculture. USDA is an equal opportunity provider and employer.

Literature Cited

Agrios, G.N. 2009. Plant Pathogens and Disease: General Introduction. Pages 613-646 in Encyclopedia of Microbiology (Third Edition). Elsevier, Amsterdam.

Aycock, R. 1966. Stem rot and other diseases caused by *Sclerotium rolfsii* or the status of Rolfs' fungus after 70 years. N. C. Agric. Exp. Stn. Tech. Bull. 174.

Backman, P. A., and Brenneman, T. B. 1997. Stem rot. Pages 36-37 in: Compendium of Peanut Diseases, 2nd ed. N. Kokalis-Burelle, D.M. Porter, R. Hodrfguez-Kabana, D.H. Smith and P. Subrahmanyam, eds. American Phytopathological Society Press, St. Paul, MN.

Baranowski, P., Jedryczka, M., Mazurek, W., Babula-Skowronska, D., Siedliska, A., and Kaczmarek, J. 2015. Hyperspectral and thermal imaging of oilseed rape (*Brassica napus*) response to fungal species of the genus *Alternaria*. PloS ONE 10:e0122913.

Bauriegel, E., Giebel, A., Geyer, M., Schmidt, U., Herppich, W. B. 2011. Early detection of *Fusarium* infection in wheat using hyper-spectral imaging. Comput. Electron. Agric. 75:304-312.

Brenneman, T. B., Branch, W. D., and Csinos, A. S. 1990. Partial resistance of Southern Runner, *Arachis hypogaea*, to stem rot caused by *Sclerotium rolfsii*. Peanut Sci. 17:65-67.

Carter, G. A., and Knapp, A. K. 2001. Leaf optical properties in higher plants: linking spectral characteristics to stress and chlorophyll concentration. Am. J. Bot. 88:677-684.

Chaerle, L. and Van Der Straeten, D. 2000. Imaging techniques and the early detection of plant stress. Trends Plant Sci. 5:495-501.

Chaerle, L., Caeneghem, W. V., Messens, E., Lambers, H., Van Montagu, M., Van Der Straeten, D. 1999. Presymptomatic visualization of plant–virus interactions by thermography. Nat. Biotechnol. 17:813-816.

Gold, K. M., Townsend, P. A., Herrmann, I., Gevens, A. J. 2019. Investigating potato late blight physiological differences across potato cultivars with spectroscopy and machine learning. Plant Sci. 110316.

Gold, K. M., Townsend, P. A., Chlus, A., Herrmann, I., Couture, J. J., Larson, E. R., and Gevens, A. J. 2020a. Hyperspectral measurements enable pre-symptomatic detection and

differentiation of contrasting physiological effects of late blight and early blight in potato. Remote Sens. 12:286.

Gold, K. M., Townsend, P. A., Larson, E. R., Herrmann, I., and Gevens, A. J. 2020b. Contact Reflectance Spectroscopy for Rapid, Accurate, and Nondestructive *Phytophthora infestans* Clonal Lineage Discrimination. Phytopathology. 110: 851-862.

Gorbet, D. W., Kucharek, T. A., Shokes, F. M., and Brenneman, T. B. 2004. Field evaluations of peanut germplasm for resistance to stem rot caused by *Sclerotium rolfsii*. Peanut Sci. 31:91-95.

Hagan, A. K., Rivas-Davila, M. E., Bowen, K. L., and Wells, L. 2004. Comparison of fungicide programs for the control of early leaf spot and southern stem rot on selected peanut cultivars. Peanut Sci. 31:22-27.

Heim, R. H. J., Carnegie, A. J. and Zarco-Tejada, P. J. 2019a. Breaking down barriers between remote sensing and plant pathology. Trop. Plant Pathol. 44:398-400.

Heim, R. H. J., Wright, I. J., Allen, A. P., Geedicke, I., and Oldeland, J. 2019b. Developing a spectral disease index for myrtle rust (*Austropuccinia psidii*). Plant Pathol. 68:738-745.

Heim, R. H. J., Wright, I. J., Chang, H. C., Carnegie, A. J., Pegg, G. S., Lancaster, E. K., Falster, D.S., and Oldeland, J. 2018. Detecting myrtle rust (*Austropuccinia psidii*) on lemon myrtle trees using spectral signatures and machine learning. Plant Pathol. 67:1114-1121.

Hillnhütter, C., Mahlein, A. K., Sikora, R. A., and Oerke, E. C. 2011. Remote sensing to detect plant stress induced by *Heterodera schachtii* and *Rhizoctonia solani* in sugar beet fields. Field Crops Res. 122:70-77.

Hillnhütter, C., Schweizer, A., Kühnhold, V., and Sikora, R. A. 2010. Remote sensing for the detection of soil-borne plant parasitic nematodes and fungal pathogens. Pages 151-165 in: Precision crop protection - the challenge and use of heterogeneity, Springer, Dordrecht.

Jacquemoud, S. and Ustin, S. L. 2001. Leaf optical properties: A state of the art. Pages 223-332 in: Proc. 8th International Symposium of Physical Measurements & Signatures in Remote Sensing. 8-12 January 2001, CNES, Aussois, France.

Jones, H. G., Stoll, M., Santos, T., Sousa, C. D., Chaves, M. M., and Grant, O. M. 2002. Use of infrared thermography for monitoring stomatal closure in the field: application to grapevine. J. Exp. Bot. 53:2249-2260.

Jones, H. G. 1999. Use of thermography for quantitative studies of spatial and temporal variation of stomatal conductance over leaf surfaces. Plant Cell Environ. 22:1043-1055.

Kincaid, C. 2005. Guidelines for selecting the covariance structure in mixed model analysis. Paper 198-30 in: Proc. 30th Ann. SAS Users Group Conf. SAS Institute Inc., Cary NC.

Mahlein, A. K., Kuska, M. T., Behmann, J., Polder, G., and Walter, A. 2018. Hyperspectral sensors and imaging technologies in phytopathology: state of the art. Annu. Rev. Phytopathol. 56:535-558.

Mahlein, A. K., Steiner, U., Dehne, H. W., and Oerke, E. C. 2010. Spectral signatures of sugar beet leaves for the detection and differentiation of diseases. Precis. Agric. 11:413-431.

Mahlein, A. K. 2016. Plant Disease Detection by Imaging Sensors – Parallels and Specific Demands for Precision Agriculture and Plant Phenotyping. Plant Dis. 100: 241-251.

Mahlein, A. K., Rumpf, T., Welke, P., Dehne, H. W., Plümer, L., Steiner, U., Oerke, E. C. 2013. Development of spectral indices for detecting and identifying plant diseases. Remote Sens. Environ. 128:21-30.

Moran, M. S., Inoue, Y., and Barnes, E. M. 1997. Opportunities and limitations for image-based remote sensing in precision crop management. Remote Sens. Environ. 61:319-346.

Mullen, J. 2001. Southern blight, Southern stem blight, White mold. *The Plant Health Instr.* DOI: 10.1094/PHI-I-2001-0104-01. *Updated 2006.*

Nilsson, H. E. 1995. Remote Sensing and Image Analysis in Plant Pathology. Annu. Rev. Phytopathol. 33:489-528.

Nilsson, H. E. 1991. Hand-held radiometry and IR-thermography of plant diseases in field plot experiments. Int. J. Remote Sens. 12:545-557.

Oerke, E. C. 2019. Precision crop protection systems. Pages 347- 398 in: Precision agriculture for sustainability, Burleigh Dodds Science Publishing, Cambridge.

Oerke, E. C., Mahlein, A. K., and Steiner, U. 2014. Proximal sensing of plant diseases. Pages 55-58 in: Detection and Diagnostics of Plant Pathogens, Springer, Dordrecht.

Oerke, E. C., Steiner, U., Dehne, H. W., and Lindenthal, M. 2006. Thermal imaging of cucumber leaves affected by downy mildew and environmental conditions. J. Exp. Bot. 57:2121-2132.

Pallas, J. E., Michel, B. E., and Harris, D. G. 1967. Photosynthesis, transpiration, leaf temperature, and stomatal activity of cotton plants under varying water potentials. Plant Physiol. 42:76-88.

Patrick, A., Pelham, S., Culbreath, A., Holbrook, C. C., De Godoy, I. J., and Li, C. 2017. High throughput phenotyping of tomato spot wilt disease in peanuts using unmanned aerial systems and multispectral imaging. IEEE Instrum. Meas. Mag. 20:4-12.

Pérez-Bueno, M. L., Pineda, M., Vida, C., Fernández-Ortuño, D., Torés, J. A., de Vicente, A.,Cazorla, F.M., and Barón, M. 2019. Detection of White Root Rot in Avocado Trees by Remote Sensing. Plant Dis. 103:1119-1125.

Pinter, P. J., Jackson, R. D., Idso, S. B., and Reginato, R. J. 1983. Diurnal patterns of wheat spectral reflectances. IEEE Trans. Geosci. Remote Sens. 2:156-163.

Punja, Z. K. 1985. The Biology, Ecology, and Control of *Sclerotium Rolfsii*. Annu. Rev. Phytopathol. 23:97-127.

Ranson, K. J., Daughtry, C. S. T., Biehl, L. L., and Bauer, M. E. 1985. Sun-view angle effects on reflectance factors of corn canopies. Remote Sens. Environ. 18:147-161.

Raza, M. M., Harding, C., Liebman, M., and Leandro, L. F. 2020. Exploring the Potential of High-Resolution Satellite Imagery for the Detection of Soybean Sudden Death Syndrome. Remote Sens. 12:1213.

Rideout, S. L., Brenneman, T. B., Culbreath, A. K., and Langston Jr., D. B. 2008. Evaluation of weather-based spray advisories for improved control of peanut stem rot. Plant Dis. 92:392-400.

Rouse Jr., J., Haas, R. H., Schell, J. A., and Deering, D. W. 1974. Monitoring vegetation systems in the Great Plains with ERTS. Pages 301–317 in: Proc. of the 3rd earth resources technology satellite-1 symposium. Greenbelt, MD: NASA.

Rumpf, T., Mahlein, A. K., Steiner, U., Oerke, E. C., Dehne, H. W., and Plümer, L. 2010. Early detection and classification of plant diseases with support vector machines based on hyperspectral reflectance. Comput. Electron. Agric. 74:91-99.

Shokes, F. M., Różalski, K., Gorbet, D. W., Brenneman, T. B., Berger, D. A. 1996. Techniques for Inoculation of Peanut with *Sclerotium rolfsii* in the Greenhouse and Field. Peanut Sci. 23:124-128.

Wang, M., Ling, N., Dong, X., Zhu, Y., Shen, Q., Guo, S. 2012. Thermographic visualization of leaf response in cucumber plants infected with the soil-borne pathogen *Fusarium oxysporum* f. sp. *cucumerinum*. Plant Physiol. Biochem. 61:153-161.

Wolfinger, R. 1993. Covariance structure selection in general mixed models. COMMUN STAT-SIMUL C. 22:1079-1106.

Wolfinger, R. and Chang, M. 1995. Comparing the SAS® GLM and MIXED procedures for repeated measures. Pages 1-11 in: Proc. 20th Ann. SAS Users Group Conf., SAS Institute Inc., Cary NC.

Xavier, T. W., Souto, R. N., Statella, T., Galbieri, R., Santos, E. S., S Suli, G., and Zeilhofer, P. 2019. Identification of Ramularia Leaf Blight Cotton Disease Infection Levels by Multispectral, Multiscale UAV Imagery. Drones. 3:33.

Zarco-Tejada, P. J., Camino, C., Beck, P. S. A., Calderon, R., Hornero, A., Hernández-Clemente, R., Kattenborn, T., Montes-Borrego, M., Susca, L., Morelli, M., Gonzalez-Dugo, V., North, P. R. J., Landa, B. B., Boscia, D., Saponari, M., and Navas-Cortes, J. A. 2018. Previsual symptoms of *Xylella fastidiosa* infection revealed in spectral plant-trait alterations. Nat. Plants. 4:432-439.

Table S1. Correlations between disease severity, southern stem rot spectral index (SSRI), and normalized leaf temperature (CTD) for the four greenhouse experiments conducted in 2019.

Pearson Correlation Coefficients Prob > |r| under H0: Rho=0 Number of Observations				
		Severity	**SSRI**	**CTD**
Experiment 1	**Severity**	1	-0.63322	0.39633
			<.0001	**<.0001**
		168	166	96
	SSRI	-0.63322	1	-0.30158
		<.0001		**0.0031**
		166	166	94
	CTD	0.39633	-0.30158	1
		<.0001	**0.0031**	
		96	94	96
Experiment 2	**Severity**	1	-0.50831	0.16533
			<.0001	**0.0392**
		156	156	156
	SSRI	-0.50831	1	-0.04294
		<.0001		0.5946
		156	156	156
	CTD	0.16533	-0.04294	1
		0.0392	0.5946	
		156	156	156
Experiment 3	**Severity**	1	-0.39626	0.11803
			<.0001	0.1177
		185	177	177
	SSRI	-0.39626	1	-0.02595
		<.0001		0.731
		177	178	178
	CTD	0.11803	-0.02595	1
		0.1177	0.731	
		177	178	178
Experiment 4	**Severity**	1	-0.73863	0.07903
			<.0001	0.3085
		168	157	168
	SSRI	-0.73863	1	-0.09626
		<.0001		0.2304
		157	157	157
	CTD	0.07903	-0.09626	1
		0.3085	0.2304	
		168	157	168

Table S2. Correlations between environmental parameters and southern stem rot spectral index (SSRI), for the four greenhouse experiments conducted in 2019.

Pearson Correlation Coefficients Prob > |r| under H0: Rho=0 Number of Observations					
		SSRI	**Air temperature**	**Solar Radiation**	**Relative Humidity**
Experiment 1	**SSRI**	1	0.1135	0.07708	-0.06228
			0.1454	0.3236	0.4254
		166	166	166	166
Experiment 2	**SSRI**	1	-0.15904	0.04153	0.10218
			0.0474	0.6067	0.2044
		156	156	156	156
Experiment 3	**SSRI**	1	-0.07393	-0.08257	-0.02369
			0.3267	0.2732	0.7536
		178	178	178	178
Experiment 4*	**SSRI**	1	-0.17371	.	0.02052
			0.0296	.	0.7986
		157	157	0	157

*In experiment 4, the watchdog sensor inside greenhouse did not have data recorded. The air temperature and relative humidity data were recorded by another watchdog sensor mounted inside the moisture chamber in the greenhouse.

Table S3. Correlations between environmental parameters and normalized leaf temperature (CTD), for the four greenhouse experiments conducted in 2019.

Pearson Correlation Coefficients Prob > |r| under H0: Rho=0 Number of Observations		CTD	Air temperature	Solar Radiation	Relative Humidity
Experiment 1	**CTD**	1	-0.31437	-0.37781	0.30383
			0.0018	**0.0001**	**0.0026**
		96	96	96	96
Experiment 2	**CTD**	1	-0.61891	-0.51349	0.58813
			<.0001	**<.0001**	**<.0001**
		156	156	156	156
Experiment 3	**CTD**	1	-0.32569	-0.25208	0.36155
			<.0001	**0.0007**	**<.0001**
		178	178	178	178
Experiment 4*	**CTD**	1	-0.25502	.	0.14163
			0.0008	**.**	0.0671
		168	168	0	168

*In experiment 4, the watchdog sensor inside greenhouse did not have data recorded. The air temperature and relative humidity data were recorded by another watchdog sensor mounted inside the moisture chamber in the greenhouse.

Fig. 1. Signs and symptoms of southern stem rot of peanut. **A.** Mycelium and necrotic lesions on an *Athelia rolfsii*-inoculated lateral stem. **B.** Drooping of terminal leaflets. **C.** Wilting of upper leaves on the inoculated lateral stem as disease progresses. **D.** Withering of the leaves and stem.

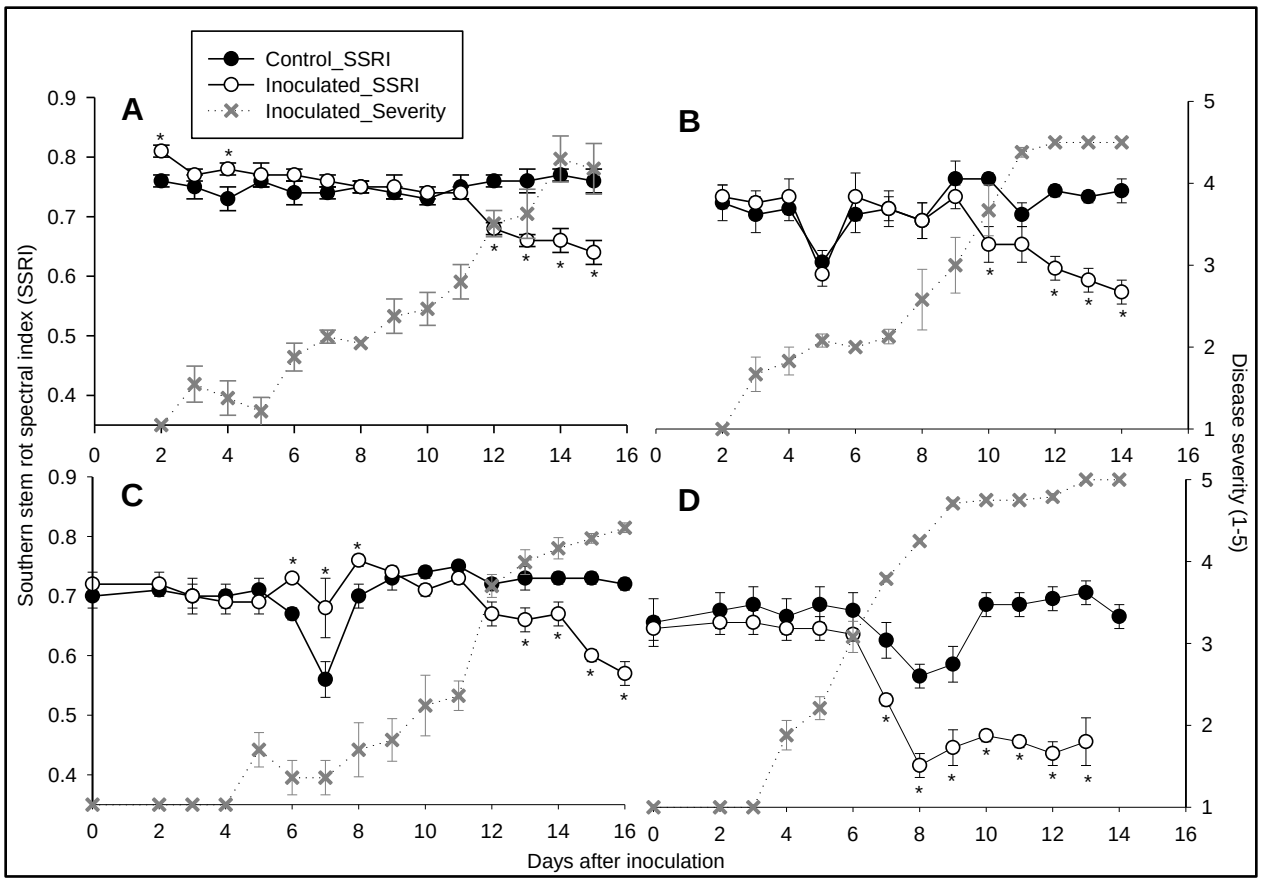

Fig. 2. Southern stem rot spectral index (SSRI) (left Y-axis, solid lines) and disease severity (right Y-axis, dotted lines) of *Athelia rolfsii*-inoculated and mock-inoculated (control) peanut plants over time in four greenhouse experiments (**A - D**) conducted in 2019. In the first, third and fourth experiments, the mock-inoculated and inoculated lateral stems were from different plants. In the second experiment, each pair of mock-inoculated and inoculated lateral stems were from the same plant. Disease symptoms were inspected visually, and spectral reflectance of one designated leaflet of the second youngest mature leaf were measured daily 2 days after inoculation. The scale of disease severity was adapted from Shokes et al. (1996) where 1 = healthy plant; 2 = necrotic lesions on stem only; 2.5 drooping of terminal leaves and lesions on stem; 3 = 25 to 50% of leaves on the inoculated stem symptomatic (wilting, leaf curling, and discoloration) and lesions on stem; 4 = >50% of leaves on the inoculated stem symptomatic and lesions on stem; 5 = withering of all the

leaves on the inoculated stem and lesions on stem. SSRI of each plant was calculated based on reflectance (R) at 550 nm and 790 nm, using the equation: SSRI = (R790 – R550) / (R790 + R550). Each dot represents the mean of disease severity or SSRI value and bars indicate the standard error of the mean. An asterisk (*) denotes significant differences of SSRI values between treatments based on a t-test at α level of 0.05.

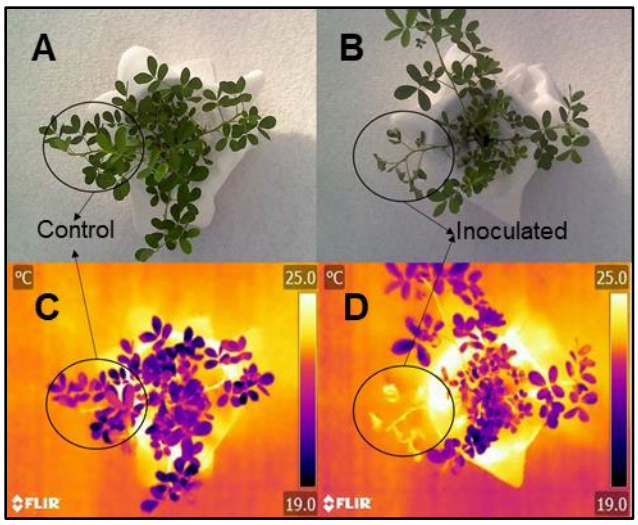

Fig. 3. Comparison of normal digital images (top) and false-color thermal images (bottom) between mock-inoculated control plants (**A**, **C**) and *Athelia rolfsii*-inoculated peanut (**B**, **D**) 12 days after inoculation in the first greenhouse experiment conducted in 2019. The treated lateral stems are circled in each image. Darker color in the thermal images indicates cooler temperature, while lighter color indicates warmer temperature. Images were taken with a FLIR T420 camera with a top view at ~ 183 cm above the ground inside the greenhouse.

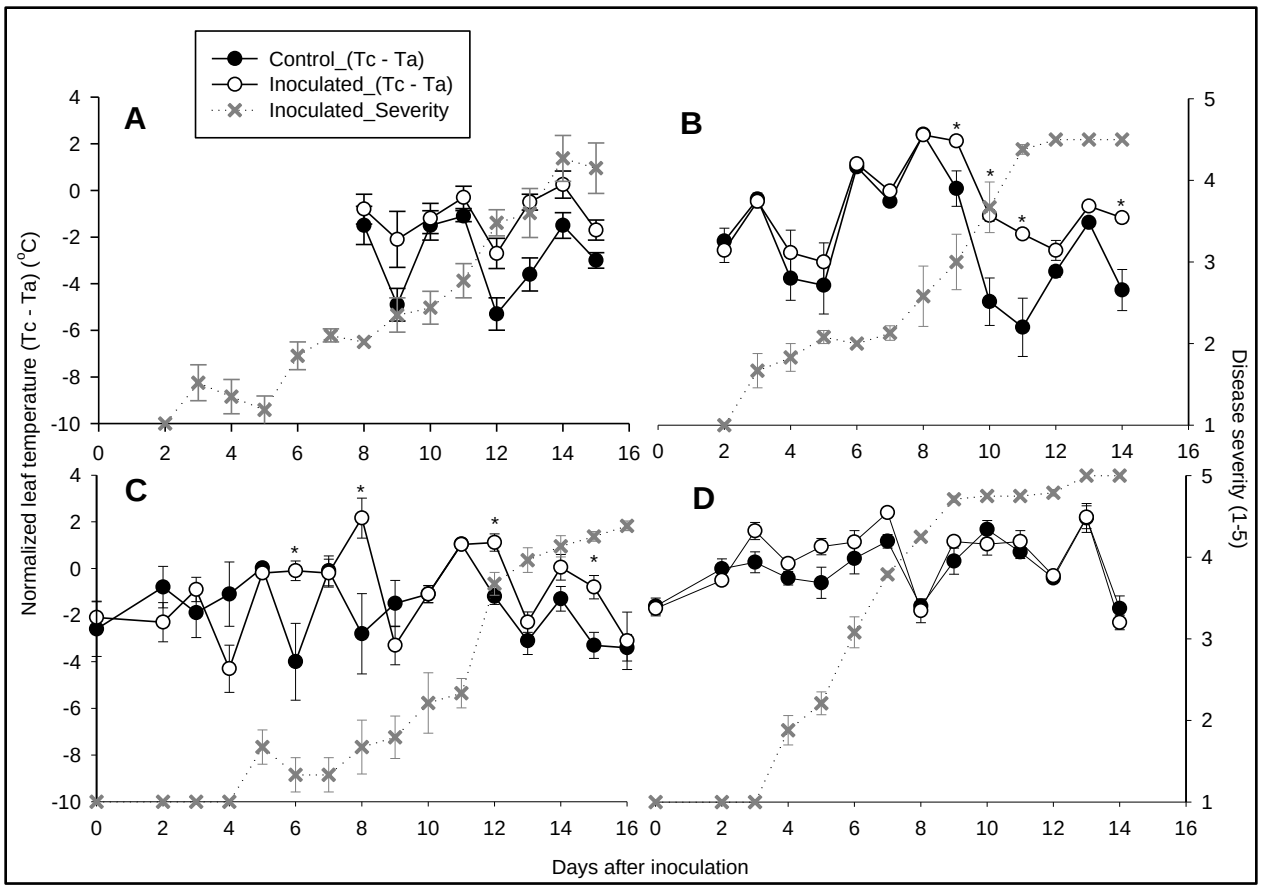

Fig. 4. Normalized leaf temperature (leaf temperature [Tc] – air temperature [Ta]) and disease severity (right Y-axis, dotted lines) of *Athelia rolfsii*-inoculated and mock-inoculated (control) peanut plants over time in four greenhouse experiments (**A** - **D**) conducted in 2019. In the first, third and fourth experiments, the mock-inoculated and inoculated lateral stems were from different plants. In the second experiment, each pair of mock-inoculated and inoculated lateral stems were from the same plant. Disease symptoms were inspected visually using a 1 to 5 scale adapted from Shokes et al. (1996). Images were taken with a FLIR T420 camera with a top view at ~ 183 cm above the ground inside the greenhouse. In each thermal image, three regions of interest (ROI, each ROI has 3 x 3 pixels) on the upper leaflets (approximately 2nd to 5th youngest mature leaf) of treated lateral stems were selected and averaged as the leaf temperature [Tc]. The air temperature [Ta] during the time when thermal images were taken on each date of measurement was measured

with a Watchdog mounted inside the greenhouse. Each dot represents the mean normalized leaf temperature and bars indicate the standard error of the mean. An asterisk (*) denotes significant differences based on t-test at α level of 0.05. In the first experiment, data were not collected until 8 days after inoculation.

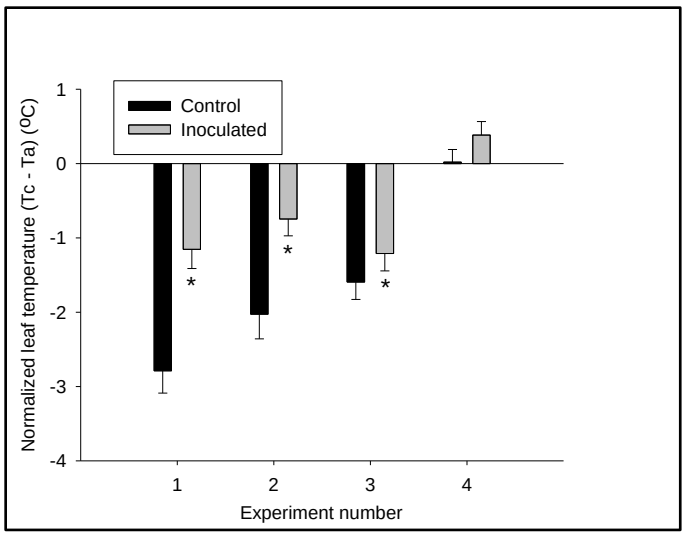

Fig. 5. Normalized leaf temperatures of mock-inoculated (control) compared to *Athelia rolfsii*-inoculated peanut lateral stems averaged across all evaluation dates for each of four greenhouse experiments conducted in 2019. Images were taken with a FLIR T420 camera with a top view at ~ 183 cm above the ground inside the greenhouse. In each thermal image, three regions of interest (ROI, each ROI has 3 x 3 pixels) on the upper leaflets (approximately 2nd to 5th youngest mature leaf) of treated lateral stems were selected and averaged as the leaf temperature [Tc]. The air temperature [Ta] during the time when thermal images were taken on each date of measurement was measured with a Watchdog mounted inside the greenhouse. Mean normalized leaf temperature was calculated by averaging the replications per treatment in each experiment across all the evaluation dates. Bars indicate the standard error, while * denotes significant differences based on a t-test at α level of 0.05.

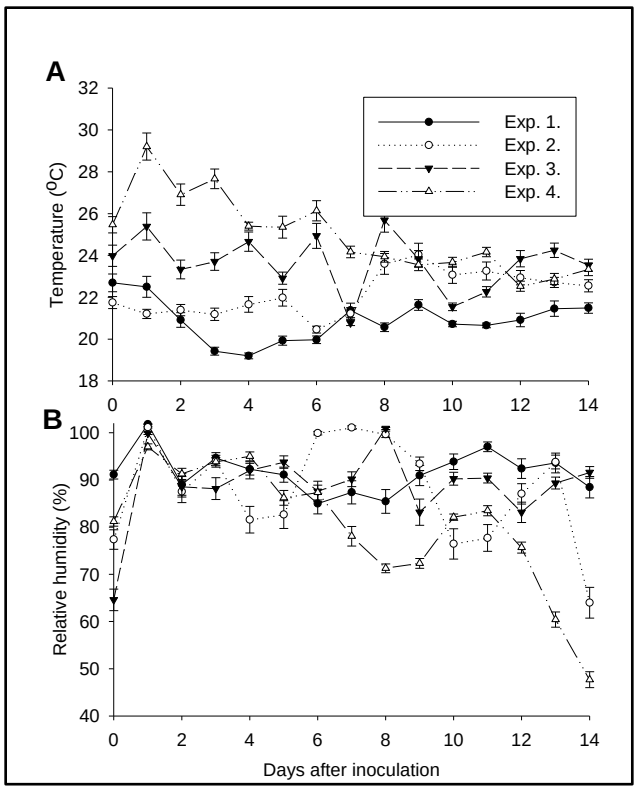

Fig. S1. Temperature (**A**) and relative humidity (**B**) inside the moisture chamber over time in the four greenhouse experiments (Exp. 1-4) conducted in 2019. Plants were placed inside the moisture chamber except daily measurement for 14 to 16 days during the first three experiments, and 7 days for the fourth experiment because plants were undergoing heat stress due to the high temperature inside the moisture chamber. Data were recorded by watchdog sensors at an interval of 15 minutes. Each dot represents the mean of each environmental factor on each date of measurement. Bars indicate standard error.

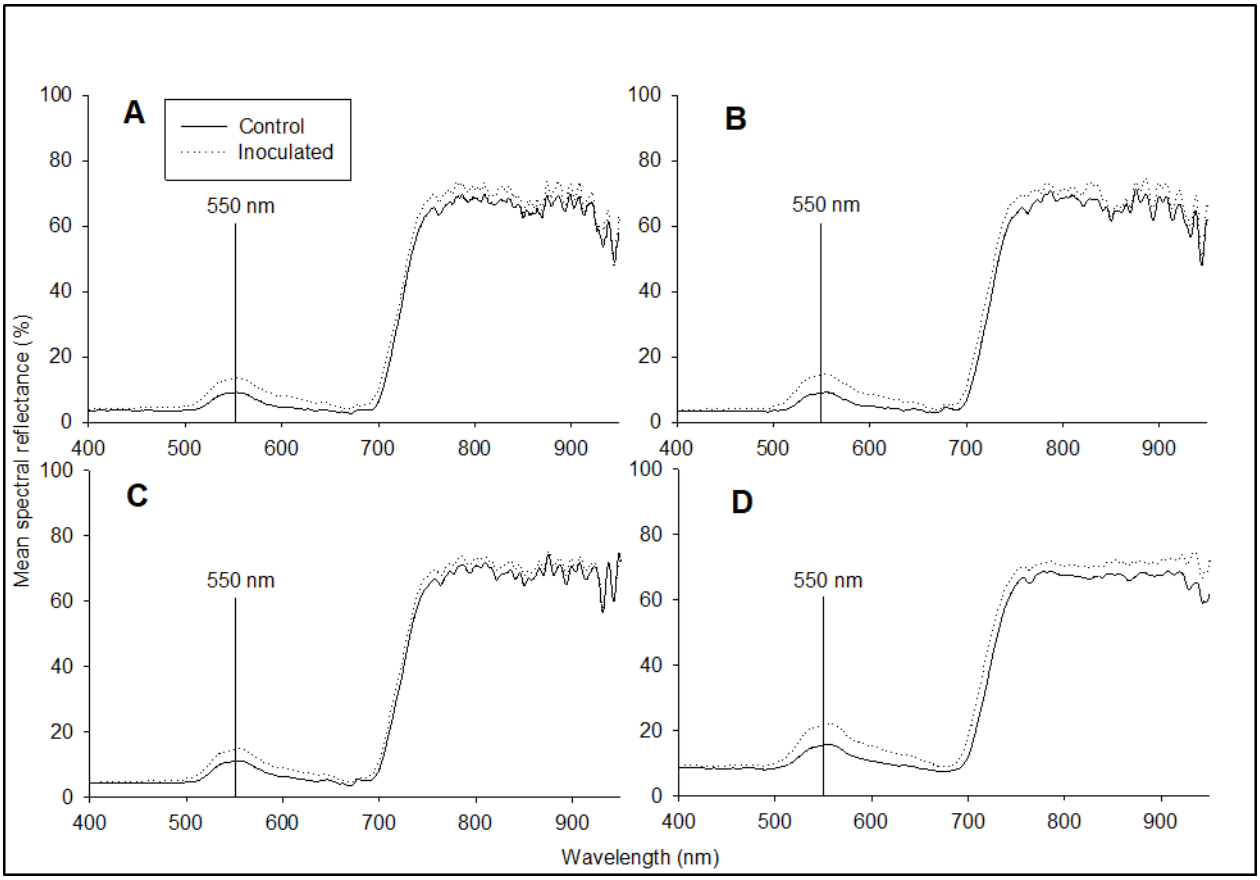

Fig. S2. Mean spectral reflectance of *Athelia rolfsii*-inoculated and mock-inoculated control peanut plants on the date when visual differences in spectra of these two treatments were first observed in four greenhouse experiments (**A** - **D**) conducted in 2019. **A** = 12 days after inoculation (DAI) in experiment 1, **B** = 10 DAI in experiment 2, **C** = 13 DAI in experiment 3, and **D** = 7 DAI in experiment 4. The spectral reflectance of an individual designated leaflet on the second youngest mature leaf of treated stems was measured with a Spectroclip-R probe using a Jaz Spectrometer in the greenhouse. The drop lines in each experiment indicated mean spectral reflectance of *A. rolfsii*-inoculated and mock-inoculated peanut plants at 550 nm.

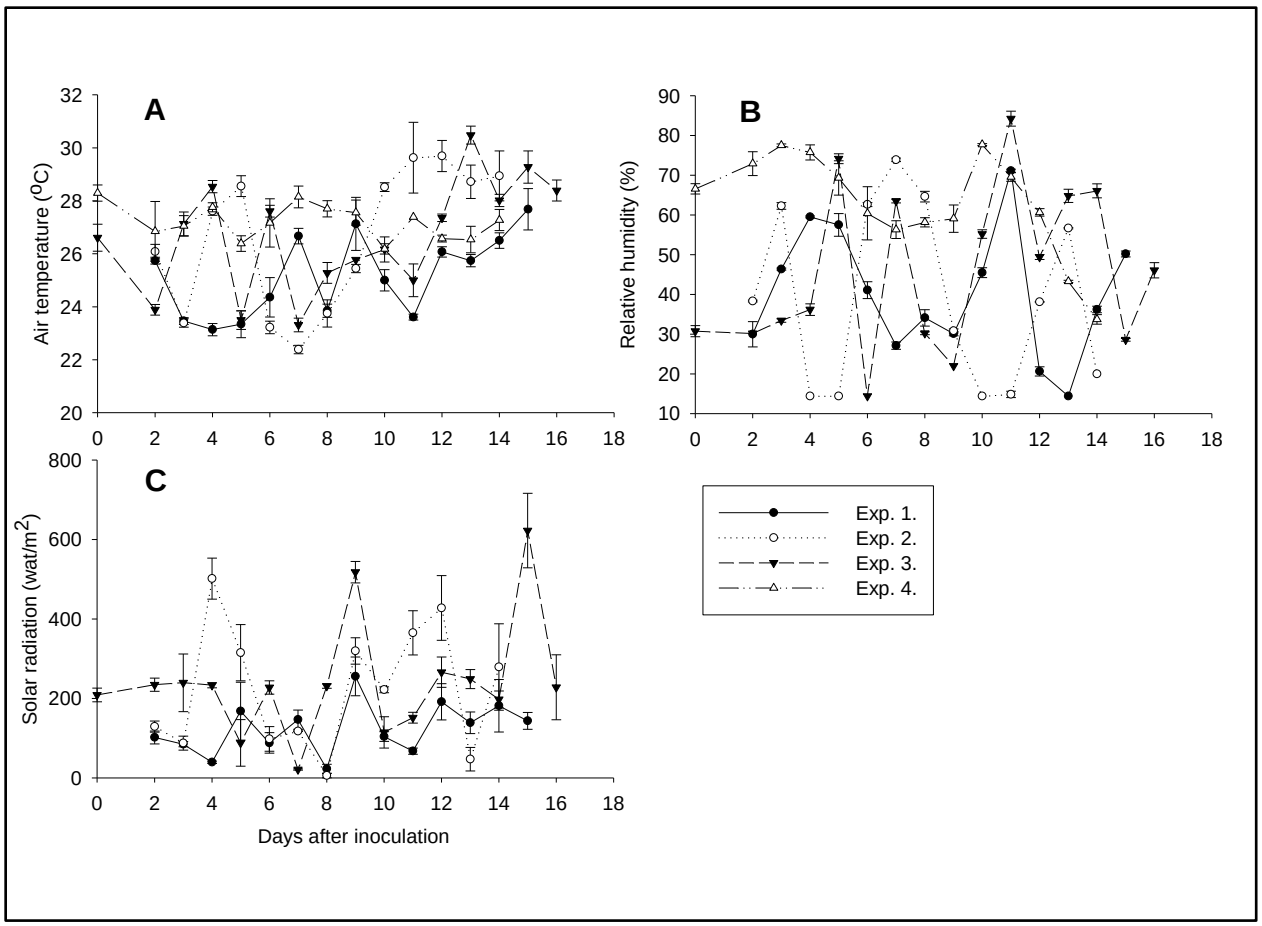

Fig. S3. The environmental factors inside the greenhouse, including air temperature (**A**), relative humidity (**B**), and solar radiation (**C**) during the time course when thermal images were taken on each date of measurement in four greenhouse experiments. Data were recorded by watchdog sensors at an interval of 15 minutes. In experiment 4, the watchdog sensor inside greenhouse did not have data recorded. The air temperature and relative humidity data were recorded by another watchdog sensor mounted inside the moisture chamber in the greenhouse. Each dot represents the mean of each environmental factor on each date of measurement. Bars indicate standard deviation.

CHAPTER 3: Identifying optimal wavelengths to detect peanut infection with *Athelia rolfsii* using hyperspectral measurements and machine learning

Xing Wei[1, 2], Marcela Aguilera[1, 3], David B. Langston Jr.[1, 2], Hillary L. Mehl[1, 2, 4], and Song Li[1]

[1]School of Plant and Environmental Sciences, Virginia Tech, Blacksburg, VA 24061; [2]Virginia Tech Tidewater Agricultural Research and Extension Center, Suffolk, VA 23437; [3]Genetics, Bioinformatics, and Computational Biology Program, Virginia Tech, Blacksburg, VA 24061; [4]United States Department of Agriculture, Agricultural Research Service, Arid-Land Agricultural Research Center, Tucson, AZ 85701

Author Contributions: Conceptualization, X.W., S.L., D.B.L., and H.L.M; methodology, X.W., S.L., D.B.L. and H.L.M.; software, X.W., M.A., and S.L.; validation, X.W. and M.A.; formal analysis, X.W.; investigation, X.W.; resources, S.L., D.B.L., and H.L.M.; data curation, X.W. and M.A.; writing—original draft preparation, X.W.; writing—review and editing, X.W., M.A., S.L., D.B.L., and H.L.M.; visualization, X.W. and S.L.; supervision, D.B.L., H.L.M., and S.L.; project administration, X.W.; funding acquisition, D.B.L. and H.L.M. All authors have read and agreed to the published version of the manuscript.

Note: This manuscript is to be submitted to the journal Remote Sensing.

Abstract: Use of hyperspectral sensors combined with machine learning is rapidly increasing in agricultural crop systems including as a tool for plant disease detection. Feature extraction and selection are commonly applied to hyperspectral data to reduce its high dimensionality and redundancy. This study was designed to identify the most important wavelengths to discriminate between healthy and diseased peanut (*Arachis hypogaea* L.) plants infected with *Athelia rolfsii*, causal agent of peanut stem rot, at different disease stages. In greenhouse experiments, daily measurements were conducted to inspect disease symptoms visually and to collect spectral reflectance of peanut leaves on lateral stems mock-inoculated and inoculated with *A. rolfsii*. Spectrum files were categorized into five classes based on foliar wilting symptoms. One feature extraction and five feature selection methods in the scikit-learn library were compared to select top 10 ranked wavelengths with and without a custom minimum distance of 20 nm. Regardless of using random forest (RF) or support vector machine with the linear kernel (SVML) as an estimator, the top 10 wavelengths selected with recursive feature elimination (RFE) outperformed ones selected by the univariate feature selection (Chi-square) and SelectFromModel (SFM) methods. Adding the minimum distance of 20 nm for top selected wavelengths improved the classification accuracy for the Chi-square and SFM methods, but not for RFE methods because wavelengths selected by RFE already spread out in different spectral regions. The overall 10-fold cross-validation accuracy for the five-class classification was 69.7% with the top 10 selected wavelengths identified by RFE-SVML feature selection method and using a SVML classifier. Wavelengths of 505, 690, and 884 nm were repeatedly selected by multiple feature selection methods. The wavelengths identified in this study may have applications for automated, sensor-based stem rot detection in peanut fields, and the methodology presented here can be adapted for soilborne disease detection in different plant systems.

Keywords: soilborne disease detection**,** *Sclerotium rolfsii***,** spectroscopy, scikit-learn, random forest, support vector machine, recursive feature elimination, feature extraction, feature selection, band selection

1. Introduction

Peanut (*Arachis hypogaea* L.) is an important oilseed crop cultivated in tropical and subtropical regions throughout the world, mainly for its seeds which contain high-quality protein and oil contents (Stalker 1997; Venkatachalam and Sathe 2006). The peanut plant is unusual because even though it flowers above ground, the development of the pods that contain the edible seed occurs below ground (Porter et al. 1997), which makes this crop prone to soilborne diseases. Stem rot of peanut, caused by *Athelia rolfsii* (Curzi) C.C. Tu & Kimbrough (anamorph: *Sclerotium rolfsii* Sacc.), is one of the most economically important soilborne diseases in peanut production (Kemerait 2012). The infection of *A. rolfsii* usually occurs first on plant tissues near the soil surface mid- to late-season following canopy closure (Backman and Brenneman 1997). The dense plant canopy provides a humid microclimate that is conducive for pathogen infection and disease development, when warm temperatures (~ 30°C) occur (Mullen 2001; Punja 1985). However, the dense plant canopy not only prevents foliar-applied fungicides from reaching below the canopy where infection of *A. rolfsii* initially occurs but also blocks visual inspection of signs and symptoms of disease.

Currently, disease assessments for peanut stem rot are based on visual inspection of signs and symptoms of this disease. The fungus, *A. rolfsii*, is characterized by the presence of white mycelia and brown sclerotia on the soil surface and infected plant tissues (Augusto et al. 2010;

Backman and Brenneman 1997). The initial symptom in plants infected with *A. rolfsii* is water-soaked lesions on infected tissues (Punja et al.1985), while the first obvious foliar symptoms are wilting of a lateral branch, the main stem, or the whole plant (Backman and Brenneman 1997). To scout for commercial fields, walking in a random manner and selecting many sites per field (~ 1.25 sites/hectare and ≥ 5 sites per field) are recommended to make a precise assessment of the whole field situation (Weeks et al. 1991). Peanut fields should be scouted once a week after plant pegging (Mehl 2020) because earlier detection before disease widespread is better to make timely crop management decisions. The present scouting method based on visual assessment is labor-intensive and time-consuming for large commercial fields, and having a high likelihood of overlooking disease hotspots. There is a need to develop a new method that can detect this disease accurately and efficiently.

Hyperspectral sensors have proven their potential for early detection of plant diseases in various plant-pathogen systems (Barreto et al. 2020; Calderón et al. 2015; Gold et al. 2020a, b, c; Hillnhütter et al. 2011, 2012; Nagasubramanian et al. 2018; Rumpf et al. 2010; Zarco-Tejada et al. 2018; Zhu et al. 2017). Visual disease rating methods are based only on the perception of red, blue, and green colors, whereas hyperspectral systems can measure changes in reflectance with a spectral range typically from 350 to 2,500 nm (Bock et al. 2020; Mahlein et al. 2018). Plant pathogens and plant diseases can alter the optical properties of leaves by changing the leaf structure and the chemical composition of infected leaves or by the appearance of pathogen structures on the foliage (Mahlein 2016; Mahlein et al. 2018). Specifically, the reflectance of leaves in the VIS region (400 nm to 700 nm), the near-infrared (NIR) region (700 to 1,000 nm), and the shortwave infrared (SWIR) region (1,000 to 2,500 nm) are typically related to leaf pigment contents, leaf cell structure, and leaf chemical and water content respectively (Carter and Knapp 2001; Jacquemound

and Ustin 2001; Mahlein 2016). A typical hyperspectral scan can generate reflectance data for hundreds of bands. This large volume of high-dimensional data poses a challenge for the data analysis to identify informative wavelengths that are directly related to plant health status (Behmann et al. 2015; Mahlein 2016).

Feature extraction and feature/band selection methods are commonly applied to hyperspectral data for dimensional reduction and spectral redundancy removal (Miao et al. 2007; Sun and Du 2019). Feature extraction methods project the original high dimensional data into a different feature space with a lower dimension (Dópido et al. 2012; Sun et al. 2014). The most commonly used feature extraction method is principal component transformation (Hsu 2007). Band selection methods reduce the dimensionality of hyperspectral data by selecting a subset of wavelengths (Yang et al. 2012; Sun and Du 2019). A variety of band selection algorithms has been used for plant disease detection, such as instance-based Relief-F algorithm (Mahlein et al. 2013), genetic algorithms (Nagasubramanian et al. 2018), partial least square (Gold et al. 2020 a, b), and random forest (Heim et al. 2018). In contrast to feature extraction methods that may alter the physical meaning of the original hyperspectral data during transformation, band selection methods preserve the spectral meaning of selected wavelengths (Yang et al. 2012; Yang et al. 2014; Sun and Du 2019).

Applications of machine learning (ML) methods have increased in agricultural production systems in the past years, especially for plant disease detection (Behmann et al. 2015; Liakos et al. 2018; Singh et al. 2016, 2020). Machine learning refers to computational algorithms that can learn from data and perform classification or clustering tasks (Samuel 1959), which are suitable to identify the patterns and trends from large amounts of data such as hyperspectral data (Behmann et al. 2015; Mahlein et al. 2018; Singh et al. 2016;). Scikit-learn library provides a number of

functions for different machine learning approaches, dimensional reduction techniques, and feature selection methods (Pedregosa et al. 2011). Results in one of our previous studies demonstrated that hyperspectral radiometric data were able to distinguish between mock-inoculated and *A. rolfsii*-inoculated peanut plants based on visual inspection of spectra after the onset of visual symptoms (Wei et al. 2021). In order to more precisely identify important spectral wavelengths that are signatures of peanut infection with *A. rolfsii*, a machine learning approach was being used in this study to further analyze the spectral reflectance data collected from healthy and diseased peanut plants infected with *A. rolfsii*. The specific objectives included, 1) to compare the performance of different machine learning methods for the classification of healthy peanut plants and plants infected with *A. rolfsii* at different stages of disease development; 2) to compare the top wavelengths selected by different feature selection methods, and 3) to develop a method to select top features with a customized minimum wavelength distance.

2. Materials and Methods

2.1 Plant Materials

The variety ‘Sullivan’, a high-oleic Virginia-type peanut, was grown in a greenhouse located at the Virginia Tech Tidewater Agricultural Research and Extension Center (AREC) in Suffolk, Virginia. Three seeds of peanut were planted in a 9.8-L plastic pot filled with a 3:1 mixture of pasteurized field soil and potting mix. Only one vigorous plant per pot was kept for data collection, while extra plants in each pot were uprooted three to four weeks after planting. Peanut seedlings were treated preventatively for thrips control with imidacloprid (Admire Pro, Bayer Crop Science, Research Triangle Park, North Carolina). Plants were irrigated 3-minutes per day automatically using a drip method. A Watchdog sensor (Model: 1,000 series, Spectrum

Technologies, Inc., Aurora, IL) was mounted inside the greenhouse to monitor environmental conditions including temperature, relative humidity, and solar radiation. The temperature ranged from 22 ℃ to 30 ℃ during the course of experiments. The daily relative humidity ranged between 14% and 84% inside the greenhouse (Wei et al. 2021).

2.2 Pathogen and Inoculation

The isolate of *A. rolfsii* used in this study was originally collected from a peanut field at the Tidewater AREC research farm in 2017. A clothespin technique, adapted from Shokes et al. (1996), was used for the pathogen inoculation. Briefly, clothespins were boiled twice in distilled water (30 min. each time) to remove the tannins that may inhibit pathogen growth. Clothespins were then autoclaved for 20 min after being submerged in full-strength potato dextrose broth (PDB) (39 g/L, Becton, Dickinson and Company, Sparks, MD). The PDB was poured off the clothespins after cooling. Half of the clothespins were inoculated with a 3-day-old actively growing culture of *A. rolfsii* on potato dextrose agar (PDA), and the other half were left non-inoculated to be used for mock-inoculation treatment. All clothespins were maintained at room temperature (21 to 23 ℃) for about a week until inoculated clothespins were colonized with mycelia of *A. rolfsii*.

Inoculation treatment was applied to peanut plants 68 to 82 days after planting. The two primary symmetrical lateral stems of each plant were either clamped with a non-colonized clothespin as mock-inoculation treatment or clamped with a clothespin colonized with *A. rolfsii* as inoculation treatment. All plants were maintained in a moisture chamber set up on a bench inside the greenhouse to facilitate pathogen infection and disease development. Two cool mist humidifiers (Model: Vicks® 4.5-liter, Kaz USA, Inc., Marlborough, MA) with maximum settings

were placed inside the moisture chamber to provide ≥ 90% relative humidity. Another Watchdog sensor was mounted inside the moisture chamber to record temperature and relative humidity every 15 minutes.

2.3 Experimental Setup

Two treatments were included, lateral stems of peanut mock-inoculated or inoculated with *A. rolfsii*. Visual rating and spectral data for this study were collected from 126 lateral stems on 74 peanut plants over four experiments where peanut plants were planted on October 19 and December 21 in 2018 and January 8 and February 22 in 2019, respectively. Each plant was inspected daily, once per day, for 14 to 16 days after inoculation. For daily assessment, plants were moved outside the moisture chamber and placed on other benches inside the greenhouse to allow the foliage to air dry before data collection. Plants were then moved back into the moisture chamber after measurements. Plants were kept inside the moisture chamber through the experimental course for the first three experiments. In the fourth experiment, plants were moved permanently outside the moisture chamber 7 days after inoculation because they were affected by heat stress.

2.4 Stem Rot Severity Rating and Categorization

Lateral stems of each plant were inspected each day visually for signs and symptoms of disease starting from 2 days after inoculation. The lateral stems of plants were categorized based on visual symptoms ratings into five classes, where ‘Healthy’ = mock-inoculated lateral stems without any disease symptoms; ‘Presymptomatic’ = inoculated lateral stems without any disease symptoms; ‘Lesion only’ = necrotic lesions on inoculated lateral stems; ‘Mild’ = drooping of

terminal leaves to wilting of < 50% upper leaves on inoculated lateral stems; 'Severe' = wilting of ≥ 50% leaves on inoculated lateral stems.

2.5 Spectral Reflectance Measurements

The second youngest mature leaf on each treated lateral stem was labeled with a twist tie immediately before the inoculation treatment. Spectral reflectance of one leaflet on this designated leaf was measured from the leaf adaxial side once per day starting 2 days after inoculation using a handheld Jaz spectrometer and an attached SpectroClip probe (Ocean Optics, Dunedin, Florida, **Fig. 1A**). The spectral range and optical resolution of the Jaz spectrometer were 200 to 1,100 nm and ~ 0.46 nm, respectively. The spectrometer was set to boxcar number of 5 and averages of 10 to reduce machinery noises. The light source for the SpectroClip probe was from a Pulsed Xenon light embedded in the Jaz spectrometer, with an active illuminated area of 5 mm in diameter. The WS-1 diffuse reflectance standard, with reflectivity >98%, was used as the white reference (Ocean Optics, Dunedin, Florida).

2.6 Data Analysis Pipeline

2.6.1 Data preparation

The data analysis pipeline is illustrated in **Fig. 1B**. The spectrum file collected by the Jaz spectrometer was in a Jaz data file format (.JAZ). Each spectrum file contains information of spectrometer settings and five columns of spectral data including W = wavelength, D = dark spectrum, R = reference spectrum, S = sample spectrum, and P = processed spectrum in percentage. Each spectrum file's name was labeled manually according to the experiment number, plant and its lateral stem ID, and date collected. Then spectrum files were grouped into five classes based on

the visual ratings of disease symptoms for each individual assessment including ‘Healthy’, ‘Presymptomatic’, ‘Lesion only’, ‘Mild’, and ‘Severe’.

2.6.2 Preprocessing of raw spectrum files

The preprocessing steps of raw spectrum files were adapted from Heim et al. (2018) using the R statistical platform (version 3.6.1). The processed spectral data and file name were first extracted from each Jaz spectral data file and saved into a Microsoft Excel comma-separated values file (.CSV). A master spectral file was created consisting of processed spectral data and file names of spectra from all five categories. Spectral data were then smoothed with a Savitzky-Golay filter using the second-order polynomial and a window size of 33 data points (Savitzky and Golay 1964). Wavelengths at two extreme ends of the spectrum (< 240 nm and > 900 nm) were deleted due to large spectral noises. Outlying spectrums were removed using depth measures in the Functional Data Analysis and Utilities for Statistical Computing (fda.usc) package (Febrero-Bande and Oviedo de la Fuente 2012). The final dataset after outlier removal consisted of 399 observations including 82 for ‘Healthy’, 79 ‘Presymptomatic’, 72 ‘Lesion only’, 73 ‘Mild’, and 93 ‘Severe’.

The spectral signals were further processed using the prospectr package to reduce multicollinearity between predictor variables (Heim et al. 2018; Stevens and Ramirez-Lopz 2014). The bin size of 10 was used in this study, meaning the spectral reflectance for each wavelength was the average spectral reflectance values of 10 adjacent wavelengths before signal binning. The spectral resolution was reduced from 0.46 nm (1,569 predictor variables/wavelengths) to 4.6 nm (157 predictor variables/wavelengths).

2.6.3 Comparison of machine learning methods for classification

The spectral data after preprocessing steps were analyzed using the Python programming language (version 3.7.10). The performance of nine common machine learning methods was compared for the classification of mock-inoculated, healthy peanut plants and plants inoculated with *A. rolfsii* at different stages of disease development. The nine machine learning algorithms tested in this study included Gaussian Naïve Bayes (NB), K-nearest neighbors (KNN), linear discriminant analysis (LDA), multi-layer perceptron neural network (MLPNN), random forests (RF), support vector machine with the linear kernel (SVML), support vector machine with the radial kernel (SVMR), gradient boosting (GBoost), and extreme gradient boosting (XGBoost). All the nine algorithms were supervised machine learning methods, but they were from diverse categories based on their learning models (Liakos et al. 2018). The Gaussian Naïve Bayes (NB) algorithm belongs to the probabilistic graphical Bayesian models (Liakos et al. 2018). The KNN uses instance-based learning models. The LDA is a commonly used dimensionality reduction technique. The MLPNN is one of the traditional artificial neural networks. The RF and the two gradient boosting algorithms uses ensemble-learning models by combining multiple decision-tree based classifiers. Support vector machine (SVM) uses separating hyperplanes to classify data from different classes with the goal of maximizing margins between each class (Cortes and Vapnik 1995; Liakos et al. 2018). The nine machine learning methods The XGBoost classifier was from the library of XGBoost (version 1.3.3) (Chen and Guestrin 2016), while all the others were from the library of scikit-learn (version 0.24.1) (Pedregosa et al. 2011). The default hyperparameters for each classifier were used in this study.

2.6.4 Comparison of feature selection methods

Five feature selection methods from the scikit-learn library were evaluated in this study. They included one univariate feature selection method (SelectKBest using a Chi-square test), two feature selection methods using SelectFromModel (SFM), and two recursive feature elimination (RFE) methods. Both SFM and RFE needed an external estimator, which could assign weights to features. SFM selects the features based on the provided threshold parameter. RFE selects a desirable number of features by recursively considering smaller and smaller sets of features (Pedregosa et al. 2011). In addition to the feature selection methods, principal component analysis (PCA), a dimensionality reduction technique, was also included in the comparison. The top 10 wavelengths or components selected from the feature selection methods were then compared to classify the healthy and diseased peanut plants at different stages.

Unlike hyperspectral sensors, multispectral sensors using typical RGB or monochrome camera with customized, selected band filters are cheaper and are more widely used in plant phenotyping research. However, the band filters typically have a broader wavelength resolution than hyperspectral sensors. To test whether our feature selection method can be used to guide the design of spectral filters, a method was developed to enforce a minimum bandwidth distance between the selected features.

2.6.5 Plot of confusion matrix

The spectral data with all bands and with only the top 10 selected wavelengths for all five classes were split into 80% training and 20% testing subsets. The models were trained using the training datasets with all bands and with the top 10 selected wavelengths. Confusion matrixes with and without normalization were plotted using the trained models on the testing datasets.

2.6.6 Statistical analysis

A stratified 10-fold cross-validation repeated in three times was used for each classification model. A one-way ANOVA test was conducted to compare the different classification models using different machine learning classifiers and different feature selection methods, respectively. If the ANOVA tests were significant, the mean separation was then performed using the Tukey honest significant difference (HSD) test with an α level of 0.05.

3 Results

3.1 Spectral reflectance curves

The average spectral reflectance of peanut leaves from different categories were first compared using one-way ANOVA test by each spectral region including ultraviolet (UV, 240 to 400 nm), visible (VIS, 400 to 700 nm), and near-infrared (NIR, 700 to 900 nm) regions. In the UV region, 'Mild' had the greatest reflectance, followed by 'Severe' and 'Lesion only', while 'Healthy' and 'Presymptomatic' had the lowest reflectance ($P < 0.0001$) (**Fig. 2B**). In the VIS region, with the exception for 'Presymptomatic' overlapping with 'Mild', there was a gradient increase of reflectance from 'Healthy' to 'Severe' ($P < 0.0001$) (**Fig. 2C**). In the NIR) region, the 'Severe' had the greatest reflectance, followed by 'Mild' and 'Presymptomatic', while the 'Lesion only' and 'Healthy' had the lowest reflectance ($P < 0.0001$) (**Fig. 2D**). The spectral reflectance curves in the NIR regions were noisier compared with the ones in the UV and VIS regions (**Fig. 2**).

3.2 Classification analysis

To determine the best classifiers for downstream analysis, we compared the performance of nine machine learning methods for the classification of models with different input classes. The classification models were divided into three different classification problems including two classes (‘Healthy’ and ‘Severe’), three classes (‘Healthy’ and ‘Mild’ and ‘Severe’), and five classes (‘Healthy’ and ‘Presymptomatic’ and ‘Lesion only’ and ‘Mild’ and ‘Severe’). Overall, there was a decrease in accuracy when the number of input classes increased (**Fig. 3**). Specifically, all machine learning methods had >90% overall accuracy except the LDA classifier for the two-class classification ($P<0.0001$). For three-class classification, KNN, RF, SVML, GBoost, and XGBoost had greater accuracy compared with NB, LDA, MLPNN, and SVMR ($P<0.0001$), and the average accuracy for all methods was approximately 80%. For the five-class classification, RF, SVML, GBoost, and XGBoost performed better than the rest of the classifiers ($P<0.0001$) (**Fig. 3**), and the accuracy for the best classifier was around 60%. The computational time of RF and SVML were also faster than GBoost and XGBoost when performing the classification using a central processing unit (CPU) (Model: E5-2683v4, 2.1 GHz, Intel, Santa Clara, CA). Based on these results, RF and SVML were selected for further analysis.

3.3 Feature weights calculated by different methods

Different machine learning methods determine the important features using different types of algorithms to decide “weights” of each feature. For example, feature scores were calculated for each wavelength using Chi-square test method. The feature scores had similar shapes for models with different input classes (2 classes, 3 classes, and 5 classes, **Fig. 4A**). In general, higher scores were found in the VIS region compared with UV and NIR regions using the Chi-square test.

Features from the regions of 590 to 640 nm all had similar scores. In contrast, random forest method calculated feature "weights" using feature importance values. Similar to the Chi-square test, greater importance values were assigned to the VIS region than UV and NIR regions for the RF method (**Fig. 4B**). Unlike the Chi-square test, the peaks of importance values mostly occurred in two regions in the VIS region including 480 to 540 nm and 570 to 700 nm. In addition, two peaks were found on two wavelengths in the NIR regions including 830 and 884 nm for the three-class and five-class model, but not for the two-class model (**Fig. 4B**). For peaks in the RF, feature importance scores were not continuous as was the case in the Chi-square curve. Instead, they were discrete peaks in the feature importance scores and two high peaks were usually separated by wavelengths with lower importance scores. Finally, for the SVML method, the weights of each feature were calculated by averaging the absolute values of coefficients of multiple classes. Generally, peaks occurred in all three regions including UV, VIS, and NIR (**Fig. 4C**). In contrast to Chi-square and RF methods, greater weights were assigned to wavelengths in the NIR regions for the SVML method (**Fig. 4**). Interestingly, for the two-class classification, the weights were much lower than those from the three- and five-class classifications. We also noticed that the absolute values of these "features weights" were not comparable between different approaches, which is expected.

3.4 Dimension reduction and feature selection analysis

To understand the performance of different machine learning methods and the differences in the feature selection process, we performed PCA analysis for the dimension reduction of the spectral data from all five classes. In the PCA plot of the first two components, 'Healthy' (green) and 'Severe' (purple) samples can be easily separated by a straight line. 'Healthy' and

'Presymptomatic' were overlapping but some 'Presymptomatic' samples appeared in a region (PCA2 > 60) that had few samples from other classes. The 'Lesion-only' category overlapped with all other categories with a higher degree of overlapping with healthy and mild samples. In comparison, 'Mild' samples overlapped with all other categories, but had a high degree of overlap with 'Severe' samples compared to other categories. The first component explained near 60% variance, while the second component accounted for > 20% variance of the data. Overall, the top 3 components explained > 90% of the variance, and the top 10 components explained >99% variance (**Fig. S2**).

To check whether unsupervised dimension reduction can be directly used as a way to select feature and perform classification, we tested the classifiers using the top 10 components or wavelengths for the five-class model (H-P-L-M-S). Feature selections were performed using Chi-square test, selection from model for random forest and SVM, and recursive feature selection for random forest and SVM. Top 10 PCA were also used as input features. Two classifiers including RF and SVML were used as classification methods for these selected features and the resulting accuracy was compared to all features without any selection. Regardless of classifiers, the top 10 components from the PCA analysis and top 10 wavelengths selected by the RFE-RF and RFE-SVML method performed as well as using all bands for the five-class classification in terms of testing accuracy ($P>0.05$), suggesting that using a few features does not reduce the model performance. RFE methods with either RF or SVML as classifiers performed better than the univariate feature selection (SelectKBest using the Chi-square test) and the two SFM methods ($P<0.0001$) (**Fig. 5A**). Interestingly, features selected using RFE performed similarly regardless of the classification method used. For example, REF-RF features had similar accuracy when tested using SVM classifier and vice versa.

3.5 Feature selection with a custom minimum distance

The spectral reflectance of wavelengths close to each other was highly correlated. It holds true, especially for wavelengths within each region for UV, VIS and NIR regions. Wavelengths from different regions were less correlated with each other (**Fig. S3**). The top wavelengths selected by some methods were neighboring or close to each other (**Table 1a**). The performance of the accuracies for 5-class classification was compared between top features with and without customized minimum distance. The top 10 features with and without a minimum distance of 20 nm from each of the five feature selection methods were used as input data for the five-class classification. Two classifiers including RF and SVML were tested. Regardless of classifiers, the top 10 features with a minimum distance of 20 nm performed better than the original top 10 features selected by Chi-square and two SFM methods ($P < 0.05$, **Fig. 5B**). The top 10 features with a minimum distance of 20 nm performed better than the original top 10 features in six out of ten methods compared ($P<0.05$) (**Fig. 6**). In the other four methods, the top 10 features with minimum distance performed the same as the original top 10 features, suggesting that using a minimum distance filtering does not decrease the model performance (see discussion).

3.6 Selected wavelengths and classification accuracy for 5 classes

The top 10 wavelengths selected by Chi-square methods were limited to two narrow spectral regions (694 to 706 nm and 586 to 611 nm) (Table 1). The top four selected wavelengths were all within the narrow 694 to 706 nm range. Additional 20 nm limits helped to increase the diversity of the spectra selected, such as adding 632 nm, 573 nm, and 527 nm in the top five selected features. However, no wavelengths were selected below 500 nm or above 720 nm with

the Chi-square method. Without 20 nm limits and using random forest, 5 out of the top 10 features were identical between the two feature selection methods. In contrast, using SVM, only 3 out of the top 10 features were identical between two feature selection methods. Regardless of the machine learning method, one wavelength, 884 nm was selected as an important feature in four method combinations (Table 1A). Among the rest of the features, 505 nm was selected by three methods, and 501, 690, 686, 694, and 763 nm were selected by two methods. There were more common wavelengths selected by different machine learning methods (six wavelengths) than between machine learning and Chi-square methods (one wavelength).

By including a 20 nm limits, three machine learning methods had the same top three wavelengths and one machine learning method had the same top two features whereas the Chi-square method only had one top feature (698 nm) remain the same because the original top four features were all within a narrow bandwidth. Regardless of the type of machine learning method used, 884 nm was consistently an important feature. Another important feature was 496 to 505 nm, which was selected by three methods. If additional wavelengths can be included, other candidate ranges include bands of 242 to 300 nm, 620 to 690 nm, 731 to 779 nm, or 807 to 826 nm. Regardless of using all bands or the top 10 selected wavelengths by RFE-SVML, the classification accuracy was low to medium for 'Presymptomatic' and 'Mild' (42 to 69%), medium for 'Lesion only' (~70%), medium to high for 'Healthy' (76 to 86%), and high for 'Severe' (89 to 94%) (**Fig. 7**). The overall classification accuracy was 73.8% using all bands and 69.0% with the top 10 selected wavelengths.

4. Discussion

In this study, one feature extraction method (PCA) and five feature selection methods in the scikit-learn library were compared to identify the most important wavelengths for the discrimination of healthy and diseased peanut plants infected with *A. rolfsii* under controlled conditions. A new method was also developed to select the top-ranked wavelengths with a custom distance. Distanced wavelengths may make the most of the wide spectral range covered by hyperspectral sensors and facilitate the design of multispectral camera filters to be deployed for the detection of peanut stem rot in the field.

Multiple feature selection methods or an ensemble of multiple methods are recommended to be applied to hyperspectral data because wavelengths selected are affected by the feature selection methods used (Chan et al. 2008; Hennessy et al. 2020). Interestingly, SFM and RFE selected similar wavelengths with slightly different rankings using the RF estimator, but selected different wavelengths using the SVML estimator. Overall, the Chi-square method tended to select adjacent wavelengths from relatively narrow spectral areas, while RFE methods with either a SVML or RF estimator selected wavelengths spreading over different spectra regions. These machine learning-based methods are preferred because of the multicollinearity in hyperspectral data, especially among wavelengths in narrow spectral regions.

Several wavelengths were repeatedly selected as top features by different feature selection methods including ones in VIS region (501 and 505 nm), Red-edge region (686, 690, and 694 nm), and NIR region (884 nm). Reflectance at 500 nm is dependent on combined absorption of chlorophyll *a*, chlorophyll *b*, and carotenoids, while reflectance around 680 nm is solely controlled by chlorophyll *a* (Gitelson and Merzlyak 1996; Merzlyak et al. 1999). Reflectance at 885 nm is reported to be sensitive to total chlorophyll, biomass, leaf area index, and protein (Thenkabail et

al. 2004). Peanut plants infected with *A. rolfsii* exhibit necrotic lesions on the stems and discoloration and wilting of foliage, thus as the disease progresses, the concentration of chlorophyll and carotenoid contents in the leaves may be altered.

Interestingly, two similar wavelengths with this study (503 and 881 nm) combined with four unique wavelengths (545, 566, 608, and 860 nm) were used to detect drought stress in wheat (Moshou et al. 2014). Wilting of the foliage is a common symptom of peanut plants infected with *A. rolfsii* and plants under drought stress (Balota and Oakes et al. 2017; Luis et al. 2016). However, compared to the wilting of the entire plant caused by drought, the typical foliar symptom of peanut plants during the early stage of infection with *A. rolfsii* is the wilting of an individual lateral branch or main stem (Backman and Brenneman 1997). In addition, the wilting of plants infected with *A. rolfsii* is believed to be caused by the oxalic acid produced during pathogenesis (Higgins 1927; Bateman and Beer 1965). Further studies should examine the capability of both the common and unique wavelengths identified in this study and Moshou et al. (2014) to distinguish between peanut plants under drought stress and plants infected with soilborne pathogens including *A. rolfsii*.

Pathogen biology and disease physiology should be taken into consideration for plant disease detection and differentiation using remote sensing (Gold et al. 2020a; Mahlein et al. 2013), which holds true also for band selection. Compared to the infection of foliar pathogens that have direct interaction with plant leaves, infection of soilborne pathogens typically will first damage the root or vascular systems of plants before inducing any foliar symptoms. This may explain why the wavelengths identified in this study for stem rot detection were different from ones reported previously for the detection of foliar diseases in various crops or trees (Conrad et al. 2020; Gold et al. 2020a, b, c; Heim et al. 2018; Mahlein et al. 2013; Zhu et al. 2017). Previously, charcoal rot disease in soybean was detected using hyperspectral imaging, and the authors selected 475, 548,

652, 516, 720, and 915 nm using genetic algorithm and SVM (Nagasubramanian et al. 2018). Stem tissues via a destructive sampling method were used in the previous report, while reflectance of leaves was measured using a handheld hyperspectral sensor in a nondestructive manner in this study.

Regardless of using all bands or the top 10 ranked wavelengths, the predicted accuracy for the classification of diseased peanut plants was low to medium for 'Presymptomatic' and 'Mild' classes. The five classes were categorized solely based on the visual inspection of the disease symptoms. It was not known if the infection occurred or not for inoculated plants in the 'Presymptomatic' class. The drooping of terminal leaves, the first foliar symptom observed, was found to be reversible and a potential response to heat stress (Wei et al. 2021). Plants with this reversible drooping symptom were included in the 'Mild' class, which may explain in part the low accuracy for this class. Future studies aiming to detect plant diseases during early infection may incorporate some qualitative or quantitative assessments of disease development using microscopy or quantitative polymerase chain reaction (qPCR) combined with hyperspectral measurements.

5. Conclusions

Accurate and efficient diagnosis of plant diseases and their causal pathogens are the critical first step to develop effective management strategies. In addition to the developed molecular and developing chemical diagnostic tools, advancements of hyperspectral sensors combined with machine learning analysis will enrich the toolbox for plant disease detection and integrated pest management (Bock et al. 2020; Mahlein 2016; Mahlein et al. 2018; Silva et al. 2021). This study demonstrates the selection of optimal wavelengths using multiple feature selection methods in the scikit-learn machine learning library to detect peanut plants infected with *A. rolfsii* at various

stages of disease development. The wavelengths identified in this study may have application for stem rot detection in peanut fields, and the methodology presented here can be adapted for soilborne disease detection in different plant systems.

Funding: This research was funded by VIRGINIA PEANUT BOARD and VIRGINIA AGRICULTURAL COUNCIL.

Acknowledgments: We would like to thank Drs. Maria Balota, David McCall, and Wade Thomason for their suggestions on the data collection. We appreciate Linda Byrd-Masters, Robert Wilson, Amy Taylor, Jon Stein, and Daniel Espinosa for excellent technical assistance and support in data collection. Special thanks to Dr. Haidong Yan for his advice on the programming languages of Python and R. Mention of trade names or commercial products in this article is solely for the purpose of providing specific information and does not imply recommendation or endorsement by Virginia Tech or the U.S. Department of Agriculture. USDA is an equal opportunity provider and employer.

Conflicts of interest: The authors declare no conflict of interest.

Literature Cited

Augusto, J., Brenneman, T., Culbreath, A., Sumner, P., 2010. Night spraying peanut fungicides I. Extended fungicide residual and integrated disease management. Plant Disease 94, 676-682.

Backman, P.A., and T.B. Brenneman. 1997. Stem rot, pp. 36-37. In Compendium of Peanut Diseases, 2nd ed. N.Kokalis-Burelle, D.M. Porter, R Hodrfguez-Kabana, D.H. Smith and P. Subrahmanyam eds. American Phytopathological Society Press, St. Paul, MN.

Balota, M., Oakes, J., 2017. UAV remote sensing for phenotyping drought tolerance in peanuts. SPIE. Proceedings Volume 10218, Autonomous Air and Ground Sensing Systems for Agricultural Optimization and Phenotyping II. doi: https://doi.org/10.1117/12.2262496

Barreto, A., Paulus, S., Varrelmann, M., Mahlein, A.-K., 2020. Hyperspectral imaging of symptoms induced by *Rhizoctonia solani* in sugar beet: comparison of input data and different machine learning algorithms. Journal of Plant Diseases and Protection 127, 441-451.

Bateman, D., Beer, S., 1965. Simultaneous production and synergistic action of oxalic acid and polygalacturonase during pathogenesis by *Sclerotium rolfsii*. Phytopathology 55, 204-211.

Bauriegel, E., Giebel, A., Geyer, M., Schmidt, U., Herppich, W.B., 2011. Early detection of *Fusarium* infection in wheat using hyper-spectral imaging. Computers and Electronics in Agriculture 75, 304-312.

Behmann, J., Mahlein, A.-K., Rumpf, T., Römer, C., Plümer, L., 2015. A review of advanced machine learning methods for the detection of biotic stress in precision crop protection. Precision Agriculture 16, 239-260.

Bock, C.H., Barbedo, J.G., Del Ponte, E.M., Bohnenkamp, D., Mahlein, A.-K., 2020. From visual estimates to fully automated sensor-based measurements of plant disease severity: status and challenges for improving accuracy. Phytopathology Research 2, 1-30.

Calderón, R., Navas-Cortés, J., Zarco-Tejada, P., 2015. Early detection and quantification of Verticillium wilt in olive using hyperspectral and thermal imagery over large areas. Remote Sensing 7, 5584-5610.

Carter, G.A., Knapp, A.K., 2001. Leaf optical properties in higher plants: linking spectral characteristics to stress and chlorophyll concentration. American Journal of Botany 88, 677-684.

Chan, J.C.-W., Paelinckx, D., 2008. Evaluation of Random Forest and Adaboost tree-based ensemble classification and spectral band selection for ecotope mapping using airborne hyperspectral imagery. Remote Sensing of Environment 112, 2999-3011.

Chen, T., Guestrin, C., 2016. Xgboost: A scalable tree boosting system. Proceedings of the 22nd acm sigkdd international conference on knowledge discovery and data mining, pp. 785-794.

Conrad, A.O., Li, W., Lee, D.-Y., Wang, G.-L., Rodriguez-Saona, L., Bonello, P., 2020. Machine learning-based presymptomatic detection of rice sheath blight using spectral profiles. Plant Phenomics. vol. 2020, Article ID 8954085. https://doi.org/10.34133/2020/8954085.

Cortes and Vapnik. 1995. Support-vector networks. Machine learning. 20: 273-297.

Dópido, I., Villa, A., Plaza, A., Gamba, P., 2012. A quantitative and comparative assessment of unmixing-based feature extraction techniques for hyperspectral image classification. IEEE Journal of Selected Topics in Applied Earth Observations and Remote Sensing 5, 421-435.

Febrero Bande, M., Oviedo de la Fuente, M., 2012. Statistical computing in functional data analysis: The R package fda. usc. Journal of Statistical Software. 51:1-28.

Gitelson, A. A., Merzlyak, M. N. 1996. Signature analysis of leaf reflectance spectra: algorithm development for remote sensing of chlorophyll. Journal of Plant Physiology 148, 494-500.

Gold, K.M., Townsend, P.A., Chlus, A., Herrmann, I., Couture, J.J., Larson, E.R., Gevens, A.J., 2020a. Hyperspectral measurements enable pre-symptomatic detection and differentiation of contrasting physiological effects of late blight and early blight in potato. Remote Sensing 12, 286.

Gold, K.M., Townsend, P.A., Herrmann, I., Gevens, A.J., 2020b. Investigating potato late blight physiological differences across potato cultivars with spectroscopy and machine learning. Plant Science, 110316.

Gold, K. M., Townsend, P. A., Larson, E. R., Herrmann, I., and Gevens, A. J. 2020c. Contact reflectance spectroscopy for rapid, accurate, and nondestructive *Phytophthora infestans* clonal lineage discrimination. Phytopathology 110, 851-862.

Heim, R., Wright, I., Chang, H.C., Carnegie, A., Pegg, G., Lancaster, E., Falster, D., Oldeland, J., 2018. Detecting myrtle rust (*Austropuccinia psidii*) on lemon myrtle trees using spectral signatures and machine learning. Plant Pathology 67, 1114-1121.

Hennessy, A., Clarke, K., Lewis, M., 2020. Hyperspectral classification of plants: a review of waveband selection generalisability. Remote Sensing 12, 113.

Higgins, B.B., 1927. Physiology and parasitism of *Sclerotium rolfsii* Sacc. Phytopathology 17, 417.

Hillnhütter, C., Mahlein, A.-K., Sikora, R., Oerke, E.-C., 2011. Remote sensing to detect plant stress induced by *Heterodera schachtii* and *Rhizoctonia solani* in sugar beet fields. Field Crops Research 122, 70-77.

Hillnhütter, C., Mahlein, A.-K., Sikora, R.A., Oerke, E.-C., 2012. Use of imaging spectroscopy to discriminate symptoms caused by *Heterodera sch*achtii and *Rhizoctonia solani* on sugar beet. Precision Agriculture 13, 17-32.

Hsu, P.-H., 2007. Feature extraction of hyperspectral images using wavelet and matching pursuit. ISPRS Journal of Photogrammetry and Remote Sensing 62, 78-92.

Jacquemoud, S., Ustin, S.L., 2001. Leaf optical properties: A state of the art. 8th International Symposium of Physical Measurements & Signatures in Remote Sensing. CNES Aussois France, pp. 223-332.

Kemerait, Jr., R.C. 2012. Peanut. In 2008 Georgia Plant Disease Loss Estimates Compiled by D.B. Langston, Jr. The University of Georgia Cooperative Extension, College of Agricultural and Environmental Sciences and College of Family and Consumer Sciences. Ap-102-1. 8p.

Kong, W., Zhang, C., Cao, F., Liu, F., Luo, S., Tang, Y., He, Y., 2018. Detection of sclerotinia stem rot on oilseed rape (*Brassica napus* L.) leaves using hyperspectral imaging. Sensors 18, 1764.

Liakos, K.G., Busato, P., Moshou, D., Pearson, S., Bochtis, D., 2018. Machine learning in agriculture: A review. Sensors 18, 2674.

Luis, J., Ozias-Akins, P., Holbrook, C., Kemerait, R., Snider, J., Liakos, V., 2016. Phenotyping peanut genotypes for drought tolerance. Peanut Science 43, 36.

Mahlein, A.-K., 2016. Plant disease detection by imaging sensors – parallels and specific demands for precision agriculture and plant phenotyping. Plant Disease 100, 241-251.

Mahlein, A.-K., Alisaac, E., Al Masri, A., Behmann, J., Dehne, H.-W., Oerke, E.-C., 2019. Comparison and combination of thermal, fluorescence, and hyperspectral imaging for monitoring Fusarium head blight of wheat on spikelet scale. Sensors 19, 2281.

Mahlein, A.-K., Kuska, M.T., Behmann, J., Polder, G., Walter, A., 2018. Hyperspectral sensors and imaging technologies in phytopathology: state of the art. Annual Review of Phytopathology 56, 535-558.

Mahlein, A.K., Rumpf, T., Welke, P., Dehne, H.W., Plümer, L., Steiner, U., Oerke, E.C., 2013. Development of spectral indices for detecting and identifying plant diseases. Remote Sensing of Environment 128, 21-30.

Mehl, H. L. 2020. Peanut Diseases. In 2020 Virginia Peanut Production Guide. Viginia Cooperative Extension. SPES-177NP. Page 91 -106. Available at, https://www.pubs.ext.vt.edu/SPES/SPES-177/SPES-177.html. Accessed on April 12, 2021.

Merzlyak, M. N., Gitelson, A. A., Chivkunova, O. B., and Rakitin, V. Y. 1999. Non-destructive optical detection of pigment changes during leaf senescence and fruit ripening. Physiologia Plantarum 106, 135-141.

Miao, X., Gong, P., Swope, S., Pu, R., Carruthers, R., Anderson, G.L., 2007. Detection of yellow starthistle through band selection and feature extraction from hyperspectral imagery. Photogrammetric Engineering and Remote Sensing 73, 1005.

Moshou, D., Pantazi, X.-E., Kateris, D., Gravalos, I., 2014. Water stress detection based on optical multisensor fusion with a least squares support vector machine classifier. Biosystems Engineering 117, 15-22.

Mullen, J. 2001. Southern blight, southern stem blight, white mold. The Plant Health Instructor. doi: 10.1094/PHI-I-2001-0104-01. Updated 2006.

Nagasubramanian, K., Jones, S., Sarkar, S., Singh, A.K., Singh, A., Ganapathysubramanian, B., 2018. Hyperspectral band selection using genetic algorithm and support vector machines for early identification of charcoal rot disease in soybean stems. Plant Methods 14, 1-13.

Pedregosa, F., Varoquaux, G., Gramfort, A., Michel, V., Thirion, B., Grisel, O., Blondel, M., Prettenhofer, P., Weiss, R., Dubourg, V., 2011. Scikit-learn: Machine learning in Python. the Journal of Machine Learning Research 12, 2825-2830.

Porter, D. M. 1997. The peanut plant, pp. 1-2. In Compendium of Peanut Diseases, 2nd ed. N.Kokalis-Burelle, D.M. Porter, R Hodrfguez-Kabana, D.H. Smith and P. Subrahmanyam eds. American Phytopathological Society Press, St. Paul, MN.

Punja, Z., Huang, J.-S., Jenkins, S., 1985. Relationship of mycelial growth and production of oxalic acid and cell wall degrading enzymes to virulence in *Sclerotium rolfsii*. Canadian Journal of Plant Pathology 7, 109-117.

Punja, Z.K., 1985. The biology, ecology, and control of *Sclerotium rolfsii*. Annual Review of Phytopathology 23, 97-127.

Raza, M.M., Harding, C., Liebman, M., Leandro, L.F., 2020. Exploring the potential of high-resolution satellite imagery for the detection of soybean sudden death syndrome. Remote Sensing 12, 1213.

Rumpf, T., Mahlein, A.-K., Steiner, U., Oerke, E.-C., Dehne, H.-W., Plümer, L., 2010. Early detection and classification of plant diseases with support vector machines based on hyperspectral reflectance. Computers and Electronics in Agriculture 74, 91-99.

Samuel, A.L., 1959. Some studies in machine learning using the game of checkers. IBM Journal of Research and Development 3, 210-229.

Savitzky, A., Golay, M.J., 1964. Smoothing and differentiation of data by simplified least squares procedures. Analytical Chemistry 36, 1627-1639.

Shokes, F.M., Różalski, K., Gorbet, D.W., Brenneman, T.B., Berger, D.A., 1996. Techniques for inoculation of peanut with *Sclerotium rolfsii* in the greenhouse and field. Peanut Science 23, 124-128.

Silva, G., Tomlinson, J., Onkokesung, N., Sommer, S., Mrisho, L., Legg, J., Adams, I.P., Gutierrez-Vazquez, Y., Howard, T.P., Laverick, A., 2021. Plant pest surveillance: from satellites to molecules. Emerging Topics in Life Sciences. doi: https://doi.org/10.1042/ETLS20200300

Singh, A., Ganapathysubramanian, B., Singh, A.K., Sarkar, S., 2016. Machine learning for high-throughput stress phenotyping in plants. Trends in Plant Science 21, 110-124.

Singh, A., Jones, S., Ganapathysubramanian, B., Sarkar, S., Mueller, D., Sandhu, K., Nagasubramanian, K., 2020. Challenges and opportunities in machine-augmented plant stress phenotyping. Trends in Plant Science. 26, 53-69.

Stalker, H., 1997. Peanut (*Arachis hypogaea* L.). Field Crops Research 53, 205-217.

Stevens, A., Ramirez-Lopez, L. 2014. An introduction to the prospectr package. *R Package Vignette, Report No.: R Package Version 0.1*, *3*.

Sun, W., Du, Q., 2019. Hyperspectral band selection: A review. IEEE Geoscience and Remote Sensing Magazine 7, 118-139.

Sun, W., Halevy, A., Benedetto, J.J., Czaja, W., Liu, C., Wu, H., Shi, B., Li, W., 2014. UL-Isomap based nonlinear dimensionality reduction for hyperspectral imagery classification. ISPRS Journal of Photogrammetry and Remote Sensing 89, 25-36.

Thenkabail, P. S., Enclona, E. A., Ashton, M. S., and Van Der Meer, B. 2004. Accuracy assessments of hyperspectral waveband performance for vegetation analysis applications. Remote Sensing of Environment 91, 354-376.

Venkatachalam, M., Sathe, S.K., 2006. Chemical composition of selected edible nut seeds. Journal of Agricultural and Food Chemistry 54, 4705-4714.

Weeks, J. R., Hartzog, D. L., Hagan, A., French, J. C., Everest, J. W., and Balch, T. 1991. Peanut pest management scout manual. ANR-598. Alabama Cooperative Extension Service. Available at, https://ssl.acesag.auburn.edu/pubs/docs/A/ANR-0598/ANR-0598-archive.pdf. Revised Aug 2000. Accessed on April 12, 2021.

Wei, X., Langston, D., Mehl, H.L., 2021. Spectral and thermal responses of peanut to infection and colonization with *Athelia rolfsii*. PhytoFrontiers. doi: http://doi.org/10.1094/PHYTOFR-07-20-0008-R

Yang, C., Lee, W.S., Gader, P., 2014. Hyperspectral band selection for detecting different blueberry fruit maturity stages. Computers and Electronics in Agriculture 109, 23-31.

Zarco-Tejada, P., Camino, C., Beck, P., Calderon, R., Hornero, A., Hernández-Clemente, R., Kattenborn, T., Montes-Borrego, M., Susca, L., Morelli, M., 2018. Previsual symptoms of *Xylella fastidiosa* infection revealed in spectral plant-trait alterations. Nature Plants 4, 432-439.

Zhu, H., Chu, B., Zhang, C., Liu, F., Jiang, L., He, Y., 2017. Hyperspectral imaging for presymptomatic detection of tobacco disease with successive projections algorithm and machine-learning classifiers. Scientific Reports 7, 1-12.

List of figures and tables

Table 1. The original top 10 features (**a**) and the top 10 features with a custom minimum distance of 20 nm (**b**) selected by different feature selection methods from the scikit-learn machine-learning library in python. Wavelengths selected repeatedly by different methods were highlighted in different colors (Purple = Ultraviolet region; Green = Green region; Red = Red or Red-edge region; Grey = Near-infrared region).

Rank\Methods	Selected wavelengths (nm)				
	Chi-square	SFM_RF	SFM_SVML	RFE_RF	RFE_SVML
(a) Originally selected features					
1	698	496	884	501	505
2	702	884	759	884	396
3	706	665	807	505	302
4	694	501	767	274	391
5	595	690	743	620	261
6	590	686	838	735	653
7	599	826	763	247	514
8	603	505	850	686	884
9	586	628	694	645	763
10	611	492	803	690	830
(b) Features with a custom minimum distance					
1	698	496	884	501	505
2	595	884	759	884	396
3	632	665	807	274	302
4	573	690	838	620	261
5	527	826	694	735	653
6	552	628	649	247	884
7	657	242	242	686	763
8	719	518	731	645	830
9	505	607	674	779	431
10	678	274	586	826	624

Notes: Chi-square = SelectKBest (estimator = Chi-square); SFM_RF = SelectFromModel (estimator = random forest); SFM_SVML = SelectFromModel (estimator = support vector machine with the linear kernel); RFE_RF = Recursive feature elimination (estimator = random forest); RFE_SVML = Recursive feature elimination (estimator = support vector machine with the linear kernel).

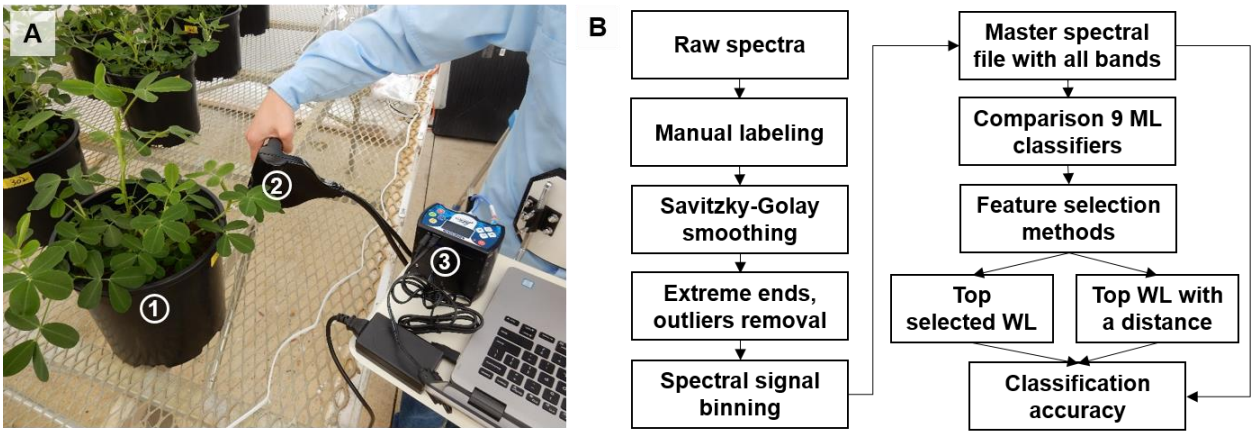

Fig. 1. **A.** Spectral reflectance measurement of peanut leaves with the Jaz spectrometer system: (1) individual potted peanut plant; (2) SpectroClip probe; (3) Jaz spectrometer. **B.** Data analysis pipeline for the wavelength selection to classify healthy peanut plants and plants infected with *Athelia rolfsii* at different stages of disease development. ML = machine learning; WL = wavelengths.

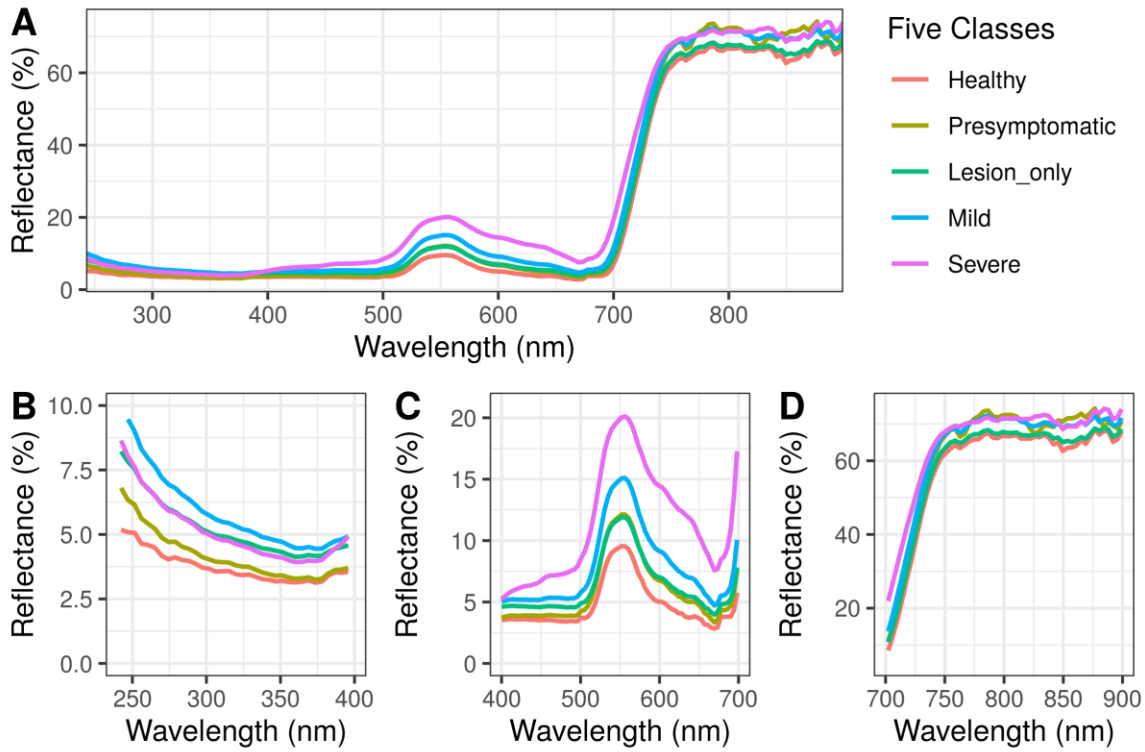

Fig. 2. Spectral profiles of healthy and peanut plants infected with *Athelia rolfsii* at different stages of disease development. **A.** Entire spectral region (240 to 900 nm); **B.** Ultraviolet region (240 to 400 nm); **C**. Visible region (400 to 700 nm). **D**. Near-infrared region (700 to 900 nm).

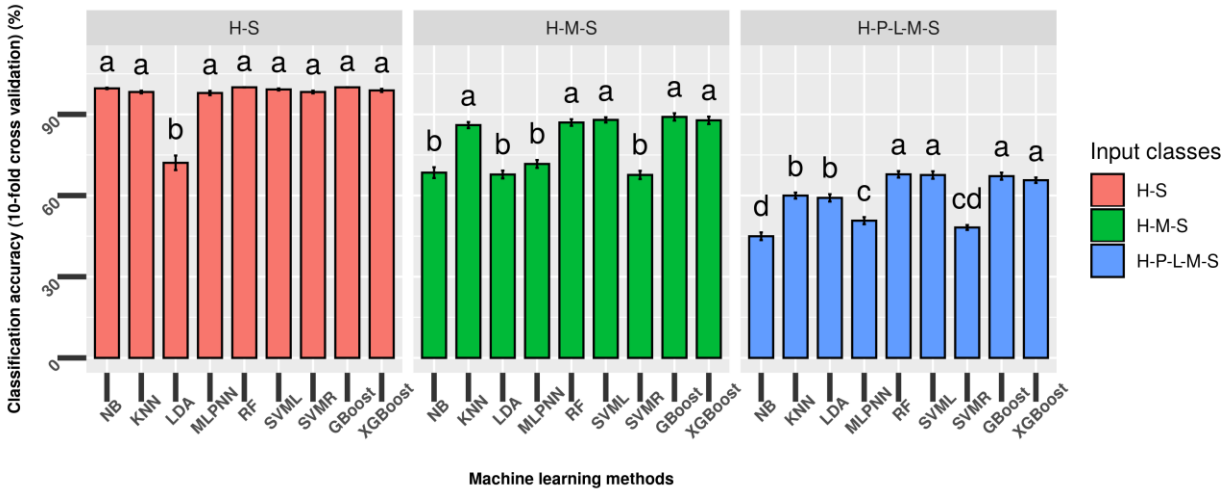

Fig. 3. Comparison of the performance of nine machine learning methods to classify the mock-inoculated healthy peanut plants and plants inoculated with *Athelia rolfsii* at different stages of disease development. Peanut plants from the greenhouse study were categorized based on visual symptomology: H = 'Healthy', mock-inoculated control with no symptoms; P = 'Presymptomatic', inoculated with no symptoms; L = 'Lesion only', inoculated with necrotic lesions on stems only; M = 'Mild', inoculated with mild foliar wilting symptoms (≤ 50% leaves symptomatic); S = 'Severe', inoculated with severe foliar wilting symptoms (> 50% leaves symptomatic). Machine learning methods tested: NB = Gaussian Naïve Bayes; KNN = K-nearest neighbors; LDA = Linear discriminant analysis; MLPNN = Multi-layer perceptron neural network; RF = Random forests SVML = Support vector machine with linear kernel; SVMR = Support vector machine with radial kernel; GBoost = gradient boosting; XGBoost = extreme gradient boosting. Bars with different letters were statistically different using Tukey honestly significant difference (HSD) test with α level of 0.05. Error bars indicate standard deviation of accuracy using stratified 10-fold cross-validation repeated three times.

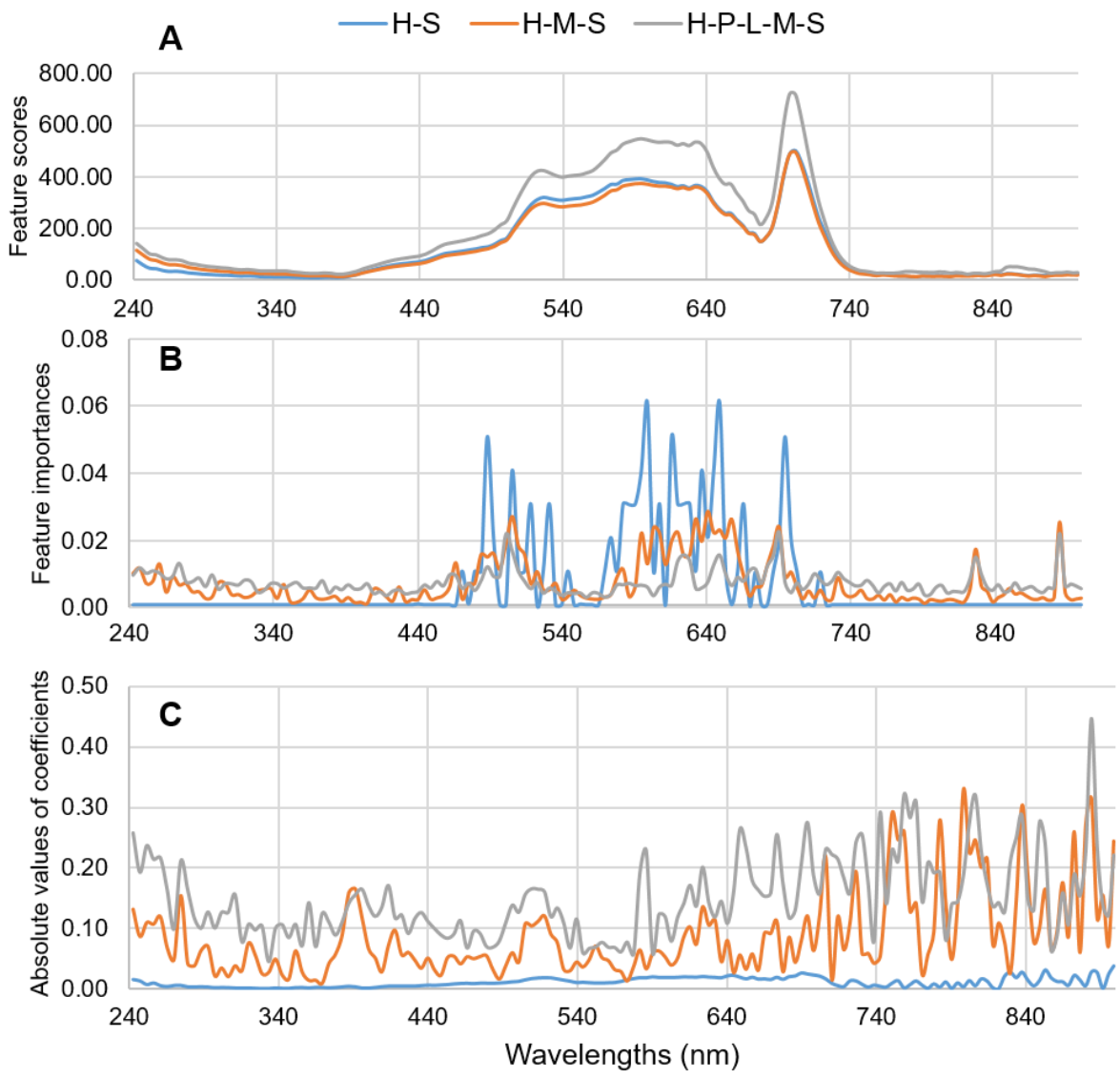

Fig. 4. The weights of each feature/wavelength calculated by three different machine learning algorithms for the classification of models with varying classes of input. **A**. the Chi-square method; **B.** Random forest; **C.** Support vector machine with a linear kernel. H = 'Healthy', mock-inoculated control with no symptoms; P = 'Presymptomatic', inoculated with no symptoms; L = 'Lesion only', inoculated with necrotic lesions on stems only; M = 'Mild', inoculated with mild foliar wilting symptoms (≤ 50% leaves symptomatic); S = 'Severe', inoculated with severe foliar wilting symptoms (> 50% leaves symptomatic).

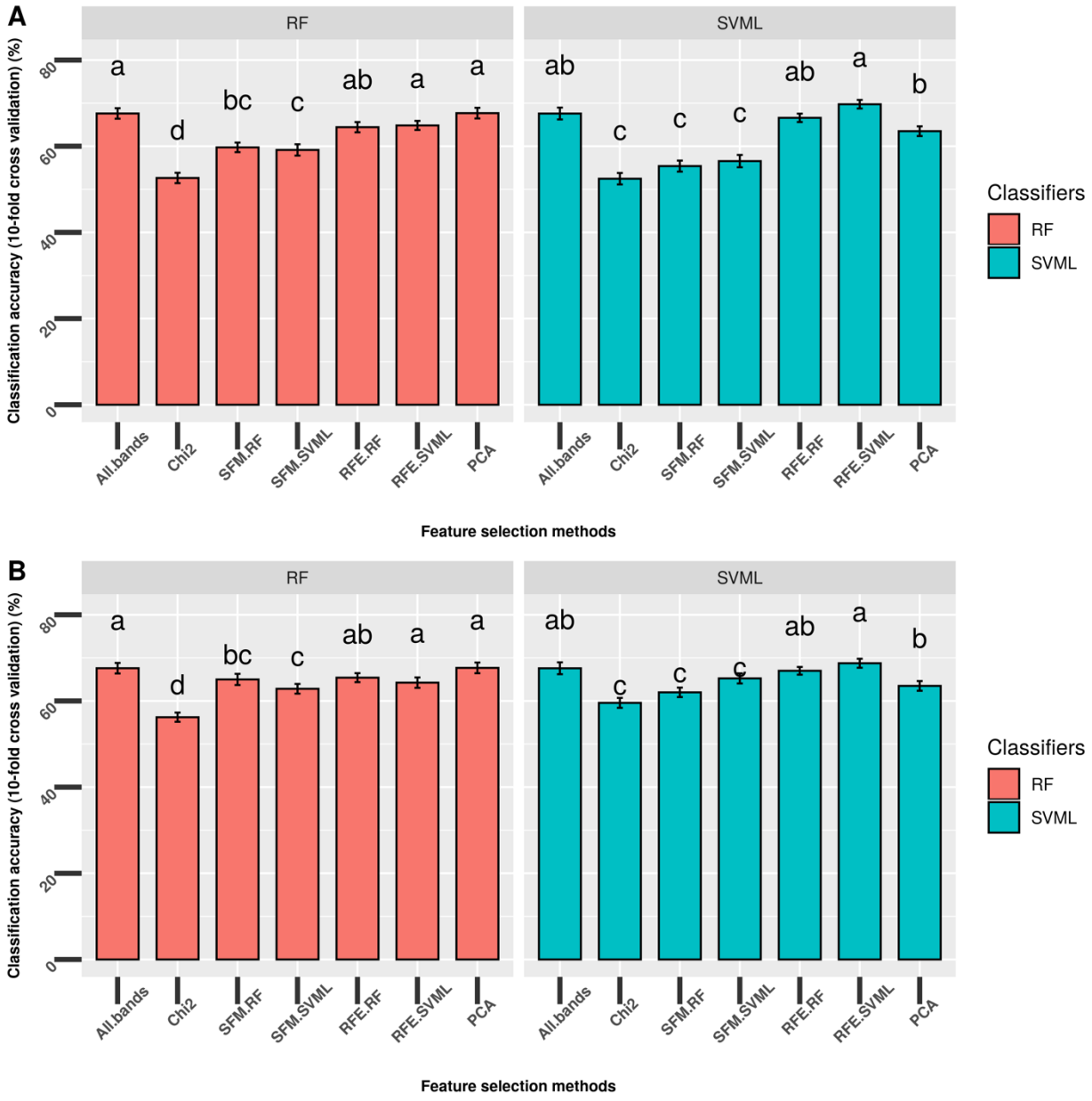

Fig. 5. Comparison of the performance of original top 10 selected wavelengths (**A**) and top 10 features with a minimum of 20 nm distance (**B**) by different feature selection methods to classify the mock-inoculated healthy peanut plants and plants inoculated with *Athelia rolfsii* at different stages of disease development (input data = all five classes). Feature selection methods tested: Chi2 = SelectKBest (estimator = Chi-square); SFM-RF = SelectFromModel (estimator = random forest); SFM-SVML = SelectFromModel (estimator = support vector machine with linear kernel);

RFE-RF = Recursive feature elimination (estimator = random forest); RFE-SVML = Recursive feature elimination (estimator = support vector machine with linear kernel). The top 10 components were used as input data for the principal component analysis (PCA) method. The two classifiers tested: RF = random forest; SVML = support vector machine with the linear kernel. Bars with different letters were statistically different using Tukey honestly significant difference (HSD) test with an α level of 0.05. Error bars indicate standard deviation of accuracy using stratified 10-fold cross-validation repeated three times.

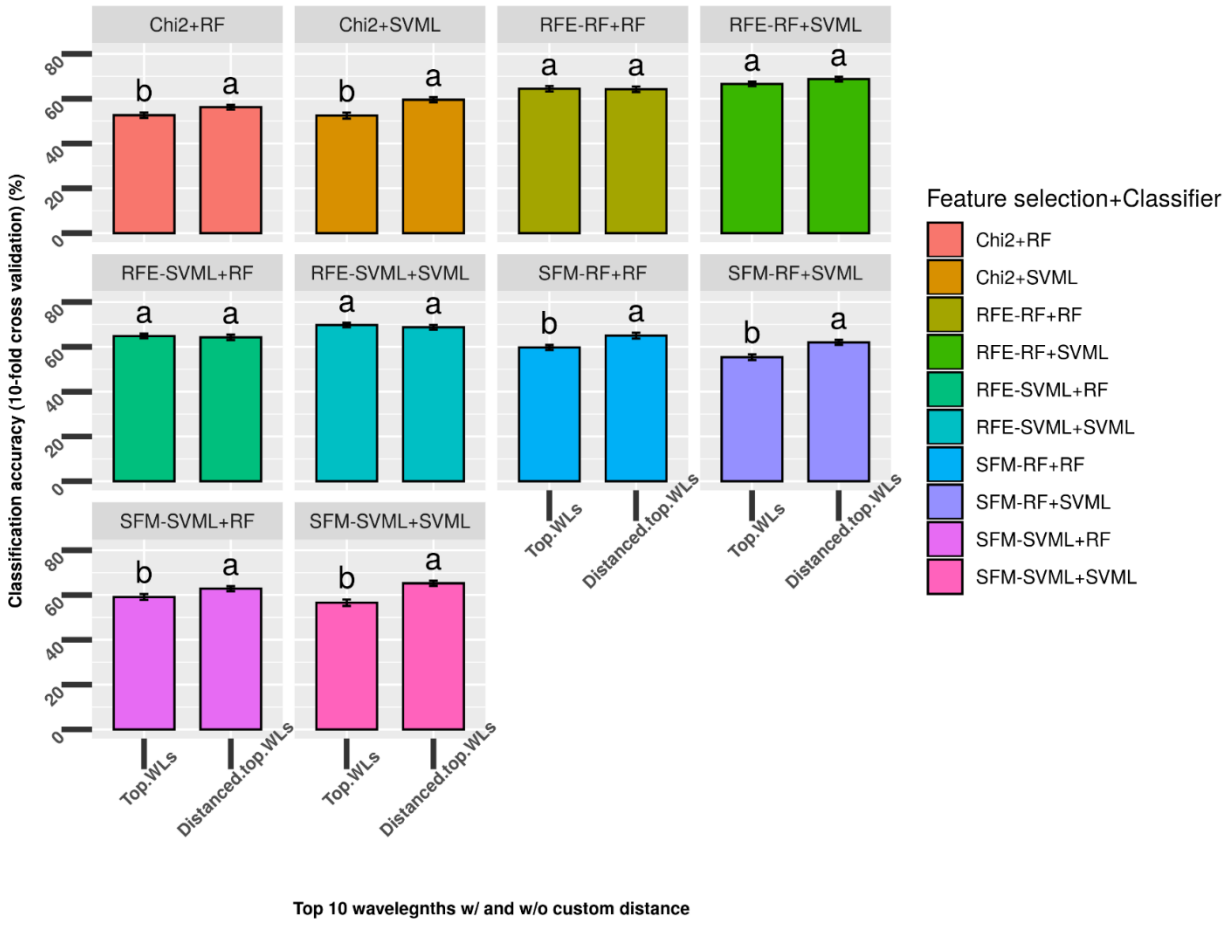

Fig. 6. Comparison of top 10 selected wavelengths (WLs) with top 10 WLs with a minimum 20 nm distance between each feature. Five features selection methods were tested, including Chi2 = SelectKBest (estimator = Chi-square); SFM-RF = SelectFromModel (estimator = random forest); SFM-SVML = SelectFromModel (estimator = support vector machine with linear kernel); RFE-RF = Recursive feature elimination (estimator = random forest); RFE-SVML = Recursive feature elimination (estimator = support vector machine with linear kernel). Each feature selection were tested using two classifiers, RF = random forest and SVML = support vector machine with the linear kernel. Bars with different letters were statistically different using Tukey honestly significant difference (HSD) test with an α level of 0.05. Error bars indicate standard deviation of accuracy using stratified 10-fold cross-validation repeated three times.

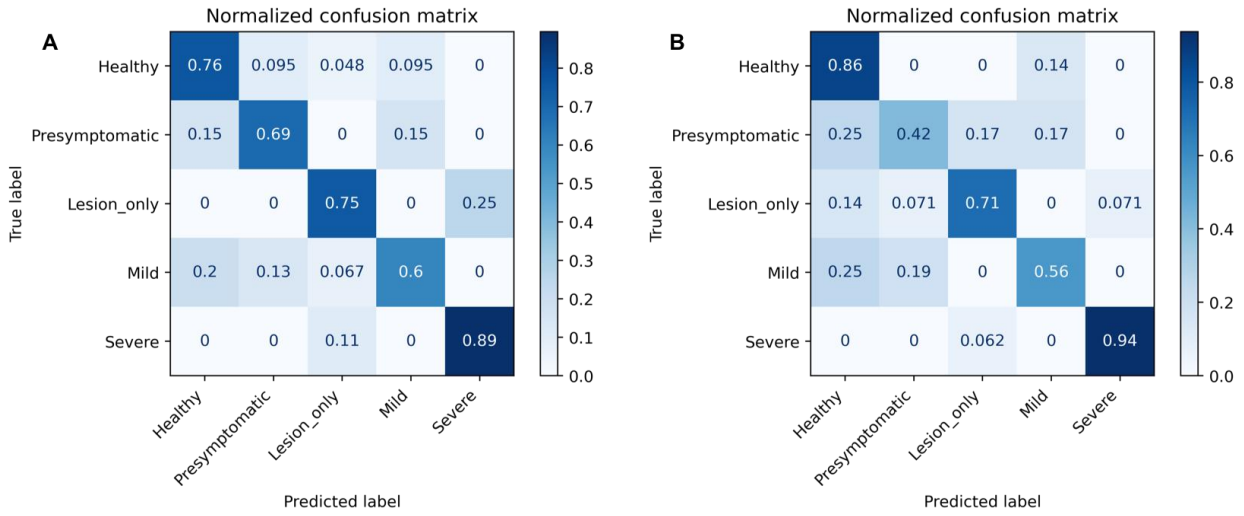

Fig. 7. Confusion matrix for using all wavelengths (**A**) and the selected top 10 wavelengths (**B**) to classify mock-inoculated healthy peanut plants and plants inoculated with *Athelia rolfsii* at different stages of disease development. Feature selection method = recursive feature elimination with an estimator of support vector machine the linear kernel (RFE-SVML); Classifier = SVML.

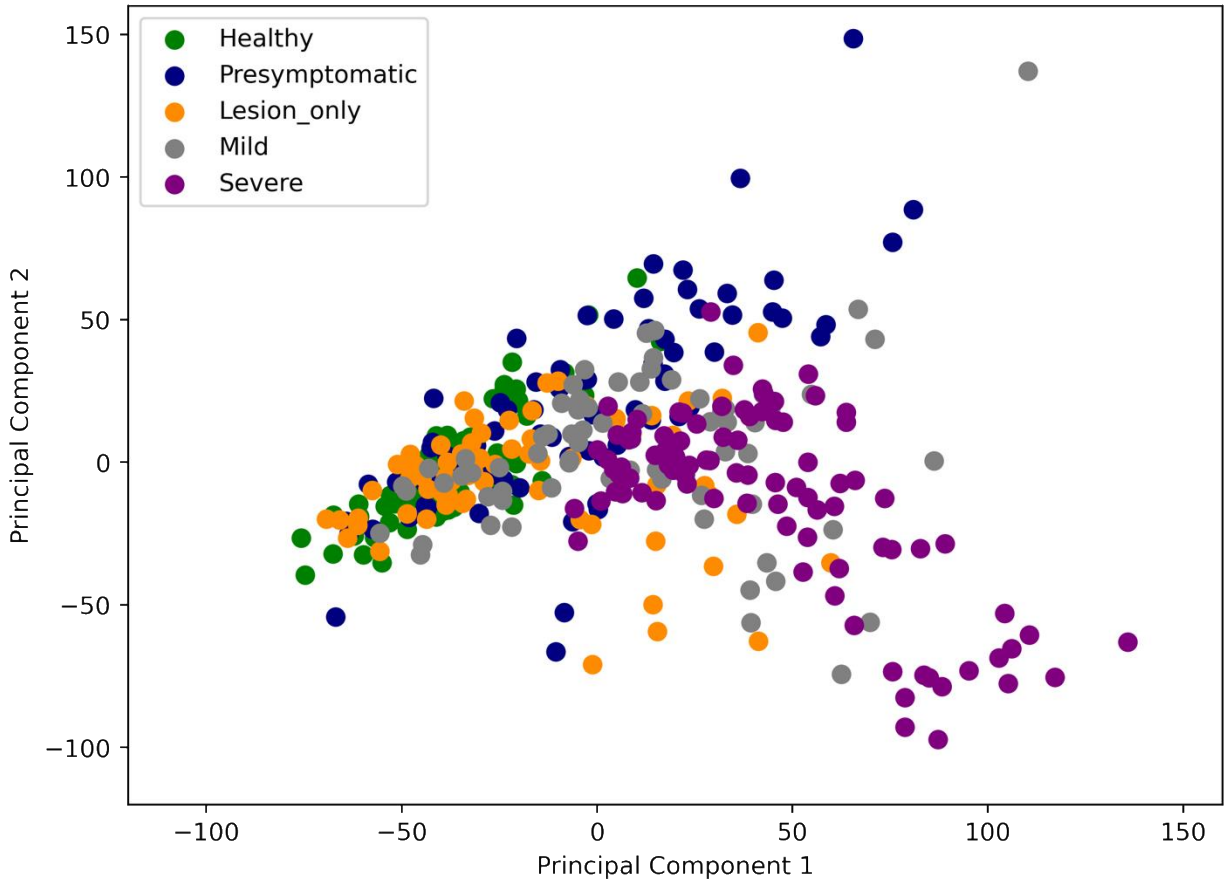

Fig. S1. The top two principal components of spectra collected from the mock-inoculated healthy peanut plants and plants inoculated with *Athelia rolfsii* at different stages of disease development. H = 'Healthy', mock-inoculated control with no symptoms; P = 'Presymptomatic', inoculated with no symptoms; L = 'Lesion only', inoculated with necrotic lesions on stems only; M = 'Mild', inoculated with mild foliar wilting symptoms (≤ 50% leaves symptomatic); S = 'Severe', inoculated with severe foliar wilting symptoms (> 50% leaves symptomatic).

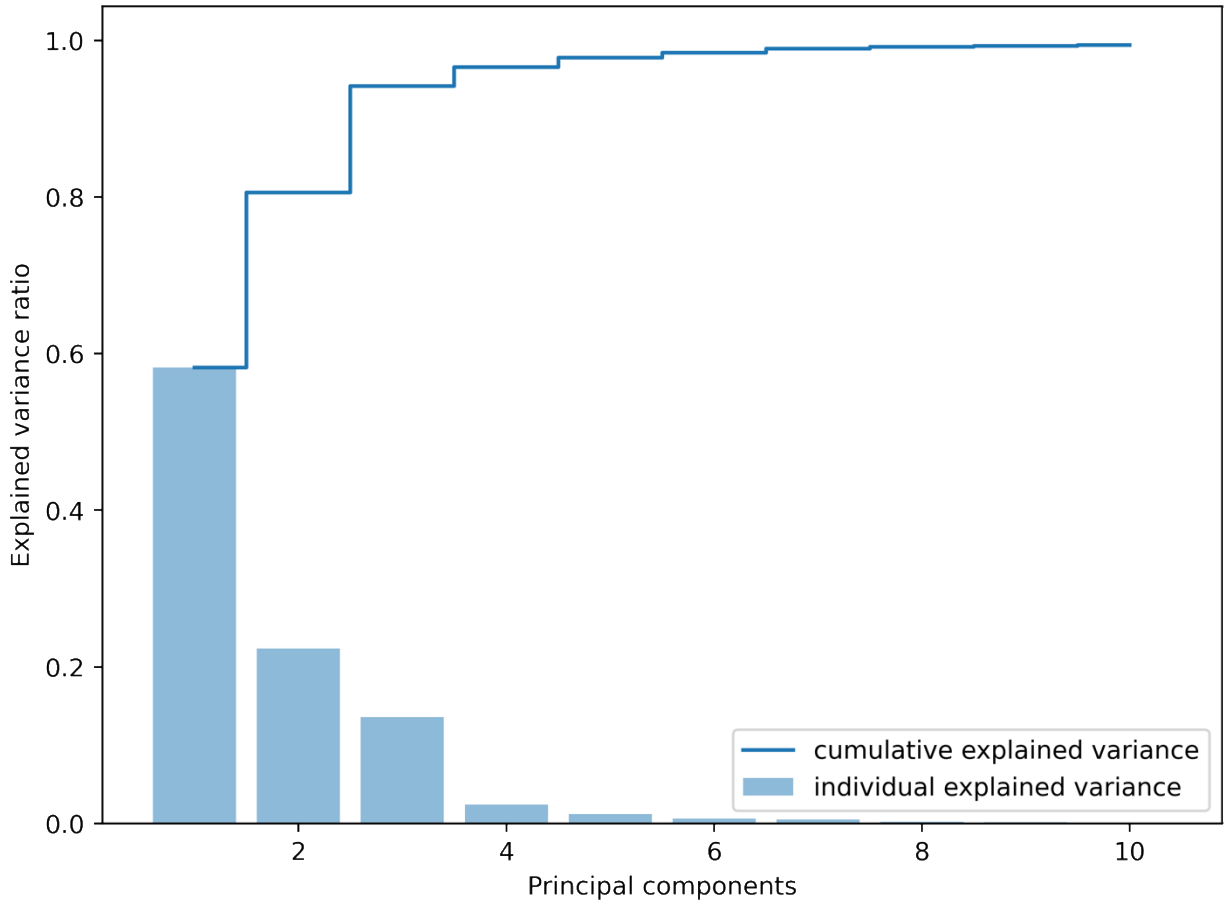

Fig. S2. The individual and cumulative explained variance for the top 10 principal components for the classification of the mock-inoculated healthy peanut plants and plants inoculated with *Athelia rolfsii* at different stages of disease development.

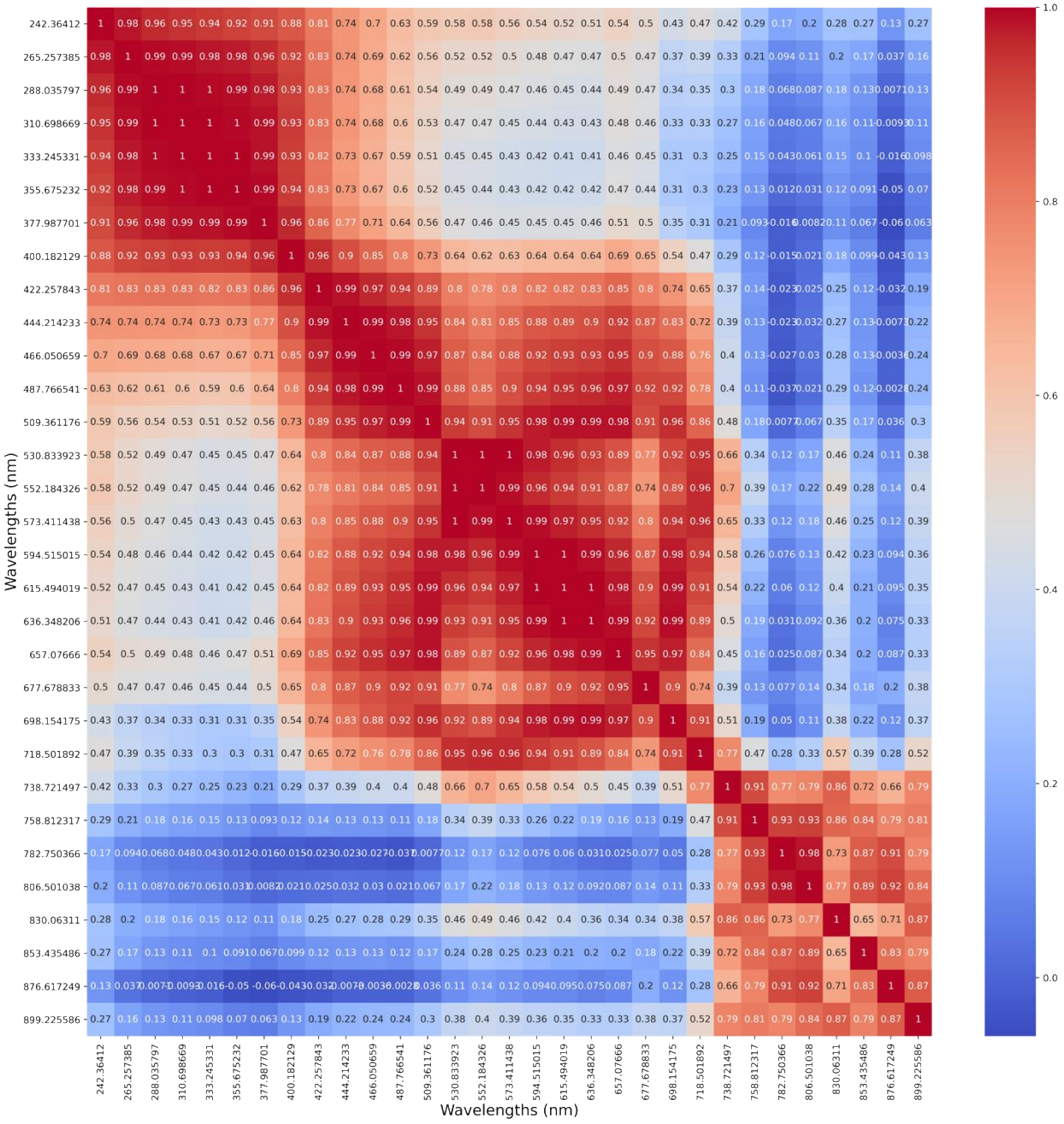

Fig. S3. Correlation heatmap of a subset of wavelengths in the spectra collected from the mock-inoculated healthy peanut plants and plants inoculated with *Athelia rolfsii* at different stages of disease development.

CHAPTER 4: Detection of soilborne disease utilizing sensor technologies: Lessons learned from studies on stem rot of peanut

Xing Wei[1,2], Marcela Aguilera[2,3], Rachael Walcheck[1,4,5], Dorothea Tholl[5], Song Li[2], David B. Langston, Jr.[1,2], and Hillary L. Mehl[1,2,6]

[1]Virginia Tech Tidewater Agricultural Research and Extension Center, Suffolk, VA, 23437; [2]School of Plant and Environmental Sciences, Virginia Tech, Blacksburg, VA 24061; [3]Genetics, Bioinformatics, and Computational Biology Program, Virginia Tech, Blacksburg, VA 24061; [4]Microbiology Undergraduate Program, Iowa State University, Ames, IA 50011; [5]Department of Biological Sciences, Virginia Tech, Blacksburg, VA 24061; [6]Current address: United States Department of Agriculture, Agricultural Research Service, Arid-Land Agricultural Research Center, Tucson, AZ 85701

Author Contributions: Studies on spectral and thermal sensors, X.W., D.B.L., and H.L.M; machine learning analysis of spectral data, X.W., M.A., and S.L.; Volatile compound studies, X.W., R.W., D.T., and H.L.M.; writing—original draft preparation, X.W. and H.L.M.; writing—review and editing, X.W., M.A., R.W., D.T., S.L., D.B.L., and H.L.M.; supervision, H.L.M.; funding acquisition, D.B.L. and H.L.M. All authors have reviewed the manuscript prior to publication.

Note: This manuscript was accepted by the journal Plant Health Progress on 12 Apr 2021.

Abstract

Soilborne plant diseases are a major constraint to crop production worldwide. Effective and economical management of these diseases is dependent on the ability to accurately detect and diagnose their signs and/or symptoms prior to widespread development in a crop. Sensor-based technologies are promising tools for automated crop disease detection, but research is still needed to optimize and validate methods for the detection of specific plant diseases. The overarching goal of our research is to use the peanut-stem rot plant disease system to identify and evaluate sensor-based technologies that can be utilized for the detection of soilborne plant diseases. Here we summarize the current state of sensor-based technologies for plant disease detection and provide examples from our own research that illustrate the advantages and limitations of different sensor-based methods for detecting soilborne diseases. In addition, the potential to adapt different sensor-based technologies to practical use in the field is discussed.

Introduction

Soilborne plant pathogens, which cause seedling, vascular, and root rot diseases, are detrimental to global food production (Katan 2017; Oerke 2006). These diverse pathogens, which include fungi, oomycetes, bacteria, viruses, and nematodes, share a common feature of spending at least part of their life cycle in the soil (Bruehl 1987; Katan 2017). Management of soilborne pathogens is challenging because the inoculum can survive in the soil without the crop host for long periods of time. In addition, these pathogens typically have a broad host range (Divya Rani and Sudini 2013), and it is laborious and time-consuming to manually detect and identify specific diseases in the field. Inexpensive and reliable disease detection, identification, and quantification are needed to optimize disease control strategies, help growers make management decision, and

maximize net profits (Bock et al. 2010; Nutter 1990; Nutter et al. 1991; Nutter et al. 1993). Sensor technologies are a promising tool for automated plant disease detection, identification, and quantification, and this is a rapidly expanding area of research (Mahlein 2016; Nutter 1990; Oerke 2020).

Sensors that can potentially be used for plant disease identification fall into two general categories: optical and non-optical (Fig. 1) (Oerke et al. 2014). Various types of optical sensors have been used for plant disease detection. These include RGB, multi- and hyperspectral reflectance, thermal, fluorescence, and light detection and ranging (LiDAR) sensors (Mahlein 2016; Oerke 2020). Among these sensors, spectral reflectance and infrared thermography (IRT) are of particular interest in plant disease detection and plant phenotyping because they can be utilized with ground-based, airborne, and satellite-based platforms (Mahlein 2016; Oerke et al. 2014). Among the non-optical type sensors, those that can detect volatile organic compounds (VOCs) emitted by the plant and/or pathogen during disease development have been utilized the most for plant disease detection. These include but are not limited to VOC trapping devices coupled with gas chromatography-mass spectrometry (GC-MS), electronic noses (e-nose), and other novel VOC sensors (Fig. 1) (Li et al. 2019; Oerke 2020). Though there has recently been an exponential increase in research aimed at utilizing various sensor technologies for plant disease detection, additional studies and technological improvements aimed at identifying and detecting disease-specific signatures are needed before they can be used as a practical tool for in-field plant disease detection and site-specific management.

The sensitivity and specificity of sensor-based methods, which highly depend on spatial resolution, are critical to detect and identify plant diseases caused by microorganisms (Oerke et al. 2014). The spatial resolution, referring to the minimum size of a pixel in image-based optical

sensors, relies on the distance between the sensor and the object (Mahlein 2016; Oerke et al. 2014). Proximal sensing platforms are suitable for disease detection at leaf and plant scale, while remote sensing with airborne platforms is useful for detecting soilborne disease patches in the field or in later stages of disease epidemics (Hillnhütter et al. 2011; Mahlein et al. 2012; Nutter et al. 2010; Oerke et al. 2014). In addition to spatial resolution, Hillnhütter and Mahlein (2008) suggested spectral resolution and temporal factors are also essential for detecting small areas in a field, a critical capacity during the early stage of disease development.

Currently, one of the major limitations to using sensors for plant disease detection is the lack of an efficient method to analyze and interpret the great amount of complex data generated with sensor measurements (Mahlein 2016; Moran et al. 1997). Machine learning algorithms are a very promising approach that can be used to collate and statistically evaluate large amounts of sensor data more efficiently and without explicit programing (Samuel 1959; Singh et al. 2016). Along with sensor technologies, machine learning approaches have been increasingly applied in precision crop management for yield prediction and detection of abiotic and biotic stresses like pest insects, diseases, and weeds (Liakos et al. 2018; Mahlein et al. 2018). Machine learning algorithms are capable of generalizing trends or patterns from large amounts of data efficiently (Singh et al. 2016), which is essential for timely application of crop management practices based on sensor technologies.

Exploring sensor-based methods to detect stem rot of peanut

Stem rot, caused by *Athelia rolfsii* (anamorph *Sclerotium rolfsii*), is one of the most economically important soilborne diseases of peanut (*Arachis hypogaea* L., also known as groundnut) worldwide. Yield loss caused by this disease is typically less than 25% but can be up

to 80% under conditions favorable to *A. rolfsii*, which include warm to hot temperatures (27 to 30 ºC) and high relative humidity (> 90%) (Backman and Brenneman 1997; Punja 1985). The initial symptoms exhibited by peanut plants infected with *A. rolfsii* are water-soaked necrotic lesions on stems, roots, pegs, or pods, while the foliar symptoms include wilting of a single lateral branch, the main stem, or the entire plant (Fig. 2) (Backman and Brenneman 1997). Signs of the pathogen include white appressed mycelium and brown round sclerotia, which are usually found at or near the soil line on and around the affected plant parts (Fig. 2).

Foliar applied fungicides are used for management of stem rot, but they are most effective when applied prior to or during the early stages of infection. As with other soilborne crop diseases, scouting via visual inspection is frequently used to detect signs and symptoms of the disease and make management decisions. However, with the expansion of data-based, site-specific crop management, there is a need and demand for automated sensor-based plant disease detection. Using the peanut-stem rot plant disease system, the overarching goals of our research are to 1) identify and evaluate multiple sensor-based technologies that can be utilized for detection of soilborne plant diseases and 2) explore the benefits and limitations of each, including their relative sensitivity and specificity as well as potential to be adapted to field use.

Spectral signatures of peanut plants infected with *A. rolfsii*

Greenhouse experiments were conducted at the Virginia Tech Tidewater Agricultural Research and Extension Center (AREC) in Suffolk, VA, to identify responses of peanut to infection with *A. rolfsii* under controlled conditions (Wei et al. 2019, 2020, and 2021). Approximately 70-day-old ‘Sullivan’ peanut plants were either inoculated with *A. rolfsii* or mock-inoculated via a clothespin technique adapted from Shokes et al. (1996). Briefly, clothespins

colonized with *A. rolfsii* were clamped on lateral stems of peanut plants (Fig. 3A). Non-colonized clothespins were clamped on mock-inoculated control stems. In each experiment, inoculated lateral stems were compared to mock-inoculated controls. Following inoculation, plants were placed inside a moisture chamber to facilitate pathogen infection and disease development. Starting 2 days after inoculation, plants were inspected daily for visual disease symptoms. The rating scale of disease severity was adapted from Shokes et al. (1996), where 1 = healthy without any disease symptoms, 2 = necrotic lesions on the inoculated stems only, 3 = up to 50% leaves on the inoculated stems symptomatic (discoloration, prevalent veins, and wilting), 4 = more than 50% leaves symptomatic, and 5 = withering of whole inoculated stems. Inside the greenhouse, plants were placed outside the moisture chamber during daily measurement, and moved back to the moisture chamber after the measurement was completed.

Spectral reflectance of a designated leaflet on the second youngest leaf on the treated lateral stem was measured daily by a Spectroclip-R probe with a handheld Jaz spectrometer (Fig. 3B), and a machine learning approach was used to analyze the resulting data and identify stem rot-associated spectral signatures. A total of 252 spectra were selected from the greenhouse experiments and assigned into three classes based on disease severity ratings: healthy (scale =1), mildly symptomatic (scale >2 but <4), or severely diseased (scale ≥ 4) based on visual symptomology. Spectral data were analyzed using the R statistical platform with methods adapted from Heim et al. (2018). Extreme ends of spectra were deleted due to noisy signals, and outlying spectra were removed using depth measures (Febrero-Bande and Oviedo de la Fuente 2012). First-order derivatives (FOD) of each spectrum were also calculated to minimize random noise thus improve classification quality (Demetriades-Shah et al. 1990). The random forest algorithm was used for both the classification and feature selection of important wavelengths (Breiman 2001;

Genuer et al. 2015; Kuhn et al. 2017). The spectral dataset was randomly split 80:20 into training and testing subsets. The training data were used to train a random forest classifier to learn patterns to distinguish between healthy and diseased plants and the testing data were used to evaluate how correctly can the trained model classify "unknown" spectra as coming from healthy versus diseased plants.

Overall, leaves of peanut plants infected with *A. rolfsii* exhibited greater reflectance compared to non-infected healthy plants in both visible (VIS) and near-infrared (NIR) regions (Fig. 4), suggesting that infection of peanut stems with *A. rolfsii* results in alteration of pigment concentrations and cell structure of the peanut leaves. Using a machine learning algorithm, it was possible to distinguish healthy, non-infected peanut plants from symptomatic *A. rolfsii*-infected plants with an overall accuracy (OA) greater than 80% (Table 1). Most wavelengths selected by the random forest algorithm as indicative of plant health were from the VIS region (Fig. 4), which agreed with the three visual observation classes of foliar symptoms 'healthy', 'mild', and 'severe'. Additional studies are needed to determine if these wavelengths represent disease-specific signatures of *A. rolfsii* infection in peanuts.

Thermal response of peanut infected with *A. rolfsii*

Thermal responses of peanut plants in the greenhouse experiments described above were measured using a Forward-Looking Infrared (FLIR) Camera at ~ 183 cm above the ground inside the greenhouse**.** When taking thermal images, plants were placed on a wood board covered with a white needled cotton batting to provide a uniform thermal background (Fig. 3C). Soil in each plastic pot was also covered with the white cotton batting. Thermal images were taken daily

following inoculation with *A. rolfsii* to measure changes in canopy temperature as the disease developed over time.

Leaflets on the *A. rolfsii*-inoculated stems had higher temperatures than leaflets on the mock-inoculated and untreated stems at 8 and 12 days after inoculation (Fig. 5B, C). The higher leaf temperature in *A. rolfsii*-infected plants might be due to the reduced water supply to the leaves and reduced evapotranspiration cooling due to fungal colonization of the vascular system of inoculated stems (Nutter 1990; Tu and Tan 1985). Detection of temperature differences between inoculated and non-inoculated peanut stems coincided with the observation of drooping of the terminal leaves on the inoculated stems. However, temperature differences between inoculated and non-inoculated stems were not consistent across all evaluation dates due to variability in environmental conditions during sensor measurements (Wei et al. 2021).

Volatile compounds emitted by *A. rolfsii* infected peanut plants

Peanut plants were inoculated in the greenhouse in order to identify VOCs released during early infection of peanut with *A. rolfsii*. Volatiles were collected from mock-inoculated control plants and plants that were inoculated with *A. rolfsii* 4 and 8 days prior to volatile collection. To inoculate/mock-inoculate peanut plants, 15-cm-diam. plugs of 3 day-old inoculated and non-inoculated agar pieces were placed on the base of the main stem of each plant. Each plant was enclosed in an oven cooking bag and tied shut with a string under the inoculation site to concentrate the emitted volatiles. VOCs were collected for 24 hours from the headspace of each plant using small pumps that pull volatiles on a charcoal trap (Fig. 3D). VOCs were then eluted from the traps with dichloromethane and analyzed by gas chromatography-mass spectrometry (GC-MS).

Emissions of compounds including hexenyl acetate, monoterpenes, the C_{16} homoterpene TMTT ((*E*,*E*)-4,8,12-trimethyltrideca-1,3,7,11-tetraene) and especially the C_{11} homoterpene DMNT ((*E*)-4,8-dimethyl-1,3,7-nonatriene) were elevated in *A. rolfsii*-infected plants 8 days after inoculation (Fig. 6). DMNT and TMTT are common VOCs that are released by angiosperms in response to herbivory and pathogen infection (Attaran et al. 2008; Tholl et al. 2011). DMNT has been previously reported as the predominant compound emitted from peanut plants infected with *A. rolfsii*. The homoterpene also occurs in volatile blends released from peanut damaged by the beet armyworm (*Spodoptera exigua*), and in response to a combination of both pathogen and herbivore attack (Cardoza et al. 2002). However, insect damage causes a substantial emission of several other compounds besides DMNT, which distinguishes this volatile blend from that induced only by fungal infection (Cardoza et al. 2002).

Advantages and limitations of different sensor-based methods for detection of soilborne diseases

Here, we define the sensitivity of a sensor-based method for plant disease detection as being indicative of how early the method can detect the pathogen infection and disease development. A highly sensitive method can detect initial pathogen infection prior to visible disease symptoms. Medium sensitivity detects the disease when symptoms just become visible. Low sensitivity methods can only detect the disease when severe symptoms have developed. We define the specificity of a sensor-based method for plant disease detection as how accurately the method can identify a specific pathogen infection and subsequent disease development. High specificity methods can identify a specific disease with an accuracy greater than 80%. Low specificity indicates the method can distinguish healthy plants and plants under stress, but cannot

determine whether plants are under abiotic or biotic stress. Methods with medium specificity fall in between the above two.

In our studies, we conducted a preliminary evaluation of three sensor-based methods for the detection of stem rot of peanut. With all three methods, it was possible to detect responses of peanut plants to infection with *A. rolfsii*, but the sensitivity and specificity of the sensor measurements varied. Spectral reflectance differed between *A. rolfsii*-infected and non-infected peanut plants, and spectral signatures identified through machine learning algorithms were able to distinguish non-infected peanut plants from those with severe stem rot symptoms. However, the algorithm was less accurate for distinguishing non-infected plants from those with mild symptoms. Thus, the ability of spectral reflectance to accurately detect stem rot during the early stages of disease development is questionable. Foliar diseases (e.g., powdery mildew, rust, and leaf spots) typically have disease-specific symptoms, while symptoms of soilborne diseases might be confounded with abiotic stress such as drought and heat stresses. Nevertheless, hyperspectral sensors have demonstrated the potential to detect diseased plants before visible symptoms developed in several other plant disease systems (Arens et al. 2016; Gold et al. 2020b; Zarco-Tejada et al. 2018) and to distinguish different diseases in various crops (Gold et al. 2020a; Hillnhütter et al. 2011; Mahlein et al. 2013). Thus, overall spectral sensors were rated with a 'medium' sensitivity and 'high' specificity in the potential of identifying soilborne diseases (Table 2).

Thermal responses of peanut to the infection of *A. rolfsii* were detected when foliar symptoms became visible, but these thermal responses were not consistent across all the evaluation dates and were highly influenced by environmental conditions such as air temperature, humidity, and solar radiation (Wei et al. 2021). These results agree with previous studies which suggest that

thermal sensors are highly sensitive in detecting the leaf temperature changes due to changes in plant transpiration rate and water status caused by abiotic and biotic stresses (Chaerle and van der Straeten 2000; Oerke and Steiner 2010; Oerke et al. 2014). However, the potential of using thermal sensors to identify a specific plant disease is limited because plants under different stresses may alter the plant physiology similarly (Nutter et al. 2010), and thermal sensors are highly sensitive to environmental conditions (Oerke et al. 2014). Thus, thermal sensors were rated with a 'medium to high' sensitivity and 'low' specificity in the potential of identifying soilborne diseases (Table 2).

Results in previous studies and ours showed that VOCs could be detected from the pathogen itself (Fravel et al. 2002) and plants during the pathogenesis of pathogen infection (Cardoza et al. 2002). The VOCs collected in *A. rolfsii*-infected peanut plants were reported in peanut plants under other biotic stresses (Cardoza et al. 2002; Fravel et al. 2002) and in other plant systems (Boué et al. 2003; Zhang et al. 2008). While VOC blends differ between pathogen and insect attack (Cardoza et al. 2002), overlap of VOC mixtures in response to multiple stressors makes it more difficult to immediately distinguish one from the other. Thus, the volatile-based detection method was rated with a 'high' sensitivity and 'low to medium' specificity to detect soilborne plant diseases (Table 2).

Currently, there are various types of spectral and thermal sensors available on the market that can be hand-held, mounted on ground-based tractors and robotic systems, airplanes, and satellites. The technical innovation and improvement of spectral and thermal sensors make them also suitable for mounting on unmanned aerial vehicles (UAVs) for large-scale mobile mapping applications (SphereOptics 2017). Therefore, the potential of field application of spectral and thermal sensors is high if the specific disease signatures (spatial and temporal) could be identified.

Recent studies demonstrated the detection of several soilborne diseases with spectral sensors mounted on the UAV (Wang et al. 2020a, b) or satellite (Raza et al. 2020). Aerial infrared thermography has proved useful in characterizing and monitoring the spatial and temporal pattern of soilborne diseases for field application (Pinter et al. 1979; Powell et al. 1976; Schmitz et al. 2004). In addition, Oerke et al. (2014) suggested thermal sensors could be used in screening disease-resistance germplasms in the inoculated experiments where identification of the specific disease is not necessary. The advantages of volatile-based sensors such as e-noses include operational simplicity, non-destructivity, bulk sampling (Cellini et al. 2017) and the potential to identify the original sources of VOCs and disease hotspots in the field based on volatile gradients (Oerke 2020; Oerke et al. 2014). The disadvantages are lower sensitivity and specificity compared to microbiological and molecular methods (Cellini et al. 2017), but these drawbacks might be irrelevant in comparison with optical sensors (Oerke 2020). Several commercial e-nose models have been applied for plant diagnosis purposes (Cellini et al. 2017), but challenges remain regarding sensor performance, sampling, and detection in open areas, and scaling up measurement (Cui et al. 2018). As an alternative to e-noses, new small-scale portable VOC sensors have been developed that appear to be robust against environmental variation of temperature, humidity, and interference (Li et al. 2019). Nevertheless, from a current perspective, VOCs may have more potential in detecting plant diseases under control conditions than in open fields and VOC-based methods could possibly be suitable as secondary techniques in combination with others.

Conclusions

Interdisciplinary research involving plant science, electronics, and computer science closely tied to practical agriculture will advance plant disease detection, identification, and

quantification using sensor technologies, thus improving plant health management (Mahlein 2016). An open and transparent culture of collaboration and communication among experts from different disciplines will foster and accelerate interdisciplinary research (Heim et al. 2019). Future research should include plants under different diseases and abiotic stresses to verify the uniqueness and robustness of these sensor-based signatures to detect soilborne diseases in the field. Sensor-based signatures can be potentially employed together with localized information such as rotation and tillage and weather conditions to provide accurate monitoring and prediction of plant disease epidemics to develop timely and efficient management practices.

Acknowledgments

Studies on spectral and thermal sensors were funded in part by Virginia Peanut Board, Virginia Agricultural Council. The VOC detection study was a research project in the Research and Extension Experimental Learning (REEL) program at Virginia Tech funded by the Agriculture and Food Research Initiative program of the National Institute of Food and Agriculture, USDA (grant no. 2017-67032-26017). We thank Drs. Maria Balota, Wade Thomason, and David McCall (members of the first author's Ph.D. committee) for their great advice on this project. We also thank Sophie LeBlanc for assistance with the VOC analysis, and Robert Wilson, Amy Taylor, Daniel Espinosa for assisting with the greenhouse measurements. Mention of trade names or commercial products in this article is solely for the purpose of providing specific information and does not imply recommendation or endorsement by the U.S. Department of Agriculture. USDA is an equal opportunity provider and employer.

Literature Cited

Arens, N., Backhaus, A., Döll, S., Fischer, S., Seiffert, U., and Mock, H. P. 2016. Non-invasive presymptomatic detection of *Cercospora beticola* infection and identification of early metabolic responses in sugar beet. Front. Plant Sci. 7:1377.

Attaran, E., Rostás, M. and Zeier, J. 2008. *Pseudomonas syringae* elicits emission of the terpenoid (*E*,*E*)-4,8,12-trimethyl-1,3,7,11-tridecatetraene in *Arabidopsis* leaves via jasmonate signaling and expression of the terpene synthase TPS4. Mol. Plant-Microbe Interact. 21:1482-1497.

Backman, P.A., and Brenneman, T.B. 1997. Stem rot, pp. 36-37. In Compendium of Peanut Diseases, 2nd ed. Kokalis-Burelle, N., Porter, D.M., Hodrfguez-Kabana, R., Smith, D. H. and Subrahmanyam, P. eds. American Phytopathological Society Press, St. Paul, MN.

Bock, C. H., Poole, G. H., Parker, P. E., and Gottwald, T. R. 2010. Plant disease severity estimated visually, by digital photography and image analysis, and by hyperspectral imaging. CRC Crit. Rev. Plant Sci. 29:59-107.

Boué, S. M., Shih, B. Y., Carter-Wientjes, C. H., and Cleveland, T. E. 2003. Identification of volatile compounds in soybean at various developmental stages using solid phase microextraction. J. Agric. Food Chem. 51:4873-4876.

Breiman, L. 2001. Random forests. Mach. Learn. 45:5-32.

Bruehl, G. W. 1987. Soilborne plant pathogens. New York: London: Macmillan Pub. Co., Collier Macmillan.

Cardoza, Y. J., Alborn, H. T., and Tumlinson, J. H. 2002. In vivo volatile emissions from peanut plants induced by simultaneous fungal infection and insect damage. J. Chem. Ecol. 28:161-174.

Cellini, A., Blasioli, S., Biondi, E., Bertaccini, A., Braschi, I., and Spinelli, F. 2017. Potential applications and limitations of electronic nose devices for plant disease diagnosis. Sensors. 17:2596.

Chaerle, L. and Van Der Straeten, D. 2000. Imaging techniques and the early detection of plant stress. Trends Plant Sci. 5:495-501.

Cui, S., Ling, P., Zhu, H., and Keener, H. M. 2018. Plant pest detection using an artificial nose system: a review. Sensors. 18:378.

Demetriades-Shah, T. H., Steven, M. D., and Clark, J. A. 1990. High resolution derivative spectra in remote sensing. Remote Sens. Environ. 33:55-64.

Divya Rani, V. and Sudini, H. 2013. Management of soilborne diseases in crop plants: an overview. Int. J. Plant, Animal Environ. Sci. 3:156-164.

Fang, Y. and Ramasamy, R. P. 2015. Current and prospective methods for plant disease detection. Biosensors. 5: 537-561.

Febrero-Bande, M. and Oviedo de la Fuente, M. 2012. Statistical computing in functional data analysis: The R package fda.usc. J. Stat. Softw. 51:1-28.

Fravel, D. R., Connick, W. J., Grimm, C. C., and Lloyd, S. W. 2002. Volatile compounds emitted by sclerotia of *Sclerotinia minor*, *Sclerotinia sclerotiorum*, and *Sclerotium rolfsii*. J. Agric. Food Chem. 50:3761-3764.

Genuer R., Poggi J.-M. and Tuleau-Malot, C. 2015. VSURF: An R package for variable selection using random forests. R J. 7:19-33.

Gold, K. M., Townsend, P. A., Chlus, A., Herrmann, I., Couture, J. J., Larson, E. R., and Gevens, A. J. 2020a. Hyperspectral measurements enable pre-symptomatic detection and

differentiation of contrasting physiological effects of late blight and early blight in potato. Remote Sens. 12:286.

Gold, K. M., Townsend, P. A., Larson, E. R., Herrmann, I., and Gevens, A. J. 2020b. Contact Reflectance Spectroscopy for Rapid, Accurate, and Nondestructive *Phytophthora infestans* Clonal Lineage Discrimination. Phytopathology. 110: 851-862.

Heim, R. H. J., Wright, I. J., Chang, H. C., Carnegie, A. J., Pegg, G. S., Lancaster, E. K., Falster, D.S., and Oldeland, J. 2018. Detecting myrtle rust (*Austropuccinia psidii*) on lemon myrtle trees using spectral signatures and machine learning. Plant Pathol. 67:1114-1121.

Heim, R. H., Carnegie, A. J. and Zarco-Tejada, P. J. 2019. Breaking down barriers between remote sensing and plant pathology. Trop. Plant Pathol. 44:398-400.

Hillnhütter, C., Mahlein, A. K., Sikora, R. A., and Oerke, E. C. 2011. Remote sensing to detect plant stress induced by *Heterodera schachtii* and *Rhizoctonia solani* in sugar beet fields. Field Crops Res. 122:70-77.

Hillnhütter, C., and Mahlein, A. K. 2008. Early detection and localization of sugar beet diseases: New approaches. Gesunde Pflanz. 60:143–149.

Katan, J. 2017. Diseases caused by soilborne pathogens: biology, management and challenges. J. Plant Pathol. 99:305-315.

Kuhn, M., Wing., J., Weston, S., Williams, A., Keefer, C., Engelhard, A., Cooper, T., Mayer, Z., Kenkel, B., R Core Team, Benesty, M., Lescarbeau, R., Ziem, A., Scrucca, L., Tang, Y., Candan, C., and Hunt, T. 2017. CARET: Classification and regression training. R package version 6.0-76. Available from https://cran.r-project.org/web/packages/caret/index.html. Accessed December 14, 2019.

Li, Z., Paul, R., Tis, T.B., Saville, A.C., Hansel, J.C., Yu, T., Ristaino, J.B., and Wei, Q. 2019. Non-invasive plant disease diagnostics enabled by smartphone-based fingerprinting of leaf volatiles. Nat. Plants, 5:856-866.

Liakos, K. G., Busato, P., Moshou, D., Pearson, S., and Bochtis, D. 2018. Machine learning in agriculture: a review. Sensors 18:2674.

Mahlein, A. K., Kuska, M. T., Behmann, J., Polder, G., and Walter, A. 2018. Hyperspectral sensors and imaging technologies in phytopathology: state of the art. Annu. Rev. Phytopathol. 56:535-558.

Mahlein, A. K., Oerke, E. C., Steiner, U., and Dehne, H. W. 2012. Recent advances in sensing plant diseases for precision crop protection. Eur. J. Plant Pathol. 133:197-209.

Mahlein, A. K., 2016. Plant Disease Detection by Imaging Sensors - Parallels and Specific Demands for Precision Agriculture and Plant Phenotyping. Plant Dis. 100: 241-251.

Mahlein, A.K., Rumpf, T., Welke, P., Dehne, H.W., Plümer, L., Steiner, U., and Oerke, E.C. 2013. Development of spectral indices for detecting and identifying plant diseases. Remote Sens. Environ. 128:21-30.

Moran, M. S., Inoue, Y., and Barnes, E. M. 1997. Opportunities and limitations for image-based remote sensing in precision crop management. Remote Sens. Environ. 61:319-346.

Nutter, F. W., Jr. 1990. Remote sensing and image analysis for crop loss assessment. In: Crop Loss Assessment in Rice (pp 93–105). International Rice Research Institute, Manila, The Philippines.

Nutter, F. W., Jr., Gleason, M. L., Jenco, J. H., and Christians, N. L. 1993. Assessing the accuracy, intra-rater repeatability, and inter-rater reliability of disease assessment systems. Phytopathology. 83**:** 806–812.

Nutter, F. W., van Rij, N., Eggenberger, S. K., and Holah, N. 2010. Spatial and temporal dynamics of plant pathogens. Pages 27-50 in: Precision Crop Protection-the Challenge and Use of Heterogeneity, Springer, Dordrecht.

Nutter, F.W., Jr., Teng, P. S., and Shokes, F.M. 1991. Disease assessment terms and concepts. Plant Dis. 75**:** 1187–1188.

Oerke, E. C. 2006. Crop losses to pests. J. Agric. Sci. 144:31.

Oerke, E. C. 2020. Remote Sensing of Diseases. Annu. Rev. Phytopathol. 58:225-252.

Oerke, E. C. and Steiner, U. 2010. Potential of digital thermography for disease control. Pages 167-182 in: Precision crop protection-the challenge and use of heterogeneity, Springer, Dordrecht.

Oerke, E. C., Mahlein, A. K., and Steiner, U. 2014. Proximal sensing of plant diseases. Pages 55-58 in: Detection and Diagnostics of Plant Pathogens, Springer, Dordrecht.

Pinter, P.J., Stanghellini, M.E., Reginato, R.J., Idso, S.B., Jenkins, A.D., and Jackson, R. D. 1979. Remote Detection of Biological Stresses in Plants with Infrared Thermometry. Science 205:585-587.

Powell, N. L., Porter, D. M., and Pettry, D. E. 1976. Use of aerial photography to detect diseases in peanut fields I. Sclerotinia blight. Peanut Sci. 3:21-24.

Punja, Z. K. 1985. The Biology, Ecology, and Control of *Sclerotium rolfsii*. Annu. Rev. Phytopathol. 23:97-127.

Raza, M. M., Harding, C., Liebman, M., and Leandro, L. F. 2020. Exploring the Potential of High-Resolution Satellite Imagery for the Detection of Soybean Sudden Death Syndrome. Remote Sens. 12:1213.

Samuel, A. L. 1959. Some studies in machine learning using the game of checkers. IBM J. Res. Dev. 3:210-229.

Schmitz, A., Kiewnick, S., Schlang, J., and Sikora, R. A. 2004. Use of high resolution digital thermography to detect *Heterodera schachtii* infestation in sugar beets. Commun. Agric. Appl. Biol. Sci. 69:359-363.

Shokes, F. M., Różalski, K., Gorbet, D. W., Brenneman, T. B., and Berger, D. A. 1996. Techniques for Inoculation of Peanut with *Sclerotium rolfsii* in the Greenhouse and Field. Peanut Sci. 23:124-128.

Singh, A., Ganapathysubramanian, B., Singh, A. K., and Sarkar, S. 2016. Machine learning for high-throughput stress phenotyping in plants. Trends Plant Sci. 21:110-124.

SphereOptics. 2017. Remote Sensing & Proximal Sensing. Available from https://sphereoptics.de/en/application/remote-sensing-proximal-sensing/. Accessed on November 14, 2020.

Tholl, D., Sohrabi, R., Huh, J.-H. and Lee, S. 2011 The biochemistry of homoterpenes – Common constituents of floral and herbivore-induced plant volatile bouquets. Phytochemistry 72:1635-1646.

Tu, J. C., and Tan, C. S. 1985. Infrared thermometry for determination of root rot severity in beans. Phytopathology, 75:840-844.

Wang, T., Thomasson, J. A., Isakeit, T., Yang, C., and Nichols, R. L. 2020a. A Plant-by-Plant Method to Identify and Treat Cotton Root Rot Based on UAV Remote Sensing. Remote Sens. 12:2453.

Wang, T., Thomasson, J. A., Yang, C., Isakeit, T., and Nichols, R. L. 2020b. Automatic Classification of Cotton Root Rot Disease Based on UAV Remote Sensing. Remote Sens. 12:1310.

Wei, X., Aguilera, M., Li, S., Langston Jr., D. B., and Mehl, H. L. 2020. Identification of sensor-based signatures of peanut infection with *Athelia rolfsii* using machine learning. (Abstr.) Phytopathology. 110:S2.207. doi: 10.1094/PHYTO-110-12-S2.207

Wei, X., Langston Jr., D. B., and Mehl, H. L. 2019. Spectral and thermal signatures of early infection of peanut with *Sclerotium rolfsii*. (Abstr.) Phytopathology. 109:S2.1. doi: 10.1094/PHYTO-109-10-S2.1

Wei, X., Langston Jr., D. B., and Mehl, H. L. 2021. Spectral and thermal responses of peanut to the infection and colonization with *Athelia rolfsii*. PhytoFrontiers. doi: 10.1094/PHYTOFR-07-20-0008-R

Zarco-Tejada, P. J., Camino, C., Beck, P. S. A., Calderon, R., Hornero, A., Hernández-Clemente, R., Kattenborn, T., Montes-Borrego, M., Susca, L., Morelli, M., Gonzalez-Dugo, V., North, P. R. J., Landa, B. B., Boscia, D., Saponari, M., and Navas-Cortes, J. A. 2018. Previsual symptoms of *Xylella fastidiosa* infection revealed in spectral plant-trait alterations. Nat. Plants. 4:432-439.

Zhang, Z. M., Wu, W. W., and Li, G. K. 2008. A GC—MS study of the volatile organic composition of straw and oyster mushrooms during maturity and its relation to antioxidant activity. J. Chromatogr. Sci. 46:690-696.

Table 1. Classification accuracy of stem rot of peanut using first-order derivative-transformed spectra of the second youngest mature leaflets on *Athelia rolfsii*-inoculated and mock-inoculated peanut stems.

Parameters	Reference			Total	User's accuracy[c] (%)
	Healthy	Mild	Severe		
Prediction					
Healthy	14[a]	2	0	16	87.5
Mild	1	10	0	11	90.9
Severe	0	2	18	20	90.0
Total	15	14	18	47	
Producer's accuracy[b] (%)	93.3	71.4	100.0		89.4[d]

[a]Numbers in the diagonals were the correctly classified samples, while off-diagonals were misclassified.

[b]Producer's accuracy was the number of correctly classified samples divided by the total number of reference samples in each class. It represents the classification accuracy for each specific class.

[c]User's accuracy was the number of correctly classified samples divided by the total number of prediction samples in each class. It represents the reliability of the classification accuracy for each specific class.

[d]Overall accuracy was the total number correctly classified samples divided by the total number of samples. It represents the overall agreement between the reference and prediction.

Table 2. Comparison of the sensitivity, specificity, and potential field application (and its platform) of using spectral, thermal and volatile sensors for the detection of soilborne diseases in the field (Oerke et al. 2014, adapted).

Sensor type	Sensitivity	Specificity	Potential field application (and its platform)
Spectral sensors	Medium	High	High (ground-based, UAV[a], airborne, and space-borne)
Thermal sensors	Medium-High	Low	High (ground-based, UAV, airborne, and space-borne)
Volatile sensors	High	Low-Medium	Low-Medium (ground-based, UAV, airborne)

[a]UAV = unmanned aerial vehicle.

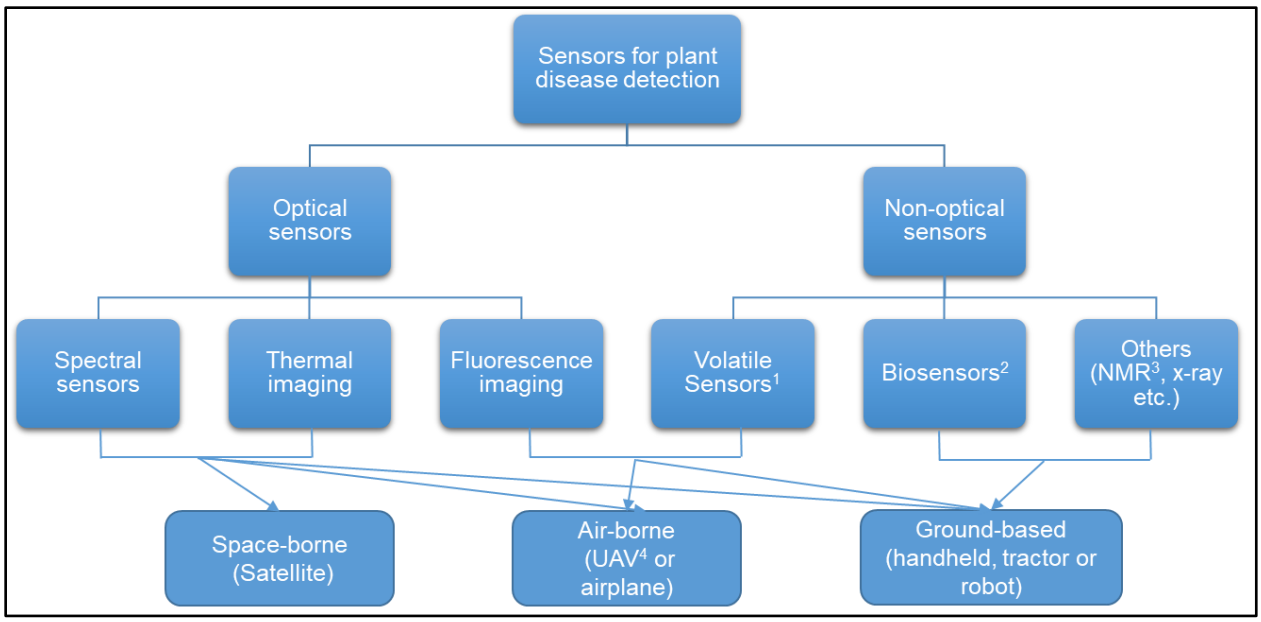

Fig. 1. Commonly used sensors for plant disease detection and their application platform (adapted based on information from Oerke et al. 2014; Mahlein 2016; Fang and Ramasamy 2015). [1]Volatile sensors include portable gas chromatography-mass spectrometry (GC-MS) systems and Electronic noses (E-nose). [2]Biosensors are sensors based on highly selective bio-recognition elements such as enzyme, antibody, DNA-RNA, and bacteriophage (Fang and Ramasamy 2015); [3]NMR = Nuclear magnetic resonance; [4]UAV = unmanned aerial vehicle.

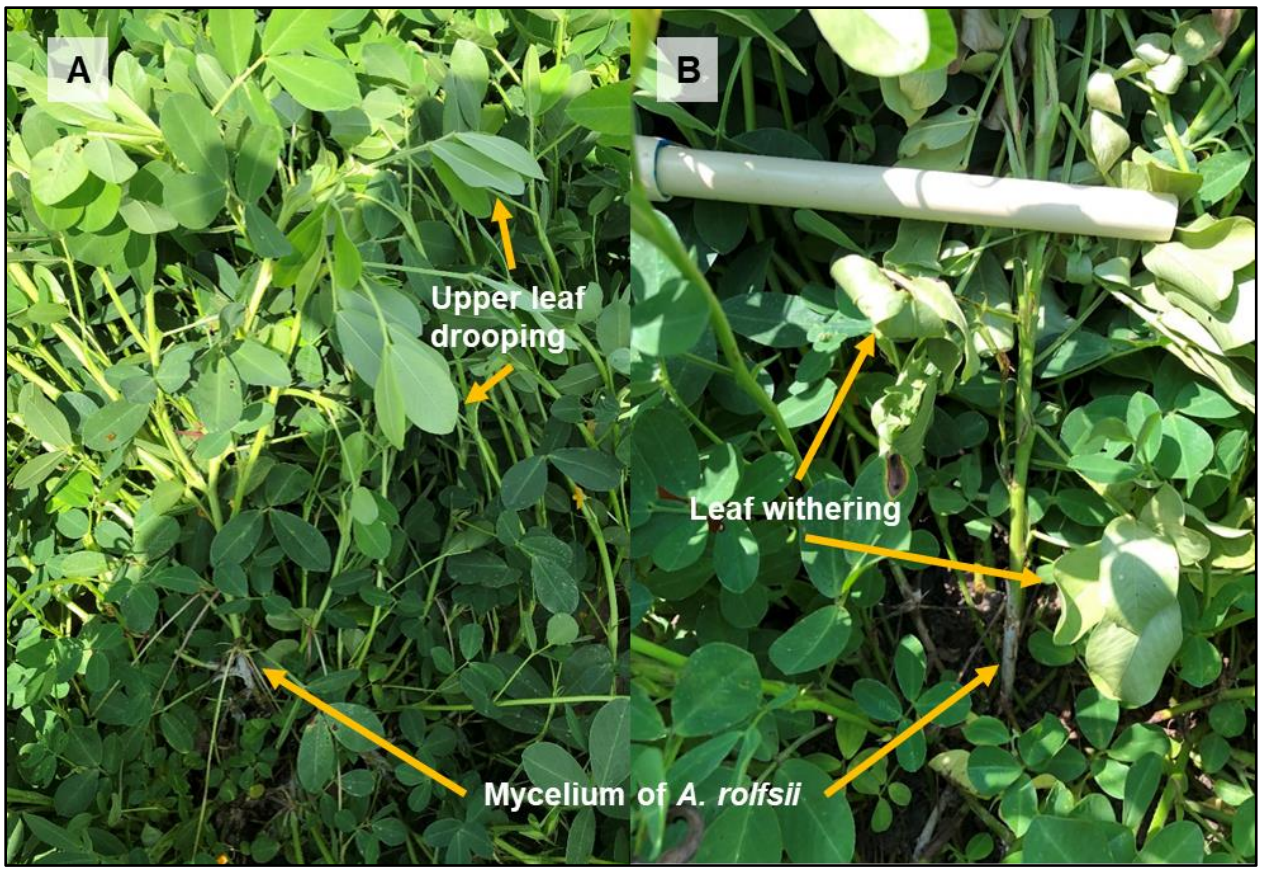

Fig. 2. Signs and symptoms of peanut plants naturally infected with *Athelia rolfsii* in the field during (**A**) early and (**B**) late infection stage.

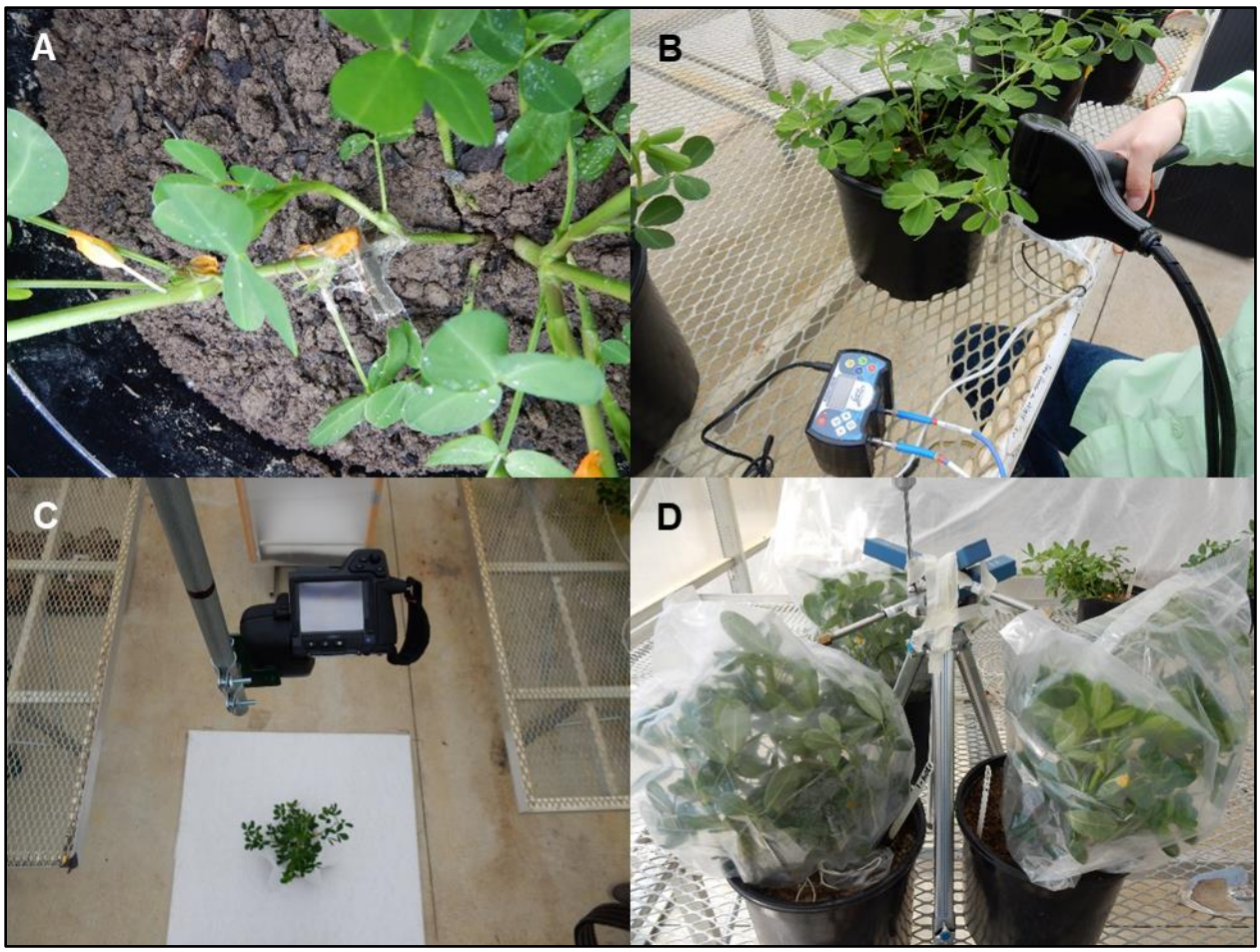

Fig. 3. A = Peanut plants were inoculated via clamping a with Athelia-rolfsii colonized clothespin on one of the two major lateral stems in each plant. **B** = Spectral reflectance of one designated leaflet of the second youngest mature leaf on treated lateral stems were measured with a Spectroclip-R probe using a handheld Jaz spectrometer. **C** = Top-view thermal images of the whole plant were taken with a FLIR T420 camera at ~183 cm above the ground inside the greenhouse. **D** = Volatile compounds were collected from the headspace of peanut plants enclosed in an oven bag using a pump with a charcoal trap.

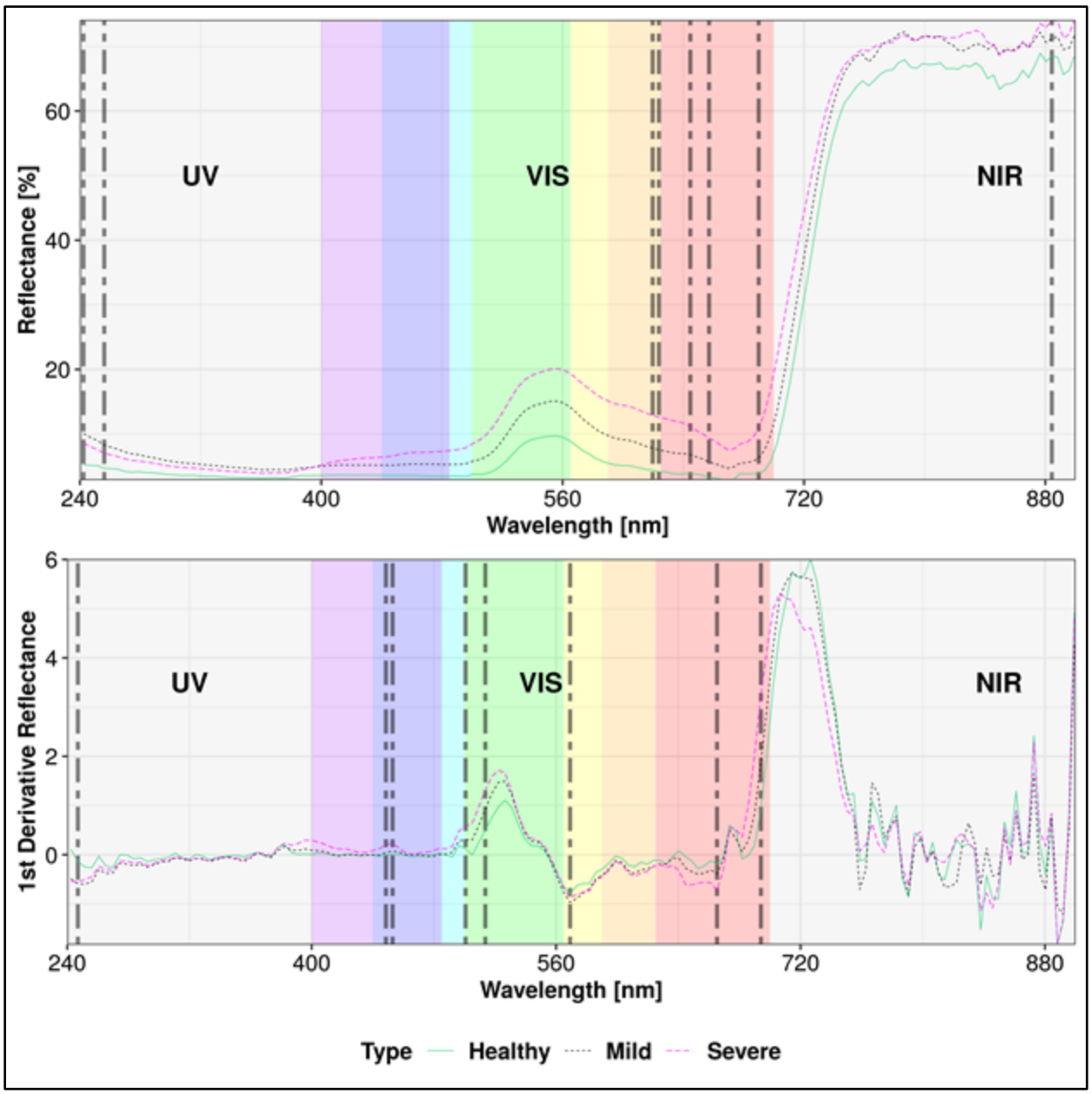

Fig. 4. Spectral signatures and selected wavelengths (as shown in drop lines) using the primary **(top)** and derivative-transformed **(bottom)** spectra of *Athelia rolfsii*-inoculated and mock-inoculated peanut plants. UV = Ultraviolet, VIS = Visible, NIR = Near-infrared.

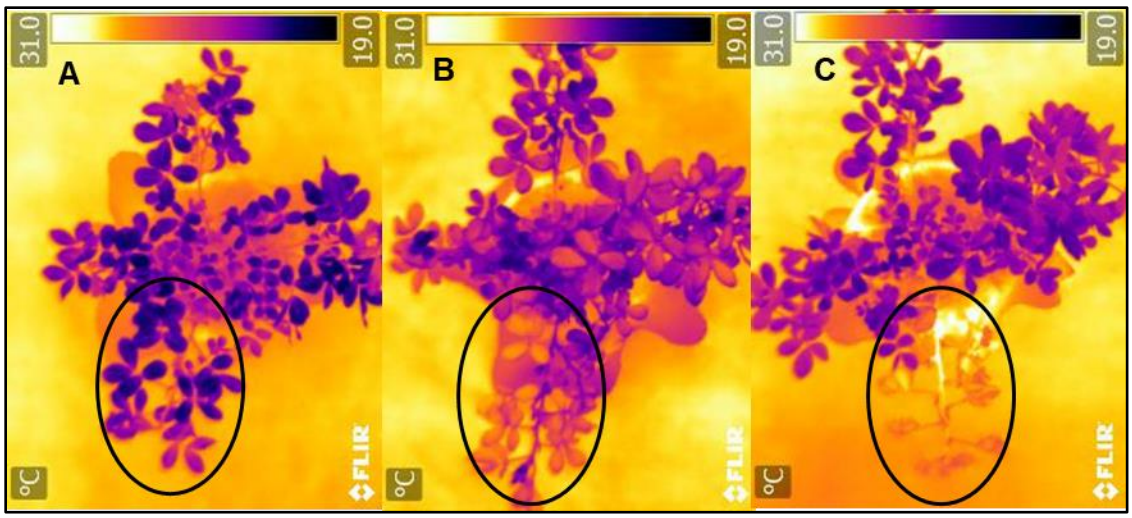

Fig. 5. Thermal images of a peanut plant inoculated with *Athelia rolfsii* in a greenhouse experiment. The lateral stem inoculated with *A. rolfsii* is circled in each thermal image, while the opposite lateral stem was mock-inoculated. **A** = 4 days after inoculation (DAI); **B** = 8 DAI; **C** = 12 DAI. Darker color indicates cooler temperature, while lighter color indicates warmer temperature. Images were taken with a FLIR T420 camera with a top view at ~183 cm above the ground inside the greenhouse.

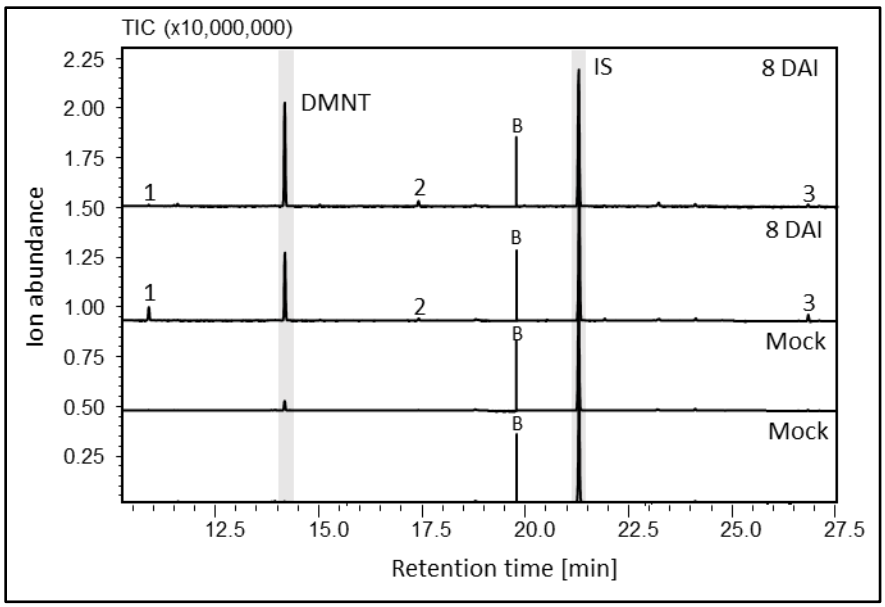

Fig. 6. Volatile emission of peanut upon infection with *Athelia rolfsii.* GC-MS chromatograms of VOCs collected from shoots and leaves of *A. rolfsii infected* peanut plants eight days after inoculation in comparison to mock-inoculated plants. DMNT= (*E*)-4,8-dimethyl-1,3,7-nonatriene, 1=hexenyl acetate, 2=putative monoterpene, 3=TMTT ((*E,E*)-4,8,12-trimethyltrideca-1,3,7,11-tetraene), IS=internal standard, B=background, TIC=total ion chromatogram. DAI=days after inoculation. Identification of compounds is based on library suggestion.

CHAPTER 5: Comparison of standard and newly registered peanut fungicides with different modes of action through bioassay of detached plant tissues with *Athelia rolfsii*

Xing Wei,[1,2] David B. Langston, Jr.,[1,2] and Hillary L. Mehl[1,2,3]

[1]Tidewater Agricultural Research and Extension Center, Virginia Tech, Suffolk, VA 23437, U.S.A.; [2]School of Plant and Environmental Sciences, Virginia Tech, Blacksburg, VA 24061, U.S.A.; [3]Current address: United States Department of Agriculture, Agricultural Research Service, Arid-Land Agricultural Research Center, Tucson, AZ 85701, U.S.A.

Author Contributions: Conceptualization, X.W., D.B.L., and H.L.M; methodology, X.W., D.B.L. and H.L.M.; formal analysis, X.W.; investigation, X.W.; resources, D.B.L., and H.L.M.; writing—original draft preparation, X.W.; writing—review and editing, X.W., D.B.L., and H.L.M.; supervision, D.B.L. and H.L.M.; funding acquisition, D.B.L. and H.L.M. All authors have reviewed the manuscript prior to publication.

Note: This manuscript is to be submitted to the journal Plant Disease.

Keywords: *Arachis hypogaea*, *Sclerotium rolfsii*, stem rot, residual activity, fungal inhibition, demethylation inhibitor (DMI), quinone outside inhibitor (QoI), succinate dehydrogenase inhibitor (SDHI)

Funding: This work was funded by the Virginia Peanut Board.

Abstract

Stem rot of peanut, caused by *Athelia rolfsii*, is an important fungal disease impacting peanut production worldwide. Foliar-applied fungicides are used to manage the disease, and several new fungicides have been recently registered for stem rot control in peanuts. This study compared fungicidal, residual, and potential systemic activity of standard and new stem rot fungicides against *A. rolfsii* using a laboratory bioassay. Peanut plants for the laboratory bioassay were grown in the field and were treated with eight fungicides ~90 days after planting, and plants were sampled weekly for five weeks following application. For the bioassay, plants were separated into the second newest fully mature leaf present at the time of fungicide application, newest fully mature leaf present at sample collection, upper stem, and crown. Each tissue type was inoculated with *A. rolfsii* then incubated at 30°C for two days. Lesion length was measured, and percent inhibition of fungal growth by each fungicide relative to the control was calculated. All fungicides provided the greatest inhibition of *A. rolfsii* on leaf tissues that were present at the time of fungicide application, followed by the newly grown leaf and upper stem. Little inhibition occurred on the crown. Fungal inhibition decreased at similar rates over time for all fungicides tested. Succinate dehydrogenase inhibitors provided less basipetal protection of upper stems than quinone outside inhibitor or demethylation inhibitor fungicides. Properties of fungicides characterized in this study, including several newly registered products, are useful for developing fungicide application recommendations to maximize their efficacy to control both foliar and soilborne peanut diseases.

Introduction

Peanut (*Arachis hypogaea* L.) is cultivated in tropical and subtropical areas worldwide, mainly for its seeds which contain high-quality protein and oil content (Stalker 1997; Venkatachalam and Sathe 2006). In 2017/18, the United States was the fourth-largest peanut producer (3.23 million metric tons), following China (17.09 million), India (6.65 million), and Nigeria (4.25 million) (USDA-FAS 2019). The area planted in peanuts in the U.S. was 576,879 hectares in 2018 (USDA-NASS 2019). Most peanuts in the U.S. are grown in three regions: southeastern U.S. (Georgia, Alabama, and Florida), southwestern U.S. (Texas, Oklahoma, and New Mexico), and the Virginia-Carolina region (North Carolina, South Carolina, and Virginia) (National Peanut Board 2019). However, peanut production in the U.S. is affected by several pests including foliar diseases, such as early and late leaf spot, and soilborne fungal diseases, such as stem rot, Sclerotinia blight, and Rhizoctonia limb rot. Estimated economic losses caused by reduced yields and costs of management practices to control diseases in Georgia alone, the top peanut producer in the U.S., were more than $160 million in 2018 (Kemerait 2020).

Stem rot of peanut is caused by a soilborne fungus, *Athelia rolfsii* (Curzi) C.C. Tu & Kimbrough (anamorph: *Sclerotium rolfsii* Sacc.). Yield losses caused by stem rot average 7 to 10% annually in the southeastern U.S. and usually much lower in states of the other two regions (Backman and Brenneman 1997), but it has become more prevalent in Virginia-Carolina (VC) region in recent years. New varieties with increased tolerance to stem rot were developed in recent years (Gorbet and Tillman 2008, 2011; Branch and Brenneman 2008, 2015; Branch and Culbreath 2011), but host resistance alone does not adequately control the disease. Cultural control practices including crop rotation and deep plowing to reduce the accumulation and persistence of pathogen inoculum in soils (Backman and Brenneman 1997), thus reducing the risk and severity of yield

loss caused by this disease. However, growers typically rely on the application of fungicides to control stem rot during the growing season (Hagan et al. 2004; Rideout et al. 2008).

Fungicides with different modes of action are labeled for stem rot control in peanut. The active ingredients of these fungicides are mainly from three chemical groups: demethylation inhibitors (DMI) (e.g., tebuconazole, prothioconazole, metconazole), quinone outside inhibitors (QoI) (e.g., azoxystrobin, fluoxastrobin, pyraclostrobin), and succinate dehydrogenase inhibitors (SDHI) (e.g., penthiopyrad, benzovindiflupyr, flutolanil) (Anco 2017; Balota et al. 2020). DMI fungicides interfere with one specific enzyme, C14-demethylase, which is involved in sterol biosynthesis in cell membranes of fungi (FRAC 2019). Therefore, DMI fungicides can cause abnormal growth and death of the fungus (Mueller et al. 2013). Both QoI and SDHI fungicides inhibit fungal respiration, but they have different target sites on the respiratory system of fungi. QoI fungicides target the cytochrome bc1 (ubiquinol oxidase) at quinone outer binding site (complex III), while SDHI fungicides act at the succinate-dehydrogenase in the complex II of the fungal respiratory system (FRAC 2019). Since these chemicals have different modes of action and target sites, they may differ from each other in their overall fungicidal activity against *A. rolfsii*.

Systemic movement of fungicides, especially basipetal movement, can provide an alternative solution to target soilborne diseases by moving downward inside the plant after foliar sprays (Augusto and Brenneman 2012). Basipetal movement of fungicides or their active derivatives takes place in the phloem sap in the symplast sieve tubes (Brudenell et al. 1995; Chollet et al. 2004; Quimette and Coffey 1990). To move basipetally, foliar-applied fungicides need to first penetrate into and diffuse through the leaf cuticles, then penetrate into the xylem apoplast and symplast membrane before moving into the sieve tubes at the site of leaf application (Kleier 1988; Kleier et al. 1998). The ability of fungicides to penetrate into the xylem apoplast is associated with

their lipophilicity or relative solubility to plant membranes, measured by an octanol-water coefficient (K_{ow}) (Kleier et al. 1998). The ability of a pesticide to concentrate in the phloem symplast and move for long distances is related to its acid strength (Augusto and Brenneman 2012; Bromilow et al. 1990; Devine 1987; Grimm et al. 1995; Neumann et al. 1985; Rigitano et al. 1987). The acid strength of a pesticide can be measured as the negative logarithm, pK_a, of the acid dissociation constant K_a (Rigitano et al. 1987).

There were previous reports on the systemicity of fungicides against *A. rolfsii* in peanut (Augusto and Brenneman 2012) and tomato (Roberts 2012). However, both of these studies were conducted a decade ago. Several new fungicide products have been labeled for stem rot control in peanut since then, including azoxystrobin + benzovindiflupyr (Elatus, registered in 2015), bixafen + flutriafol (Lucento, 2019), inpyrfluxam (Excalia, 2020), and mefentrifluconazole (Provysol, 2020). These new products have been demonstrated to be effective in field trials (Langston and Mehl 2021), but different properties of fungicides that may contribute to their efficacy have not been directly compared.

Most peanut fungicides are recommended to be applied every 14 to 21 days according to their labels. Multiple applications of fungicides are needed for one growing season because the activity of fungicides decreases over time, and fungicide needs to be applied to new crop growth. The residual activity of a fungicide can be influenced by the application rate and method, systemicity of the fungicide products, the targeted disease, the level of disease pressure, and environmental factors such as rain and sun exposure (Augusto et al. 2010a; Miorini et al. 2017). Currently, there is a lack of study on the residual activity of different peanut fungicides after foliar application. Therefore, this study was designed to compare the inhibition of *A. rolfsii* by standard and new stem rot fungicides on different peanut tissue types using a laboratory bioassay. Results

provide insights into the relative fungicidal, residual, and potential systemic activity of these fungicides that can be used to improve fungicide application recommendations for control of stem rot in peanut.

Materials and Methods

Field trials. 'Sullivan' peanuts were planted on the 16th and 26th of May 2020, respectively, in Field 16A and Field 66 at Virginia Tech Tidewater AREC's Hare Road Research Farm in Suffolk, VA. The soil at these two field sites was Kenansville loamy fine sand and Nansemond, Emporia, Eunola. The seeding rate was 13 seeds/m (13.45 kg/ha). Management of soil fertility, plant growth, insects, and weeds followed standard practices of the Virginia Cooperative Extension system (Balota et al. 2020; Flessner and Taylor 2019). Plots consisted of four 7.62 m long rows spaced 0.91 m apart. The middle two rows of each plot received fungicide treatments. Plots were arranged in a randomized complete block design with eight treatments (seven stem rot fungicides plus a "non-treated" control) and four replicates per treatment. Application rates and chemical properties of fungicides tested in this study are listed in Table 1. Approximately 90 days after planting (DAP), fungicide treatments were applied at 186 liters/ha with 262 kPa through a tractor plot sprayer equipped with two 8002 TwinJet nozzles per row. A nonionic surfactant (NIS) (Induce, Helena Chemical Company, Collierville, TN) was added to each fungicide solution at 0.125% v/v prior to application. To control leafspot and prevent pre-mature defoliation of the crop, fungicides previously reported to have no significant field activity against *A. rolfsii* (Culbreath et al. 1995) were applied to all plots including the stem rot fungicide "non-treated" control, for leafspot control. Approximately 60 DAP, all plots in both fields were sprayed with chlorothalonil (1.261 kg a.i./ha, Bravo Weather Stik, Syngenta Crop Protection, Inc., Greensboro, NC) and

approximately 100 DAP, fields were sprayed with pydiflumetofen (0.050 kg a.i./ha, Miravis, Syngenta Crop Protection, Inc., Greensboro, NC). While pydiflumetofen is an SDHI fungicide like some tested in this study, previous research has indicated this active ingredient provides little suppression against stem rot (Wei et al. 2018, 2019, and 2020). One of the fields also received thiophanate-methyl (0.394 kg a.i./ha, Topsin, United Phosphorus, Inc., King of Prussia, PA) as a rescue treatment against late leaf spot 113 DAP (Fig. 1).

Plants were sampled and evaluated in a laboratory bioassay weekly for five weeks after applying fungicide treatments. One to three days before the fungicide application, fifteen plants per plot were arbitrarily selected and labeled with flagging tape. These fifteen labeled plants were divided into five groups of three plants designated for each of the five sampling dates. For each labeled plant, the second youngest mature leaf on the primary lateral stem near the center of each plot was labeled with a twist tie. Sampling and initiation of the bioassay for each sampling date were completed over two days with plants for two replicates of fungicide treatments collected each day. On each day of sampling, the designated plants from each plot were dug and placed in a pre-labeled Ziploc bag then transported from the field to the laboratory in coolers.

Laboratory bioassay. On the same day of collection, four plant tissue sections were separated from each plant: the labeled leaf, the youngest mature leaf on the primary lateral stem, the upper stem, and the crown (Fig. 2A). For each replicate, plant sections were placed on moist paper towels inside a plastic container (32.2-liter in volume). The paper towels were placed on light grids (Plaskolite, Columbus, OH) and screen mesh (Saint-Gobain North America, Malvern, PA) to hold plant sections in position. In addition, 2 L of double-distilled water was added to the bottom of each container. Each plant section was then inoculated with an agar plug (5 mm in diameter) from a 3-day-old actively growing *A. rolfsii* grown on full-strength potato dextrose agar

(39 g/L; Becton, Dickinson and Company, Sparks, MD). The pathogen isolate was originally collected from a peanut field at the Tidewater AREC research farm in 2017. The mycelial plug was aseptically placed with the colonized portion face down on the middle of each leaflet and on the proximal end of each stem and crown section (Fig. 2B). The plastic containers were sealed with clear plastic wrap immediately after inoculation. Inoculated plant tissues were maintained in a temperature-controlled incubator (Thermo Fisher Scientific, Waltham, MA) at 30°C. Two days after inoculation, lesion length was measured on each plant section using a digital caliper (General Tools & Instruments, Secaucus, NJ). The length and width of necrotic lesions on each leaflet were measured and averaged as the mean lesion length for the leaflet sections, while the length of the necrotic lesion was recorded for each stem or crown section.

Data analysis. The experiment was a randomized complete block design with 8 fungicide treatments, 5 sampling dates, 4 replicates/blocks, and the experiment was conducted twice using plants collected from two different fields in 2020. A total of 960 peanut plants (120 plants per fungicide treatment) were sampled from the fields and tested in the laboratory bioassay. Lesion length for each experimental unit was calculated by averaging measurements of the group of 3 plants that were collected from the same plot on each sampling date. Percent fungal inhibition by each fungicide treatment was calculated using the following equation: percent inhibition = 100 × (average of lesion length of control – lesion length of fungicide treatment) / average lesion length of control.

An analysis of variance by each tissue type was first performed with field, fungicide, sampling date, and their interactions as fixed factors. The interaction effect of field with fungicide and sampling date was not significant ($P>0.05$) for all tissue types indicating that results were reproducible across the two fields/experiments. Mixed models were then constructed for the

statistical analysis of lesion length of control treatment (response variable 1), percent inhibition by all stem rot fungicide treatments combined (response variable 2), and percent inhibition of each stem rot fungicide (response variable 3). The fixed factors included sampling date (weeks after treatment), tissue type, and sampling date × tissue type interaction for response variables 1 and 2; and fungicide, sampling date, and fungicide × sampling date interaction for response variable 3. Field and block nested in the field were set as random factors for each mixed model. A one-sample t-test was performed to determine if the percent inhibition was greater than 0% for each tissue type on each sampling date, and for each fungicide treatment by each tissue type. In the mixed models, means of each fixed factor were separated using Tukey's Honest Significant Difference (HSD) test at α level of 0.05. All the statistical analysis was conducted using JMP Pro 15.0.0 (SAS Institute Inc., Cary, NC).

Results

During the course of field trials, there were rain events almost weekly from early August to late September in 2020 on the research farms in Suffolk, VA (Fig. 1). The application of stem rot fungicides in Field 16A was followed by a rain event the next day, but for Field 66, rain did not occur until nearly a week after application. However, the leaf spot rescue treatment of thiophanate-methyl and chlorothalonil in Field 66 was followed by a rain event the day after fungicides were applied (Fig. 1).

In the laboratory bioassay, lesion length for the control treatment (Fig. 3A) and percent inhibition by stem rot fungicide treatments (Fig. 3B) were first compared among different tissue types over the five sampling dates. For the lesion length of control treatments, sampling date and the interaction between sampling date and tissue type were not significant ($P > 0.05$), indicating

the lesion length for each tissue type did not change over the five-week experimental course. The labeled leaf had the greatest lesion development, followed by newly grown leaflets and upper stem section, while the crown section had the least lesion development ($P < 0.0001$). For percent inhibition by averaging over all stem rot fungicide treatments compared to control, there were significant effects for sampling date, tissue type, and their interaction ($P < 0.0001$). Across five sampling dates, the labeled leaf had the greatest percent inhibition, followed by the newly grown leaf and upper stem section, while the crown section had the least percent inhibition ($P < 0.0001$).

The effect of fungicide treatment, sampling date and their interaction on percent inhibition was examined by each tissue type. There was no significant fungicide by sampling date interaction for any tissue types except for the new leaf (Table 2). Therefore, each main treatment factor was analyzed separately. The sampling date effect was significant for the labeled leaf, newly grown leaf, and upper stem, but not for the crown section (Table 2). For the labeled leaf, inhibition of *A. rolfsii* was greatest one week after fungicide treatment and then decreased over time, indicating a decrease in fungicide activity (Fig. 3B). However, fungal growth was inhibited by fungicide treatments (percent inhibition significantly greater than 0%) on the labeled leaf for all five sampling dates (one-sample t-test, $P < 0.0001$). Fungal growth on the newly grown leaf and upper stem section was inhibited up to four and three weeks following fungicide treatment, respectively ($P < 0.001$). For the crown section, however, fungicides inhibited fungal growth only at two weeks after application ($P = 0.021$).

The effect of fungicide treatment on percent inhibition of *A. rolfsii* was significant for the labeled leaf and upper stem section, but not for the crown section (Fig. 4) (Table 2). Percent inhibition on the labeled leaf was similar for all fungicides except for bixafen + flutriafol, which provided greater percent inhibition than azoxystrobin and inpyrfluxam. For the upper stem,

azoxystrobin inhibited *A. rolfsii* more than benzovindiflupyr and inpyrfluxam. Among all tissue types, only the newly grown leaf had a significant fungicide by sampling date interaction (Table 2). One week after fungicide treatment, mefentrifluconazole inhibited *A. rolfsii* less than azoxystrobin, azoxystrobin + benzovindiflupyr, inpyrfluxam, and prothioconazole + tebuconazole ($P = 0.0033$) (Fig. 5). There was no significant difference among fungicide treatments for the rest of the sampling dates ($P > 0.05$) (data not shown).

Discussion

In this study, the fungicidal and residual activities of different peanut fungicides, including products with new or relatively new active ingredients, were compared side-by-side with different peanut tissue types using a laboratory-based bioassay. All of the foliar-applied fungicides evaluated provided inhibition of *A. rolfsii* for up to two weeks on plant tissues that received a direct application. Percent inhibition of *A. rolfsii* decreased over time, and the activity of all fungicides decreased at a similar rate. Results indicate that fungicides are most effective for up to two weeks after application, but by three weeks after application fungicidal activity decreases significantly. Thus, this supports the current recommendation that stem rot fungicides should be applied every two weeks when disease pressure is high (Anco 2017; Anco and Chapin 2016).

Regardless of their modes of action, all stem rot fungicides provided the greatest inhibition of *A. rolfsii* on the labeled leaf, followed by the newly grown leaf. The inhibition on the labeled leaf indicates fungicides were effective in controlling *A. rolfsii* on plant tissues that had direct contact with fungicides. The inhibition on newly emerged leaves suggests a potential acropetal (upward) movement of these foliar-applied fungicides (Augusto and Brenneman 2012). Alternatively, newly grown leaves (especially for ones collected on the first sampling date) may

have come into direct contact with the fungicides when they were applied, but the concentration of chemicals was likely less on these tissues than the labeled leaves. Since the stem rot fungicides tested in this study are also labeled for control of foliar diseases, the potential acropetal movement of these chemicals to newly emerged leaves is beneficial in managing leaf spot diseases in peanuts.

The inhibition of *A. rolfsii* by stem rot fungicides on the upper stem indicates a possible basipetal (downward) movement of these chemicals. In this study, azoxystrobin outperformed benzovindiflupyr and inpyrfluxam, both of which are SDHI fungicides, in protecting the upper stem. Basipetal movements of chemicals depend on their phloem mobility within plant tissues. Weakly acidic compounds with pK_a values between 2 and 6.5 and log K_{ow} values from 1 to 3 had optimal phloem mobility (Brudenell et al. 1995; Smith et al. 1995; Wright et al. 1994). However, none of these three chemicals were within the ranges for optimal phloem mobility (Table 2). Interestingly, the rates of SDHI fungicides were one to five-fold less than azoxystrobin when applied together with benzovindiflupyr (as Elatus) or applied alone (as Quadris) (Table 1).

Little evidence of protection of the crown section was found with these stem rot fungicides in this study. This may be explained, in part, by the fact that there was much less lesion development on the crown sections than other plant tissues regardless of control or stem rot fungicide treatments. The crown sections used in this study were much shorter in length than the two leaf tissues and upper stem (data not shown), and they represent older growth compared to other plant tissues tested. It has previously been reported that *A. rolfsii* infection and disease development decrease with increasing plant age (Rideout 2002). Thus, the crown sections might be less susceptible to *A. rolfsii* than other plant tissues tested in this study.

The newly registered peanut fungicides were demonstrated to be effective against *A. rolfsii* (Langston and Mehl 2021). It is known that the infection of *A. rolfsii* firstly occurs on the crown

or lower parts of lateral stems inside the plant canopy or belowground tissues, where the overwintering sclerotia of this pathogen reside (Backman and Brenneman 1997). Thus, the tissues that were more susceptible in the current bioassay such as leaf tissues and upper stem are not typically infected by *A. rolfsii* in the field. Under field conditions, when fungicide applications are followed by rain events or irrigation, the fungicide is believed to be washed down to the stem and crown (Taylor 1996; Woodward et al. 2012). The increased moisture/humidity due to rain also increases the pathogen infection and disease pressure. Greater efficacy (differences between treatment and control) is typically found in this scenario because there is more disease, and the fungicide is being physically transported to the tissues that need protection at the same time. However, in the current study, only one of the two field trials had the application of stem rot fungicides followed by a rain event (Fig. 1). Thus, there may have been less physical transport of fungicides down to crown tissues than would occur in the presence of rain or irrigation events.

The limited systemic movement of fungicides evaluated in the current study highlights the importance of using fungicide application methods that facilitate direct coverage of plant tissues that need to be protected from infection by *A. rolfsii* (Augusto et al., 2010a, 2010b; Shew 2021; Woodward et al. 2012). However, stem rot usually occurs during the mid to late growing season when the plant canopy covers the soil between rows and produces a warm and humid environment conducive to pathogen growth (Aycock 1966; Shokes et al., 1996). It is difficult for foliar-sprayed fungicides to penetrate into lower stems inside plant canopy and roots, pegs and pods underground because of the density of plant leaves, but it is in these plant tissues in the lower canopy that infection of soilborne pathogens initially occurs. To facilitate the penetration of fungicides into lower plant canopies, growers are recommended to apply stem rot fungicides with high spray volumes (187 liter/ha) (Shew 2021), to spray at night when the peanut leaves are folded (Augusto

et al., 2010a, 2010b), or to apply irrigation after fungicide spray to wash the fungicide residues on the foliage into the inner and lower plant tissues (Woodward et al. 2012), or to schedule stem rot fungicide application just prior to rain events.

In the current study, the conclusion that there was potentially basipetal movement of fungicides into tissues below the upper plant canopy was based on the assumption that fungicides did not come into direct contact with the upper stem and crown section on the day of fungicide application. For future studies, it is recommended to include sampling on the day that fungicides are applied so it will be possible to assess the extent to which fungicides come into contact with the different tissues immediately following application. Overall, this study suggests re-treatment interval and application methods of peanut fungicides should be carefully considered when developing fungicide programs to maximize their efficacy to control both foliar and soilborne peanut diseases.

Acknowledgments

We thank Dr. Wade Thomason, Quyen Do and Young Hu Yun for their suggestions on the experimental design and statistical analysis. We thank Richard (Steve) Byrum, Linda Byrd-Masters**,** and Navjot Kaur for technical support. We thank Dr. Sally Taylor, Dr. Sean Malone, and Matthew Wilkins for providing and maintaining one of the peanut fields for this study. Mention of trade names or commercial products in this article is solely for the purpose of providing specific information and does not imply recommendation or endorsement by the Commonwealth of Virginia or the U.S. Department of Agriculture. USDA is an equal opportunity provider and employer.

Literature Cited

Anco, D. 2017. Peanut Disease Management. In 2017 South Carolina Pest Management Handbook. Clemson Cooperative Extension. APT-17. Page 190-201. Available at, https://dc.statelibrary.sc.gov/bitstream/handle/10827/24248/CU_ES_PMH_SC_Pest_Management_Handbook_2017.pdf?sequence=1&isAllowed=y. Accessed on December 31, 2019.

Anco, D. and Chapin, J. W. 2016. Peanut Disease Management. In 2016 South Carolina Pest Management Handbook. Clemson Cooperative Extension. APT-16. Page 184-196. Available at, https://www.clemson.edu/extension/agronomy/pestmanagement/introduction.pdf. Accessed on December 31, 2019.

Augusto, J. and Brenneman, T. B. 2012. Assessing systemicity of peanut fungicides through bioassay of plant tissues with *Sclerotium rolfsii*. Plant Dis. 96: 330-337.

Augusto, J., Brenneman, T. B., Culbreath, A. K. and Sumner, P. 2010a. Night spraying peanut fungicides I. Extended fungicide residual and integrated disease management. Plant Dis. 94: 676-682.

Augusto, J., Brenneman, T. B., Culbreath, A. K. and Sumner, P. 2010b. Night spraying peanut fungicides II. Application timings and spray deposition in the lower canopy. Plant Dis. 94: 683-689.

Aycock, R. 1966. Stem rot and other diseases caused by *Sclerotium rolfsii*. N. C. Agric. Exp. Stn. Tech. Bull. 174.

Backman, P.A., and T.B. Brenneman. 1997. Stem rot. In Compendium of Peanut Diseases, 2nd ed. N.Kokalis-Burelle, D.M. Porter, R Hodrfguez-Kabana, D.H. Smith and P. Subrahmanyam eds. Page 36-37. American Phytopathological Society Press, St. Paul, MN.

Balota, M., Jordan, D., Mehl, H., Shortridge, J., and Talor, S. 2020 Virginia Peanut Production Guide. Viginia Cooperative Extension. SPES-177NP. Available at, https://www.pubs.ext.vt.edu/SPES/SPES-177/SPES-177.html. Accessed on April 12, 2021.

Branch, W. D. and Brenneman, T. B. 2008. Registration of 'Georgia-07W' Peanut. J. Plant Regist. 2: 88-91.

Branch, W. D. and Brenneman, T. B. 2015. Stem rot (white mold) and tomato spotted wilt resistance among peanut genotypes. Peanut Sci. 42: 18-22.

Branch, W. D. and Culbreath, A. 2011. Registration of 'Georgia-10T'peanut. J. Plant Regist. 5: 279-281.

Bromilow, R. H., Chamberlain, K., and Patil, S. G. 1990. A rapid method using *Ricinus communis* for the estimation of phloem translocation of xenobiotics. Pestic. Sci. 30: 1-12.

Brudenell, A. J. P, Baker, D. A., and Grayson, B. T. 1995. Phloem mobility of xenobiotics: tabular review of physiochemical properties governing the output of the Kleier model. Plant Growth Regul. 16: 215-231.

Chollet, J. F., Rocher, F., Jousse, C., Delétage-Grandon, C., Bashiardes, G., and Bonnemain, J. L. 2004. Synthesis and phloem mobility of acidic derivatives of the fungicide fenpiclonil. Pest Manage. Sci. 60: 1063-1072.

Culbreath, A. K., Brenneman, T. B., Bondari, K., Reynolds, K. L., and McLean, H. S. 1995. Late leaf spot, southern stem rot, and peanut yield responses to rates of cyproconazole and chlorothalonil applied alone and in combination. Plant Dis. 79: 1121-1125.

Devine, M. D. 1989. Phloem translocation of herbicides. Rev. Weed. Sci. 4: 191-213.

Flessner, M., and Taylor, S. V. 2019. Pest Management Guide: Field Crops, 2019. Virginia Cooperative Extension. 456-016 (ENTO-288P). Available at, https://www.pubs.ext.vt.edu/456/456-016/456-016.html. Accessed on February 21, 2021.

Fungicide Resistance Action Committee (FRAC). 2019. FRAC Code List© 2019. Available at, https://www.frac.info/docs/default-source/publications/frac-code-list/frac-code-list-2019.pdf?sfvrsn=98ff4b9a_2. Accessed on December 31, 2019.

Gorbet, D. W. and Tillman, B. 2011. Registration of 'York' peanut. J. Plant Regist. 5: 289-294.

Gorbet, D. W. and Tillman, B. L. 2008. Registration of 'Florida-07' peanut. J. Plant Regist. 3: 14-18.

Grimm, E., Grube, A., Jahnke, S., and Neumann, S. 1995. Retention of xenobiotics along the phloem path. Planta. 197: 11-18.

Hagan, A. K., Rivas-Davila, M. E., Bowen, K. L., and Wells, L. 2004. Comparison of fungicide programs for the control of early leaf spot and southern stem rot on selected peanut cultivars. Peanut Sci. 31: 22-27.

Kemerait, Jr., R. C. 2020. Peanut. In 2018 Georgia plant disease Loss estimates Compiled by E. L. Little. The Univerisity of Georgina Cooperative Extension. Annual publication 102-11. Page 13. Available at, https://secure.caes.uga.edu/extension/publications/files/pdf/AP%20102-11_1.PDF. Accessed on April 8, 2021.

Kleier, D.A. 1988. Phloem mobility of xenobiotics. I. Mathematical model unifying the weak acid and intermediate permeability theories. Plant Physiol. 86: 803-810.

Kleier, D. A., Grayson, B. T. and Hsu, F. C. 1998. The phloem mobility of pesticides. Pestic. Outlook 9: 26-30.

Langston, Jr., D. B. and Mehl, H. L. 2021. Applied research on field crop disease & nematode management 2020. Viginia Cooperative Extension. SPES-296NP. Available at, https://resources.ext.vt.edu/. Accessed on April 8, 2021.

Miorini, T. J., Raetano, C. G., and Everhart, S. E. 2017. Control of white mold of dry bean and residual activity of fungicides applied by chemigation. Crop Prot. 94: 192-202.

Mueller, D. S., Wise, K. A., Dufault, N. S., Bradley, C. A., and Chilvers, M. A.,eds. 2013. Fungicides for Field Crops. American Phytopathological Society, St. Paul, MN.

National Peanut Board. 2019. Peanut country, U.S.A. Available at, https://www.nationalpeanutboard.org/peanut-info/peanut-country-usa.htm. Accessed on December 15, 2019.

Neumann, S. E. Grimm, and F. Jacob. 1985. Transport of xenobiotics in higher plants. I. Structural prerequisites for translocation in the phloem. Biochem. Physiol. Pflanz. 180: 257-268.

Quimette, D.G. and Coffey, M. D. 1990. Symplast entry and phloem translocation of phosphanate. Pestic. Biochem. Physiol. 38: 18-25.

Rideout, S. L. 2002. The influence of environment and host growth for improved fungicide applications for control of southern stem rot of peanut. Ph.D. dissertation, University of Georgia, Athens.

Rideout, S. L., Brenneman, T. B., Culbreath, A. K., and Langston Jr., D. B. 2008. Evaluation of weather-based spray advisories for improved control of peanut stem rot. Plant Dis. 92: 392-400.

Rigitano, R. L., Bromilow, R. H., Briggs, G. G., and Chamberlain, K. 1987. Phloem translocation of weak acids in Ricinus communis. Pestic. Sci. 19: 113-133.

Roberts, M. J. 2012. Understanding the role of environment and the use of fungicides for improved control of southern blight of tomato. M.S. thesis, University of Georgia, Athens.

Shew, B. 2021. Peanut disease management. In 2021 Peanut Information. North Carolina Cooperative Extension and North Carolina State Univerisity. AG-331. Available at, https://content.ces.ncsu.edu/peanut-information. Accessed on April 8, 2021.

Shokes, F. M., Różalski, K., Gorbet, D. W., Brenneman, T. B., Berger, D. A. 1996. Techniques for Inoculation of Peanut with *Sclerotium rolfsii* in the Greenhouse and Field. Peanut Sci. 23: 124-128.

Smith, P. H., Chamberlain, K., Sugars, J. M., and Bromilow, R. H. 1995. Fungicidal activity of N-(2-cyano-2-methoximinoacetyl) amino acids and their derivatives. Pestic. Sci. 44: 219-224.

Stalker, H.T. 1997. Peanut (*Arachis hypogaea* L.). Field Crops Res. 53: 205-217.

Taylor, S. 1996. Effect of time interval prior to rainfall on the efficacy of tebuconazole against *Cercosporidium personatum*. (Abstr.) Proc. Am. Peanut Res. Educ. Soc. 28:51.

United States Department of Agriculture – Foreign Agricultural Service (USDA-FAS). 2019. World Agricultural Production. Page 26. Available at, https://apps.fas.usda.gov/psdonline/circulars/production.pdf. Accessed on December 15, 2019.

United States Department of Agriculture, National Agricultural Statistics Service (USDA-NASS). 2019. Acreage. ISSN: 1949-1522. The NASS, Agricultural Statistics Board, USDA, Washington DC. 16p.

Venkatachalam, M., Sathe, S. K., 2006. Chemical Composition of Selected Edible Nut Seeds. J. Agric. Food Chem. 54: 4705-4714.

Wei, X., Byrd-Masters, L., and Mehl, H. L. 2018. Comparison of foliar fungicide programs for leaf spot and soilborne disease control in peanut in Virginia, 2017. Plant Disease Management Reports. 12:CF041

Wei, X., Byrd-Masters, L., and Mehl, H. L. 2019. Comparison of in-furrow and foliar applications of fungicides for leaf spot and soilborne disease control in peanut in Virginia, 2018. Plant Disease Management Reports. 13:CF145

Wei, X., Byrd-Masters, L., and Mehl, H. L. 2020. Evaluation of in-furrow and foliar applications of fungicides to control leaf spot and soilborne diseases in peanut in Virginia, 2019. Plant Disease Management Reports. 14:CF166

Woodward, J. E., Brenneman, T. B., and Mullinix, Jr, B. G. 2012. Irrigation timing impacts the efficacy of foliar-applied fungicides toward foliar and soilborne pathogens of peanut. Plant Dis. 96: 1785-1790.

Wright, K. M., Prior, D. A., and Oparka, K. J. 1994. Observations on the accumulation of five xenobiotic chemicals in phloem versus parenchyma tissues of celery. Pestic. Sci. 42: 17-24.

List of tables and figures

Table 1. Fungicides with different modes of action compared for control of *Athelia rolfsii* in the current study.

Trade name	**Active ingredient(s)**	**Fungicide abbreviation**	**FRAC code[z]**	**Rates (kg a.i. h^{-1})**	**Lipophilicity (Log K_{ow})[y]**	**Acidity (pK_a)[x]**
Provost Silver	(prothioconazole+ tebuconazole)	(PTC+ TEB)	(3+ 3)	(0.200+ 0.200)	2.7 3.7	6.9 2.3 (est)
Quadris	azoxystrobin	AZX	11	0.446	3.7	N/A
Aprovia[w]	benzovindiflupyr	BZF	7	0.076	4	N/A
Elatus	(benzovindiflupyr+ azoxystrobin)	(AZX+ BZF)	(11+ 7)	(0.200+ 0.100)	4 3.7	N/A N/A
Lucento	(bixafen+ flutriafol)	(BIX+ FLT)	(7+ 3)	(0.074+ 0.127)	4.7 2.3	N/A N/A
Provysol	mefentrifluconazole	MFC	3	0.205	4	N/A
Excalia	inpyrfluxam	INP	7	0.075	3.8	N/A

[z]Fungicide resistance action committee (FRAC) code:11 = quinone outside inhibitors (QoIs); 3 = demethylation inhibitors (DMIs); 7 = succinate dehydrogenase inhibitors (SDHIs)

[y]Log K_{ow} = the computed octanol/water partition coefficient (PubChem, https://pubchem.ncbi.nlm.nih.gov)

[x]pKa = a specific type of equilibrium constant that is used to measure the propensity of a larger object to separate (dissociate) reversibly into smaller components (PubChem, https://pubchem.ncbi.nlm.nih.gov)

[w]Aprovia is NOT labeled for peanut

Table 2. Summary statistics on the effects of fungicide treatment, sampling date (weeks after fungicide treatment), and their interaction on the percent inhibition against *Athelia rolfsii*.

Factors	DF Num	DF Den	Crown[z]		Labeled leaf[y]		New leaf[x]		Upper stem[w]	
			F Ratio	P	F Ratio	P	F Ratio	P	F Ratio	P
Sampling date	4	238	2.08	0.084	55.58	**<.0001**	18.33	**<.0001**	22.09	**<.0001**
Fungicide	6	238	1.26	0.2789	6.83	**<.0001**	1.95	0.0743	2.95	**0.0086**
Sampling date*Fungicide	24	238	1.02	0.4357	1.20	0.2469	2.33	**0.0007**	1.24	0.2126

Different plant tissue types separated from each plant for the laboratory bioassay:

[z]Crown = a section from the main stem around the crown (half aboveground half belowground)

[y]Labeled leaf = the 2nd youngest mature leaf on the primary lateral stem near the center of each plot labeled prior to the application of fungicide treatments

[x]New leaf = the newly grown first mature leaf on the primary lateral stem on each sampling date

[w]Upper stem = a 2-internode-long stem section on the primary lateral stem starting immediately from the labeled leaf towards the crown of each plant

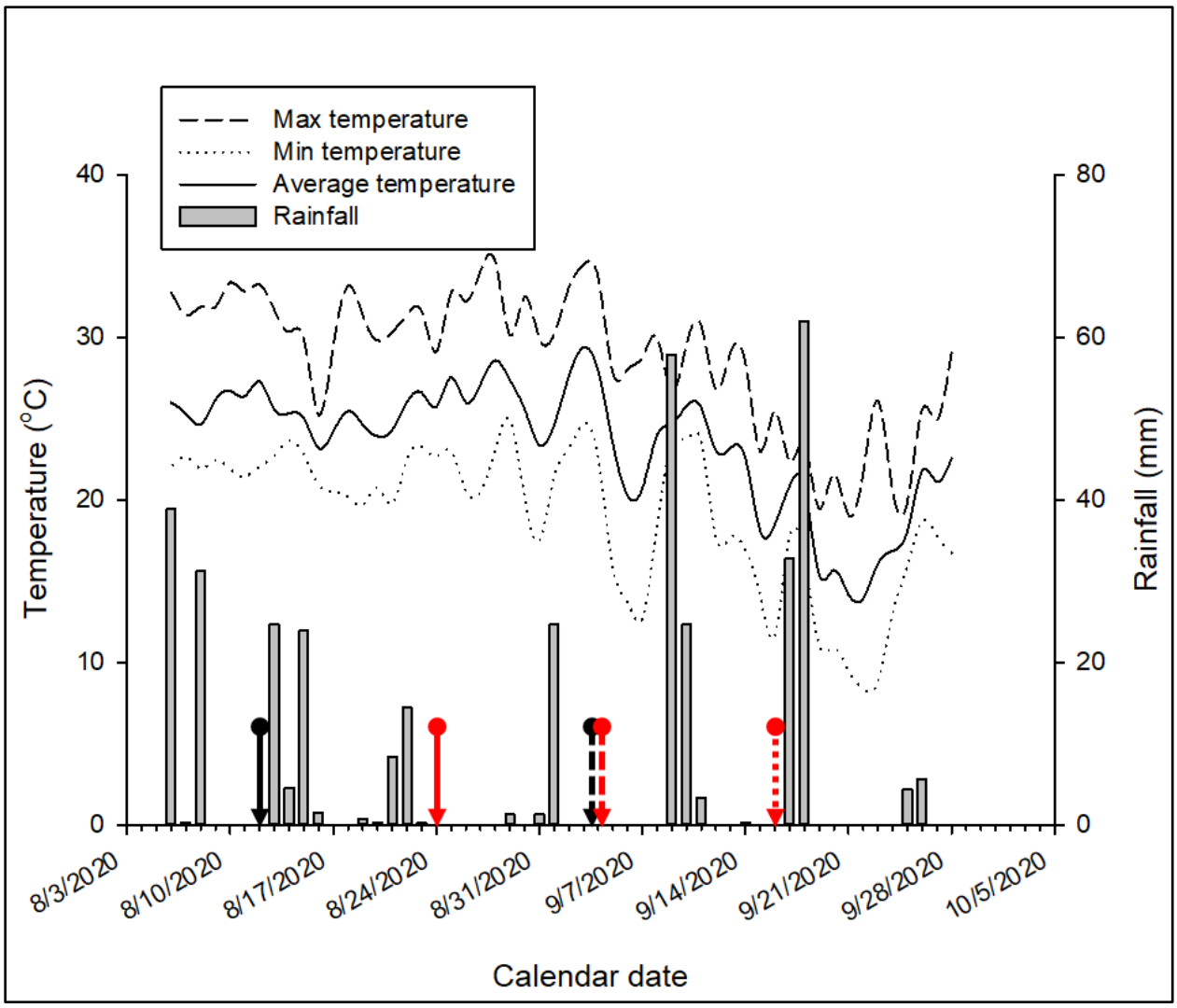

Fig. 1. Ambient temperature (**left y-axis**) and rainfall (**right y-axis**) during the course of field trials. Arrow drop lines indicate different fungicide applications: black line = Field 16A, red line = Field 66; solid line = stem rot fungicides, square dot line = application of pydiflumetofen (Miravis) and round dot line = application of thiophanate-methyl (Topsin) and chlorothalonil (Bravo Weather Stik).

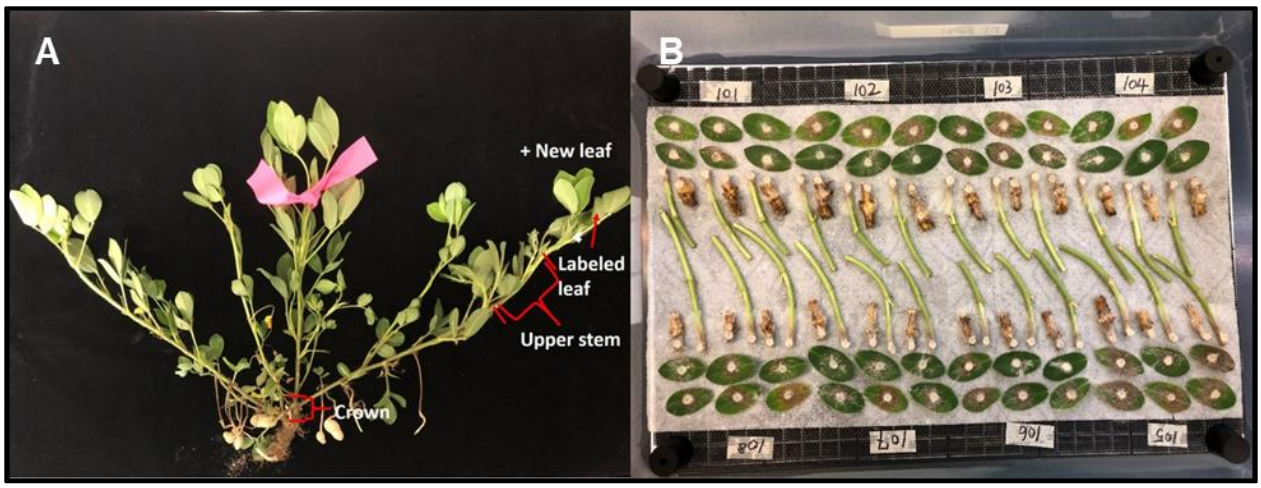

Fig. 2. Tissues sampled from each peanut plant consisting of labeled leaf, newly grown leaf, upper stem and crown (**A**), and an example of laboratory bioassay of different peanut tissues inoculated with mycelial plugs of *Athelia rolfsii* (for one replication of fungicide treatments on one evaluation date of one field) (**B**).

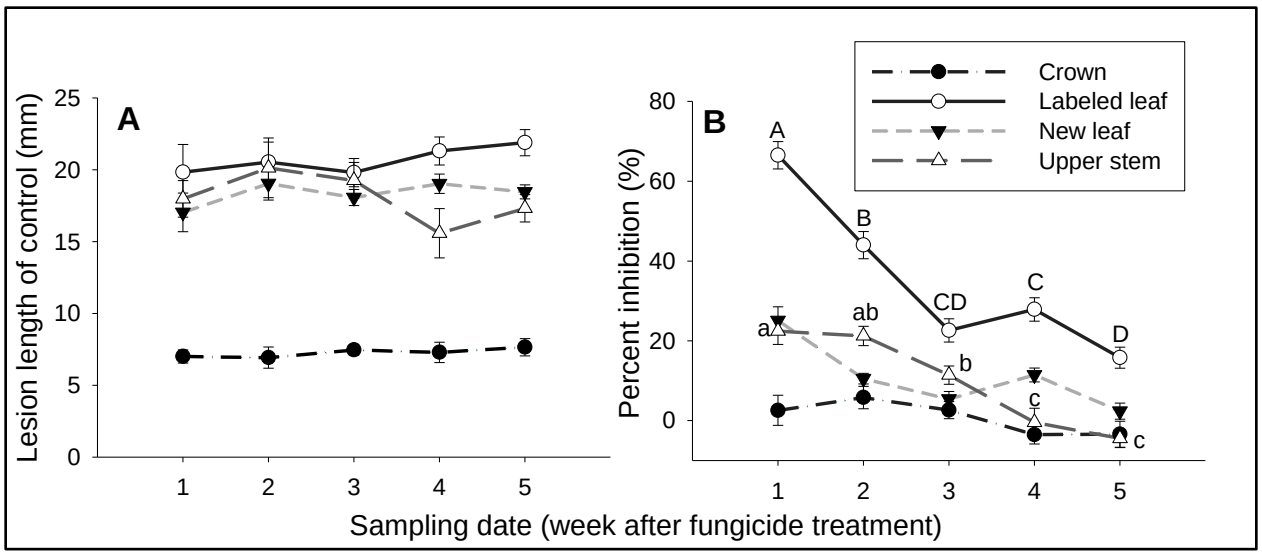

Fig. 3. Average of lesion length of control treatment (chlorothalonil) (**A**) and percent inhibition by stem rot fungicide treatments compared to control (**B**) on different peanut plant tissues inoculated with *Athelia rolfsii* on different sampling dates (week after fungicide treatment). Error bars indicate standard error, while means with different letters denote significant differences based on Tukey HSD at α of 0.05 (capital letters for labeled leaf, low-case letters for upper stem).

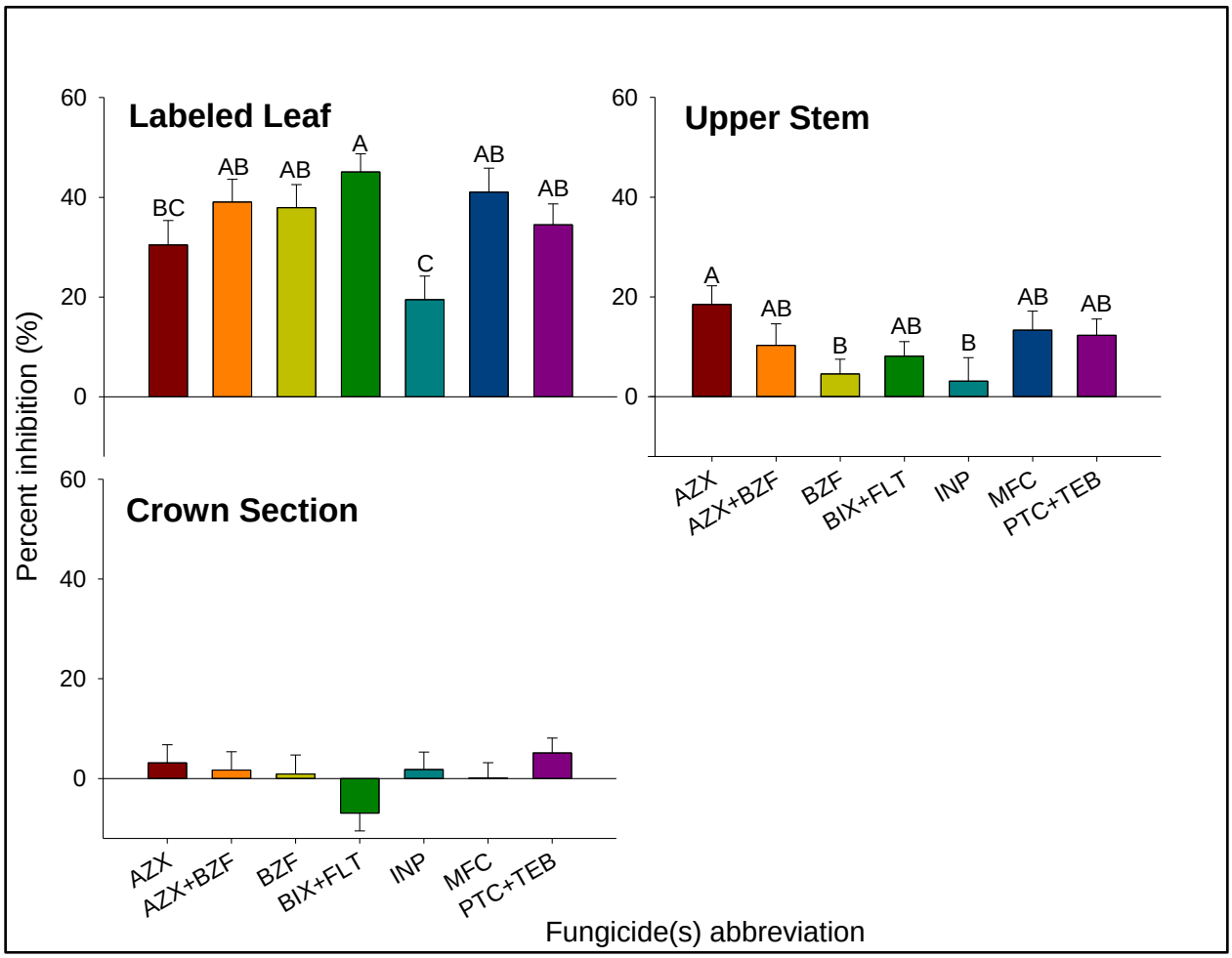

Fig. 4. Percent inhibition of different stem rot fungicide treatments against *Athelia rolfsii* across five sampling dates for labeled leaf, upper stem, and crown section. AZX = azoxystrobin; BZF = benzovindiflupyr; BIX = bixafen; FLT = flutriafol; INP = inpyrfluxam; MFC = mefentrifluconazole; PTC = prothioconazole; TEB = tebuconazole. Error bars indicate standard error, while means with different letters denote significant differences based on Tukey HSD at α of 0.05.

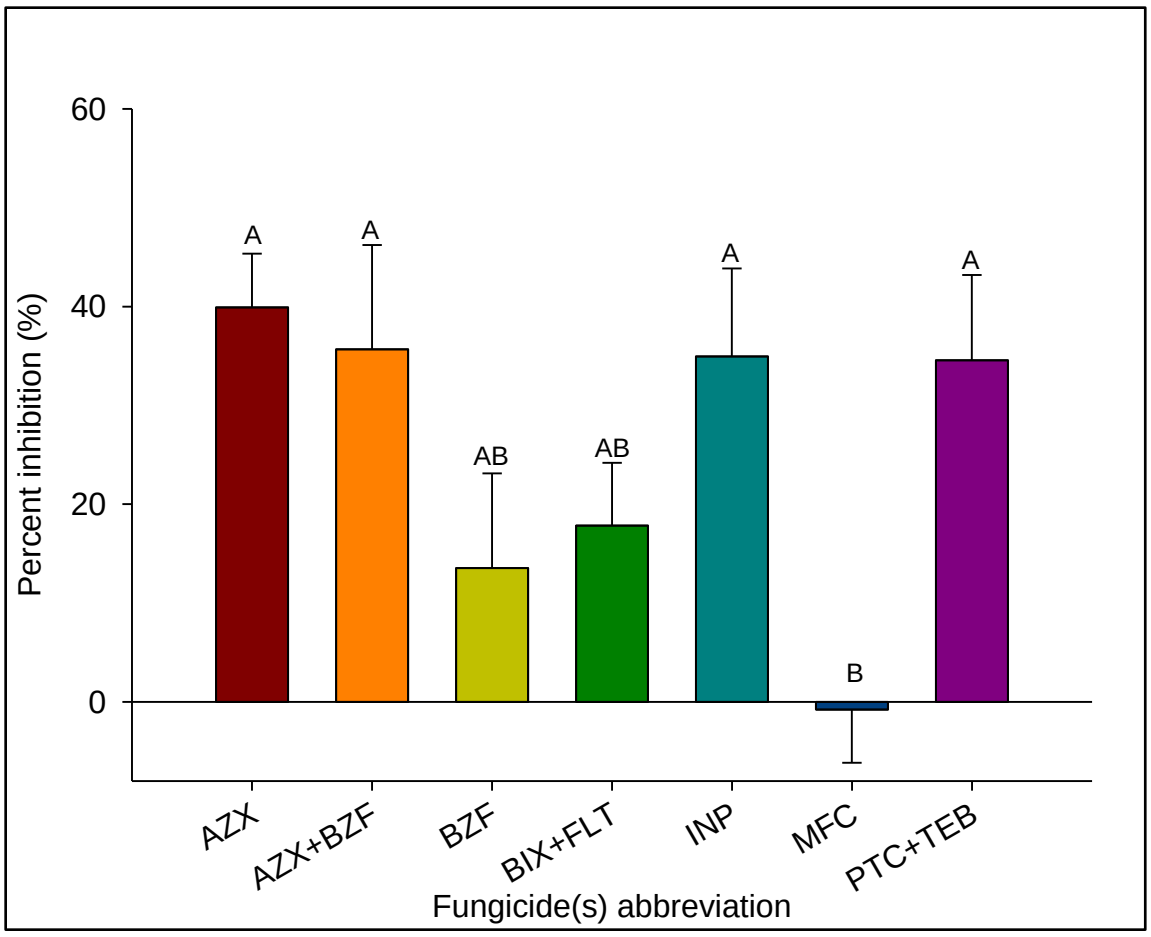

Fig. 5. Percent inhibition of different fungicide treatments against *Athelia rolfsii* on the newly grown leaf at 1 week after stem rot fungicide application. AZX = azoxystrobin; BZF = benzovindiflupyr; BIX = bixafen; FLT = flutriafol; INP = inpyrfluxam; MFC = mefentrifluconazole; PTC = prothioconazole; TEB = tebuconazole. Error bars indicate standard error, while means with different letters denote significant differences based on Tukey HSD at α of 0.05.